TADAS JUKNIUS

APPLICATIONS OF DIAMOND LIKE CARBON AND SILVER NANOCOMPOSITES FOR PREPARATION OF EXTERNAL USE PHARMACEUTICALS

DOCTORAL DISSERTATION

Kaunas
2021

KAUNAS UNIVERSITY OF TECHNOLOGY

TADAS JUKNIUS

APPLICATIONS OF DIAMOND LIKE CARBON AND SILVER NANOCOMPOSITES FOR PREPARATION OF EXTERNAL USE PHARMACEUTICALS

Doctoral dissertation
Technological Sciences, Materials Engineering (T 008)

Kaunas, 2021

The doctoral dissertation was prepared during years 2013–2018 at Kaunas University of Technology, Institute of Materials Science. Part of the research was performed at Lithuanian University of Health Sciences, Institute of Microbiology and Virology under cooperation agreement.

Scientific Advisor:
Prof. Hab. Dr. Sigitas TAMULEVIČIUS (Kaunas University of Technology, Technological Sciences, Materials Engineering – T 008).

The dissertation was edited by: English language editor dr. Armandas Rumšas Publishing House *Technologija*, Lithuanian language editor Violeta Meiliūnaitė (Publishing House *Technologija*)

The official defence of the dissertation will be held at 10:00 a.m. on the 3 of February, 2022 at the public meeting of the Dissertation Defence Board of the Materials Engineering Science Field in the Dissertation Defence Hall at Kaunas University of Technology.
Address: Donelaičio 73-403, Kaunas, LT-44249, Lithuania.
Phone: (+370) 37 300 042; fax: (+370) 37 324 144; email: doktorantura@ktu.lt

The doctoral dissertation was sent out on 3 January, 2022.
The doctoral dissertation is available on the internet at http://ktu.edu and at the library of Kaunas University of Technology (Donelaičio 20, Kaunas, LT-44239, Lithuania).

KAUNO TECHNOLOGIJOS UNIVERSITETAS

TADAS JUKNIUS

DEIMANTIŠKOSIOS ANGLIES IR SIDABRO NANOKOMPOZITŲ PANAUDOJIMAS RUOŠIANT IŠORINIO POVEIKIO VAISTINES FORMAS

Daktaro disertacija
Technologijos mokslai, medžiagų inžinerija (T 008)

Kaunas, 2021

Disertacija buvo rengta 2013–2018 metais Kauno technologijos universitete, Medžiagų mokslo institute. Dalis tyrimų buvo atlikti Lietuvos sveikatos mokslų universitete, Mikrobiologijos ir virusologijos institute, pagal bendradarbiavimo sutartį.

Mokslinis konsultantas:
prof. habil. dr. Sigitas TAMULEVIČIUS (Kauno technologijos universitetas, technologijos mokslai, medžiagų inžinerija – T 008).

Disertaciją redagavo: anglų kalbos redaktorius dr. Armandas Rumšas (leidykla „Technologija“), lietuvių kalbos redaktorė Violeta Meiliūnaitė (leidykla „Technologija“).

Medžiagų inžinerijos mokslo krypties disertacijos gynimo taryba:
prof. habil. dr. Arvaidas GALDIKAS (Kauno technologijos universitetas, technologijos mokslai, medžiagų inžinerija, T 008) – **pirmininkas**;
prof. habil. dr. Yuri DEKHTYAR (Rygos technikos universitetas, Latvija, gamtos mokslai, fizika, N 002);
prof. habil. dr. Valdimaras JANULIS (Lietuvos sveikatos mokslų universitetas, biomedicinos mokslai, farmacija, M 003);
prof. dr. Daiva MIKUČIONIENĖ (Kauno technologijos universitetas, technologijos mokslai, medžiagų inžinerija, T 008);
doc. dr. Ieva PLIKUSIENĖ (Vilniaus universitetas, technologijos mokslai, medžiagų inžinerija, T 008).

Disertacija bus ginama viešame medžiagų inžinerijos mokslo krypties disertacijos gynimo tarybos posėdyje 2022 m. vasario 3 d. 10:00 val. Kauno technologijos universitete, Disertacijų gynimo salėje.

Adresas: K. Donelaičio g. 73-403, Kaunas LT-44249, Lietuva.
Tel. (+370) 37 300 042; faks. (+370) 37 324 144; el. paštas doktorantura@ktu.lt

Disertacija išsiųsta 2022 m. sausio 3 d.
Su disertacija galima susipažinti interneto svetainėje http://ktu.edu ir Kauno technologijos universiteto bibliotekoje (K. Donelaičio g. 20, Kaunas LT-44239).

List of figures

List of tables

List of abbreviations

AAS	– atomic absorbtion spectroscopy
ATP	– adenosine triphosphate
Ag-NPs	– silver nanoparticles
B.C.E.	– before the common era
BP	– benzylpenicillin
CNS	– central nervous system
CRP	– C-reactive protein
DLC	– diamond like carbon
DLC:Ag	– silver dopped diamond like carbon
DC	– direct current
eV	– electronvolt
EDS	– energy dispersive spectroscopy
EGF	– epidermal growth factor
GoS	– group of samples
I.U.	– international units
keV	– kiloelectronvolt
Mf	– McFarland units
MRSA	– methicillin resistant Staphylococcus aureus
NPs	– nanoparticles
PPM	parts per million
RF	– radio frequency
ROS	– reactive oxygen species
SS	– saline solution
SEM	– scanning electron microscopy
SCCM	– standard cubic centimeters per minute
SIAL	– silver ion accumulation layer
S. aureus	– Staphylococcus aureus
SPR	– surface plasmon resonance
UV	– ultraviolet
UBMS	– unbalanced magnetron sputtering

INTRODUCTION

The relevance of this scientific work is based on infected wound healing problems and the aim of this dissertation is to create external use pharmaceuticals, such as a bandage, with silver ions as an antimicrobial agent, which would sustain good healing properties of infected wounds *in-vivo*, compared with the ordinary bandages. For such a bandage, thin film coatings were taken from KTU Institute of Materials Science; these were manufactured and fully investigated, and the scientific data were published by scientists Prof. habil. Dr. Sigitas Tamulevičius, Dr. Šarūnas Meškinis, Prof. Dr. Tomas Tamulevičius and others. In the current work, DLC:Ag thin film coatings were modified and applied for a bandage prototype.

It is well known that pathogenic bacteria strains can exist everywhere in our environment on widely used things, e.g., phones, keys or pens [1]. People are risking their health whenever having contact with contaminated surfaces, especially if working in places where minor injuries, such as small cuts in a finger can occur. Minor injuries with bacteria contaminated surfaces may have lethal consequences [2]. For example, one of the most dangerous bacteria is methicillin resistant *Staphylococcus aureus* (MRSA), which can cause serious wound inflammation with almost no possibility of getting cured by using antimicrobial drugs due to antibiotic resistance [3]. Centuries ago, many people would die due to wound infections and sepsis until penicillin was discovered by Alexander Fleming in 1929 [4]. In 1945, he won the most prestigious medical award – the Nobel Prize in Physiology/Medicine [4]. Since the 1960s, the treatment of *S. aureus* bacteria caused infections has become more complicated due to the growth of the antibiotic resistance by *Staphylococcus* strains. It is estimated that 65% of all *S. aureus* infections are caused by MRSA strains [5]. The growing usage of antibiotics in farms as feed additives [6] and the overuse of antibiotics in hospitals [7] increased the antibiotics-tolerating bacteria strains. For example, flies play an important role when transferring MRSA bacteria from the farm environment to hospitals or residential houses [3, 8, 9]. For that reason, widely used antimicrobial drugs have become useless, and new antimicrobials are required for infections and wound treatment.

Wounds, in terms of the injury type, are closed – when the soft-tissue layers are damaged beneath the skin, when the traumatic origin is, for example, after animal bites, or open – after injuries with sharp tools, or when sutured after a surgical intervention [10, 11]. Most problematic wounds are the chronic ones, when primary healing was unsuccessful, and secondary intervention and treatment is needed [10]. Chronic wounds usually appear after bacterial infection or when other factors, such as diabetes, burns, blood circulation failures are involved, or when the immune system causes a serious inflammation, and wounded tissues suffer from degeneration [12, 13]. The correctly chosen method of treatment is essential for successful results. One of the factors affecting the wound treatment time is scab formation, which can prolong the treatment time [11]. The moisture rich wound environment, when a scab does not cover the wound surface, can promote wound tissue angiogenesis and collagen proliferation [14, 11].

Today, the wound care has become a major challenge due to the antibiotics resistant bacteria strains, and new effective wound care products are required. One of the most promising antimicrobial materials is silver nanoparticles and silver ions [15, 16, 17]. The usage of silver as an antimicrobial agent for the treatment of infections has a long history. In 1884, Benno Crede – a German obstetrician – used 1% silver nitrate solution to cure blindness which was caused by post-partum infections for newborns [18]. Later on, when the effectiveness of silver-based medicaments was tested, and when side effects were determined, the US Food and Drug Administration [19] approved colloidal silver for wound treatment in 1920 [18]. Nowadays, moisture rich external use pharmaceuticals with anti-stick properties [20], such as creams, foams, hydrogels, hydrocolloids and polymeric films, meshes containing water with silver ions, are available on the market due to their antimicrobial properties and are used in the clinical practice [21,22].

In the clinical practice and current experiments, strong antimicrobial properties containing bandages are needed due to the unknown number of bacteria in the wound bed, and the best silver ion release properties containing thin film coating should be elected for the prototype. In such an advanced bandage, silver NPs and silver ions could be employed for a strong and long-lasting effect. Costly materials, such as silver, in dressings and bandages should be used in small amounts, and the optimum antimicrobial properties with minimum silver concentration are a desirable aspiration. For example, the authors of [23, 24] determined that the higher silver concentration does not ensure the best antimicrobial performance, and the overuse of silver in coatings is non-economical for bandages.

NPs synthesized into the water media have the propensity to aggregate in a solution [25] and pollute pharmaceuticals with remains of chemical synthesis. Another method for silver NPs synthesis is UV irradiation (365 nm, 500 W); silver salt can be reduced by using the photo-reduction method [26]. The basic methods of chemical NPs synthesis can change the chemical structure of the bandage background [27], or a bandage can be polluted with the chemical reaction remains. For the manufacturing of chemicals free bandages, the DC magnetron sputtering method was the optimum solution in the current research, because it is one of the cleanest methods to manufacture silver nanoparticles and stabilize them into a carbon matrix [28]. In the current process, silver nanoparticles are stabilized in the DLC matrix [15, 29], and thin film coatings with silver nanoparticles have no toxic chemical remains or background changes of a sputtered tray [30]. In order to improve the silver ion release properties from DLC:Ag coatings, the RF plasma etching technology for different time intervals could be applied, as, in the current work, several groups of samples were investigated so that to determine the chemical composition, the surface morphology changes, the nanoparticle size distribution, thereby determining the correlation with the silver ion diffusion to water.

In the current research work, a new bandage of a patented construction was created by applying the DLC thin film coating. For silver ion accumulation, a 3D silicone net filled with gelatin was attached so that to avoid direct contact with the wound tissues and to solve the stick-to-wound problem while sustaining the long-lasting antimicrobial properties.

Research problem

Around the world, the issue of infected wounds has become a major problem due to the extent of the growth of antibiotics resistant bacteria. The new generation of chemical antibiotics in pharmaceuticals involved in wound dressings and bandages has become more popular due to the good healing effect. On the other hand, good products are still overpriced and available for a minor part of the worldwide population. Nanotechnology based products can have the same or even better effects without using large amounts of expensive materials, and the presently applied technology could help to decrease the antimicrobial product pricing and increase the accessibility for the majority of the human population.

Diamond like carbon (DLC) coatings are widely used in electronics, optics and medicine implant segments, but cases when DLC coatings are used in external use pharmaceuticals are rare. It was a real challenge to apply DLC:Ag coatings to antimicrobial bandages because not of all DLCs have suitable properties for such applications. DLCs have several prominent advantages – they can be manufactured without chemicals which can be toxic to humans or can cause side effects. Besides, DLCs can be sputtered on textiles, and, most importantly, silver nanoparticles can be stabilized on coated surfaces. This property is important for safe-to-use products.

It is believed that the new bandage prototype might help to cure infected wounds more effectively and that the potential products will be accessible for a broad target audience.

Research objective

This research is aimed at the creation of external use pharmaceuticals, such as wound dressings or bandages, applying diamond like carbon and silver nanocomposite (DLC:Ag) coatings as the source of silver ions which act as the antimicrobial agent. The pharmacological evaluation is the second important step towards to the early stage bandage prototype.

Dissertation tasks

1. To investigate the chemical composition, surface morphology changes and nanoparticle size distribution of DLC:Ag groups of samples after RF plasma etching.
2. To determine the optimum plasma etching time of DLC:Ag surface and its correlation with the silver ion diffusion to water.
3. To perform antimicrobial tests, to determine the lowest silver ion concentration still maintaining antimicrobial properties, and to determine the best group of samples for the bandage prototype.
4. To determine the visual differences and similarities of the antimicrobial effects of silver ions, silver NPs and the widely used antibiotic benzylpenicillin for bacteria cells.
5. To prepare external use pharmaceuticals (bandages) with DLC:Ag coatings and to perform silver-ion-release and antimicrobial tests *in-vitro*.
6. To evaluate the pharmacological effect for lab animals and the bandage antimicrobial effect *in-vivo*.

Research methods

In the current scientific work, the microbiology methods (disc diffusion, serial dilution, and the spread plate technique) with pathogenic and referential bacteria were used to investigate the antimicrobial properties of silver ions and the prepared DLC:Ag samples. For the sample surface analysis and the silver content detection in samples, scanning electron microscopy (SEM) and energy dispersive X-ray spectroscopy were used. In order to detect silver ions in water, atomic absorption spectroscopy was applied. The samples were manufactured by applying the DC magnetron sputtering technology, whereas surface modification was performed with RF plasma etching. The bandage prototype was assembled by hand and tested with guinea pigs so that to determine the wound healing effect and the antimicrobial effect *in-vivo*.

Scientific novelty of the work

1. The methodology of producing antimicrobial properties demonstrating DLC:Ag nanocomposite thin films on textile, including oxygen plasma processing, was established, thereby enabling the creation of long-lasting antimicrobial materials which would sustain stability for more than 2 years.
2. Detailed antimicrobial testing of silver ions and NPs was performed for the antimicrobial effect for cell walls, and the optimum silver ion concentration for the best antimicrobial performance was determined.
3. A bandage prototype was created, and the unique structure was patented in Lithuania, and a PCT patent was obtained.

Dissertation structure

This dissertation contains the following chapters:

Chapter 1 presents the literature review. The literature review includes the history of silver application and explains the antimicrobial mechanism of silver, its toxicity for organism and the antimicrobial properties of DLC:Ag coating, respectively. Various bandages which are used in the clinical practice for wound care are reviewed. The novel method for the observation of bacteria cell wall changes caused by an antimicrobial agent is presented. Finally, information about wound healing and wound healing problems is briefly described.

Chapter 2 presents the materials and methods employed in this thesis. The chapter concisely describes the chemical reagents used in the experiments and generally explains all the methods applied in the current research work.

Chapter 3 is dedicated to the results and their discussion: this chapter contains the research results data about DLC:Ag thin film materials used in external use pharmaceuticals and presents the results of the performed antimicrobial tests. Furthermore, observation in the real time of the antimicrobial agent action mechanism and pharmacological evaluation of the created bandage data is presented.

Chapter 4 contains conclusions: the final reviews, conclusions and applications for the created external usage pharmaceuticals are presented.

The dissertation contains 132 pages, 26 figures and 6 tables and 8 annexes. The list of references features 256 items.

Personal input of the author

The presented results were obtained during experiments performed at Kaunas University of Technology and Lithuanian University of Health Sciences.

The dissertation author brought the idea to create the silver nanoparticles-based bandage. The internal structure of the bandage as well as the prepared external use of pharmaceuticals (bandage) was suggested and implemented by the author. Most of the experiments were planned and performed by the author, including all the microbiology experiments and tests with lab animals. DLC:Ag coatings were prepared by Vitoldas Kopustinskas and dr. Andrius Vasiliauskas, SEM analysis and EDS spectroscopy was performed by prof. Tomas Tamulevičius, AAS spectroscopy was conducted by Irina Abelit.

The current researches were funded by the joint KTU and LSMU projects NANOBIOSENSOR where the author was working as a junior researcher. Tadas Juknius performed the microbiology experiments with a team of scientists at LSMU. The second joint KTU and LSMU scientific project, directly related to the dissertation, was NANOSMARTPLASTER, where the author was the project initiator. The author performed experiments related to the bandage prototyping process and was employed as a junior researcher.

The results data were processed in consultation with Prof. Sigitas Tamulevičius, Prof. Tomas Tamulevičius and Associate Prof. Modestas Ružauskas.

1. LITERATURE REVIEW

In this chapter of literature review, the problems and achievements of wound treatment, thin films preparation, antimicrobial bandages and other external use pharmaceuticals used in the clinical practice are presented.

1.1 Physiology processes of wound healing

The wound healing process is influenced by a variety of factors, for example, it was determined that dehydrated wounds undergo a slower healing process [31], and small chirurgical interventions usually are very helpful in the successful treatment process of chronic wounds, but extra procedures of gangrening dead tissues, like cleaning out with a saline solution or dilute vinegar 0.5% acetic acid, are very useful [32]. Wounds developed after burns are most dangerous due to the high risk of infections, and, for example, at the beginning of the 20th century, one of the prevailing mortality reasons (over 50%) was related with injuries [33]. Hardly burned skin usually loses the epithelium layer which acts as the normal skin barrier for antimicrobial defense mechanisms [31]. Skin epidermis contains four different types of cells, but the most important ones are keratinocytes – they constitute 80–90% of the cellular epidermis and form a barrier from the outer environment, including the bacteria [33]. It is known that bacteria attached to the skin or the wound surface can form a biofilm which is from 10 to 1000 times more resistant to the biocidal agents comparing with loose bacteria, and it is very difficult to eliminate pathogens completely [34] from injured skin surfaces. Wounds after various injuries are unprotected; they are a nutrition-rich place for bacteria to grow [35]. Without protection, the skin becomes vulnerable to invasive microbial infections [18], and this can result in sepsis subsequently leading to death [34].

Wound healing is a complex biological process where various biomolecules, biochemical pathways and physiological processes are involved in the course to hemostasis [27, 28]. The main problem in the wound healing process is the prevention of transit from a healing wound towards to the chronic non-healing wound condition [36, 37]. Chronic wounds tend to get stuck in the inflammatory phase [32], and this condition requires a lot of efforts to heal the wound completely without serious residual effects [37–39]. The wound healing process can be comprised of three stages:

The inflammation stage begins after the injury or any other type of wound occurrence and extends depending on the organism's condition and its defense mechanism [33, 40, 41]. During this process, blood vessels are disrupted around the wound's bed, and they can release such clotting factors as fibrinogen which coagulates thereby forming a net for blood platelets which get stuck in the fibrin net [42]. After this process, a fibrin clot appears on the damaged area [33]. Afterwards, the increased vascular permeability leads to the leakage of plasma fluid from blood vessels [43]. The leakage process can be explained as a process when vessels expand in diameter and form micro-gaps between the vessel's cells, thus allowing the white blood cells, antibodies, and other molecules such as growth factors to migrate into the wound's bed [33, 43]. Other blood-shaped elements, such as neutrophils, release

chemokines to amplify the immune response and attract more leukocytes into the inflammation zone [33]. At this stage, the inflammation level increases, and symptoms like erythema, edema or pain start occurring, and the local temperature increases respectively [44]. Inflammation in the damaged tissues often leads to functional disorders [40, 45]. C-reactive protein (CRP) in the blood plasma [46] initiates neutrophils and macrophages to eliminate microorganisms by phagocytosis [33]. The phagocytosis process starts when CRP binds to phosphocholine on the microbe's wall surface, damages it and enhances the phagocytosis process by macrophages [46, 47]. CRP is mainly used as a marker to detect the inflammation process [46].

The proliferative stage (epithelization, angiogenesis and matrix formation) starts when activated macrophages eliminate neutrophils, and this stage can overlap with the inflammatory stage [41, 48]. Macrophages release the growth factors which initiate the new connective tissue mass formation, which is commonly termed as the granulation tissue (it contains new blood vessels) formation [33]. During this stage, the granulation tissue formation and the excretion of collagen by fibroblasts begins with the purpose to regenerate the damaged tissues [49]. Fibroblasts can also differentiate into myofibroblasts and contract the wound tissues [33]. During the granuloma tissue formation stage, the number of fibroblasts increases, and synthesis of collagen intensifies, respectively [50]. The formation of vascularized mass in the healing wound is amplified by the proliferating fibroblasts and mucopolysaccharide in exudate [43]. Furthermore, the collagen and extracellular matrix deposition promotes the angiogenesis process, and newly formed micro vessels can ensure blood circulation, which increases the speed of granulation tissue formation with the irregular texture in a naturally pink color [19]. The wound regeneration or reepithelization process begins from the wound margin and epidermal appendages [37].

The maturation stage. During this stage, the synthesized collagen improves the tensile strength of the skin, and the scar formation process begins [33]. At this stage, the number of inflammatory cells decreases to the normal level, and the gaps between the vessel's cells in the blood vessels contract; thus, vessels regress to the original structure, and the wound tissues are remodeling for the retrieval of the skin functions [49].

1.2 Healing processes of bacteria infected wounds

A healthy organism has a healthy skin, which is one of the most important organs playing an important role in the survival, and the skin can protect the body from dehydration, infections and sun radiation. It also helps to regulate the body temperature [31]. The many microbiota (Fig. 1) on the skin surface can live for any extended amount of time and do no harm for the health; for example, 1 million bacteria reside per square centimeter on the human skin [51, 52], and we do not feel any bad consequences regarding this fact. Usually, the skin surface is acidic, it contains sweat which is salt-laden, and the skin is coated with natural antimicrobial peptides which work as antibiotics [52]. Due to these conditions, the skin surface always sustains the bacterial balance, because, if it were otherwise, other pathologies

would occur [53]. In pathological cases (skin diseases, cuts, ulcers) when pathogenic microorganisms enter into the wound [54], there are all the necessary nutrients available for multiplication; consequently, serious wound infections develop [55]. Very often, the wound care can become a complicated procedure due to the accidents such as traumatic burns or blast injuries, pathologies like skin diseases, or diabetes-caused chronic inflammations [56].

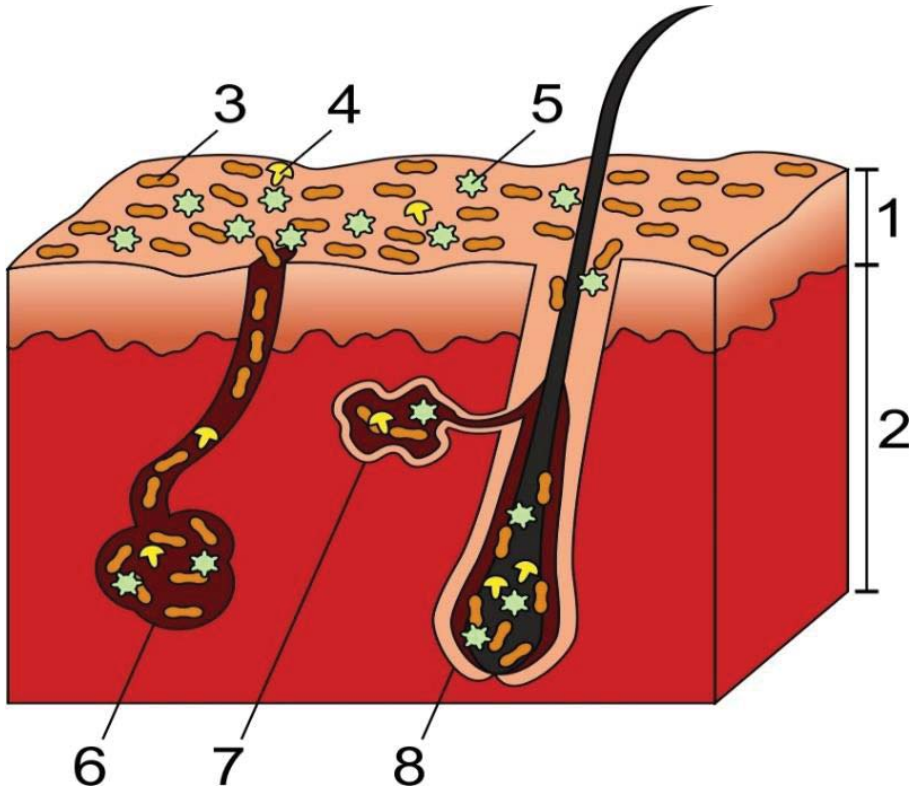

Fig. 1. Skin structure and microbiota on the skin surface [52]: epidermis (1), dermis (2), bacteria (3), fungi (4), virus (5) on the surface of the skin, sweat glands (6) and sebaceous glands (7) with a hair follicle (8) can provide nutrition for microbiota which in the case of an infection can act as pathogens; they may cause inflammation leading to tissue damage, but usually the microbiota population is regulated by skin secretion (sweat and antimicrobial peptides) and the natural skin epidermis layer

Open chronic wounds as well as the emergence of the genetic factors can negatively influence the life quality and exert a financial burden [33]. Wounds can be described as a disruption of the skin structure and function [31], and proper treatment is one of the most important procedures for patients.

1.2.1 Healing process of MRSA bacteria infected wounds

Centuries ago, people noticed that wounds which occurred after unclean (polluted with dirt) cuts and injuries can cause serious inflammation of the damaged tissues or could even lead to fatal consequences due to sepsis [57]. Every injury can 'open the gates' for pathogenic microorganisms, such as methicillin-resistant *Staphylococcus aureus* (MRSA) to the organism. MRSA can cause wound inflammation with bad outcomes leading to long term consequences [58]. The increased MRSA infection rates in hospitals appear to be unstoppable [59]. Regarding MRSA, the wound treatment becomes a complicated process. For example, chronic wounds are one of the major clinical problems, as, only in the USA, in the course of a research conducted in 2016, 6.5 million [60] patients were affected by chronic wounds [61], which may lead to serious infections. The treatment of wounds usually becomes complicated due to the bacteria biofilm which can be from 500 to 5,000 times more resistant to antibiotics than free non-biofilm bacteria [60].

Wound infection treatment caused by MRSA is a complicated process; nowadays, for the MRSA treatment, antibiotic therapies are used when more than one type of antibiotic is applied for treatment at one time [34]. Good results were observed when antimicrobial agents, such as biaryl hydroxyketone, nafcillin and cephalothin, are used as quorum-quenching agents [62] to replace methicillin which has no effect in difficult clinical cases. On the other hand, studies show that only silver containing wound dressings have a strong antimicrobial effect [63] and are the most promising strategy.

1.3 Silver as antimicrobial agent

Silver in the early history was used as money and jewelry; also, tools like silver plates and water containers were manufactured [64]. The unique antimicrobial properties of silver were noticed before 4000 B.C.E., and it was mainly used for water purification [2, 65]. Historical sources describe that a Persian King drank water from silver water containers only, and Macedonians used small silver plates to increase the wound healing speed [65]. Ancient Romans noticed that silver coins have unique properties – they could prevent water from turning sour and prevent contamination over long traveling periods [66]. The most famous ancient medical doctor – Hippocrates – used silver preparations for ulcers treatment, whereas later silver (specifically, silver salts dissolved in water) became a widely used antimicrobial agent [65]. The antimicrobial properties of silver were used in most advanced scientific projects. In the 20th century, silver was used in Apollo space programs for water purification, [13, 66] in the Mir space station [67], and in the Space shuttle missions [18, 68].

There is a wide range of silver containing medical products, such as antimicrobial wound dressings, bandages, solutions and silver-plated medical tools [69, 70]. It was determined that nanocrystalline silver and platinum coated medical devices and implants can reduce the risk of inflammation after surgical procedures due to the antimicrobial properties of silver [71], and extensive possibilities of silver application make silver one of the most valuable materials for infection treatment.

Nowadays, silver nanoparticles can be used in cashew gum [72] in odontology for gums infection treatment [73] or in general medicine [74] to reduce the number of infections after vascular surgery, and for the treatment of complicated wounds [16, 75, 76].

1.3.1 Silver-containing bandages

A wide variety of chemical drugs are used in hospitals for wound treatment. It is known that external use pharmaceuticals for infected wounds can be such products as: solutions, gels, creams, and bandages [24]. Bandage-type wound care products are used in hospitals [76], armed forces [77], and as the first aid at home. The main purpose of a bandage is to stop bleeding and to prevent the wound from contamination with dirt and bacteria [24, 78]. Most of wound dressings are made from sterile cotton, yet they also can be composed of other natural materials and could be denoted by minor antimicrobial properties [79]. Scientific studies claim that bacterial cellulose is denoted by the potential to be one of the best materials for wound treatment due to its biocompatibility, non-toxicity, mechanical stability and a high moisture content [36]. It could be added that, for the treatment of wounds, such polysaccharides as chitosan can be used in the clinical practice due to its biocompatibility, non-toxicity, and it can be applied in tissue engineering for the positive effect for the wound healing process due to its bioactivity against inflammatory cells [80].

Ionized silver (Ag^{+1}) has been employed in burn wound treatment due to the antimicrobial properties for over 200 years [64]. Silver as an antimicrobial agent became popular for applications in wound dressings, e.g., cotton bandages [81, 82]. Such bandages with silver can be described as the ordinary cotton or other dry material-based bandages with a thin-coated silver net on the surface, or else they contain metallic silver incorporated in some other form in the cotton background [83]; these are suitable for minor injury treatment. Also, silver dressings are used in extreme cases, such as war medicine, when the injuries are extremely difficult; for instance, silver-nylon dressing *Silverlon* [77] is successfully used and has helped to save many lives.

Nowadays, more advanced silver containing and moisture rich or hydrogel based wound dressings are being used [24, 78, 79]. Silver dressings, according to some authors [44], can reduce pain. An experimental study with people revealed that nylon dressings with silver can reduce pain after surgical intervention during the healing period. The pain reduction mechanism is explained by providing an occlusive barrier [44, 77].

Many studies show that silver inside bandages can strongly improve antimicrobial and wound healing properties, but most advanced bandages with silver is silver nanoparticles incorporated in multilayer water rich dressings made from hydrogels [20, 23] (water absorbent materials). The most advanced bandages are expected to feature such properties as: ability to maintain the wound-optimum moisture, absorption of extra exudate, allowance of gas diffusion, thermal insulation, antibacterial activity, biocompatibility, non-toxicity, mechanical stability, and low adherence to the wound surface [36]. Numerous researches have been performed to

implement the goals of the excellent properties containing bandage, and most promising studies can be briefly presented as follows.

One of the most popular categories of bandages is hydrogel based with silver micro-nanoparticles inside. Nanoparticles are incorporated into the hydrogel matrix and can extract silver ions into water and water based media, such as wound fluids [84, 85]. For example, these are *Acticoat*™ and *PolyMem Silver*® bandages made from hydrogels like 2-acrylamido-2-methylpropane sulfonic acid sodium salt that are incorporated with silver nanoparticles [85]. In order to enhance the healing process, dressings like Alginate-hyaluronan composite [86] or keratin-based hydrogels [87] can be successfully used as well. Moreover, water rich or hydrogel bandages with silver ions (without nanoparticles) can also be used effectively for wound treatment [83].

Bandages with biomaterials have to feature moistening properties so that to stop wound tissue dehydration and prevent infections [10, 23]. Nowadays, some wound care products contain growth factors to speed up the healing process; also, a technology has been developed to imitate the Extra Cellular Matrix in wounds which can form the structural carcass for growing cells [31]. There is a scientific study presenting dressings with nicotinamide (an anti-inflammatory drug) with silver NPs which were manufactured by using alginate (as the reducing and stabilizing agent), and it was reported that such a type of dressings strongly increases the healing speed of burn wounds on the lab rats model [88]. Other types of wound dressings to be marked are bioengineered dressings. These types of dressings can be made from human or animal skin components which can imitate the normal skin structure and architecture [72]. Dressings of this type can replace the epidermal layer and provide a structural scaffold necessary for regenerating cells [31, 32]. Also, bioengineered dressings due to their unique structure can sustain the optimal moisture level inside the wound bed and stimulate the healing process by releasing the epidermal growth factor (EGF) [89] in order to achieve the best healing effect.

Nanofiber (150 nm) mats with silver nanoparticles have the potential to be a promising technology against bacteria in wounds; the authors of experimental study [59] claim that nanofiber mats with silver nanoparticles (Ag-NPs, 25 nm diameter), enveloped in chitosan, can strongly enhance the antimicrobial properties of antimicrobial products, made from improved nanofiber materials. The authors of study [90] determined that nanocrystalline silver is denoted by strong antimicrobial properties and that similar technologies can be successfully applied in external use pharmaceuticals. One of such examples when nanocrystalline particles are used in a solid stable matrix could be DLC:Ag thin films sputtered on textiles, and silver NPs in coatings is one of the most promising materials for external use pharmaceuticals [15, 29].

1.3.2 Antimicrobial mechanism of silver ions

The mechanisms which can describe the antimicrobial effect of silver for a wide range of microorganisms are being widely discussed. The two main mechanisms have been determined based on a number of studies: mechanical and Ag ions influence, respectively. The most popular concept is the silver ion

interaction with the cell wall, the cell's internal elements and molecules [10]. The other mechanism is the mechanical cell wall interaction of Ag NPs [91, 26] which can also release silver ions [92], and many authors agree that the two main antimicrobial mechanisms can work together and cumulatively increase the antimicrobial effect [24, 26, 93].

It is widely agreed that silver ions do the damage for bacteria internal structures, but, at first, silver must be dissolved in water or water rich media [94]. Silver as a metal is zero-valent and has no antibacterial properties [10, 95]. Antimicrobial properties are developed when a silver metal atom is released from the elemental silver via oxidative dissolution [96] and becomes the positively charged silver ion. Only the Ag^{+1} state is stable for use as an antimicrobial agent, whereas other cations, i.e., Ag^{+2} and Ag^{+3} are highly reactive and short-lived [97] and are not suitable for the treatment of bacterial infections. It is known that the bacteria cell wall has the negative charge, and it can interact with the positively charged of Ag^{+} ions, and thereby silver ions can accumulate at a high affinity in the membrane [98].

It is well known that Ag ions in the plasmic membrane of bacteria can interact with the thiol groups [99] and bind with the cell surface the proteins containing Fe-S groups [100]. Ag ions can induce changes (yet NPs do not cause this effect) in the plasmic membrane or depolarize it [97, 98]. This destabilization process of the outer membrane can influence morphological changes in the cell [100], and, according to the authors of [101], bacteria after interactions with silver ions were affected, and irregular-shaped pits on the bacteria surface were observed.

The generation of free radicals by silver NPs may be another mechanism which can induce damage to the cell membrane and initiate the death of the cell [102]. These authors also discussed the reactive oxygen species (ROS) [24] which can directly influence the damage for the cell membranes due to Ag^{+} accumulation [102]. Among other things, it has been suggested that a silver ion can block the electron transport system, which leads to the cell death [103]. As a result, all of these above listed silver ion interactions are fatal for bacteria strains.

The bacterial cell wall acts as the Ag ion barrier preventing silver ion migration to the bacterial membrane, but silver ions can penetrate inside the bacteria cell by using the general bacteria poirins, and, as a result, they can block the activity of cytoplasmic proteins, stop ATP functions [104], DNA normal chain replication [102] and transcription processes [97, 105]. Silver can inhibit oxidative enzymes, such as yeast alcohol dehydrogenase, block the respiratory chain functions and lead to the cell's death [97, 106]. On top of that, the authors of [107] claim that Ag^{+} can rupture the bacteria cell wall when Ag ions merge to the negatively charged cell wall. Other research data presents that low silver ion concentrations can induce massive proton leakage through the bacteria cell membrane [106], and proton leakage usually has fatal consequences for the bacteria cell [106, 107].

There is one more silver antimicrobial action mechanism to be mentioned – photocatalytic mechanism – according to which, oxygen molecules from the cell and the hydrogen atoms of the thiol groups are affected by catalytic oxidation reactions [108], and the two thiol groups are covalently linked together by disulfide links (R-

S-S-R), hence, the cell respiration process is blocked, and bacteria loses the ability to survive [23, 24].

1.3.3 Antimicrobial mechanism of Ag NPs

It is known that nanoscale particles like carbon aggregates (not only Ag NPs) can cause permanent bacteria cell wall damage, thereby causing the release of the intracellular content out, thus leading to the cell's death [109]. There is consensus that NPs accumulation, by attaching on the surface, can initiate the 'pits formation' process and induce cell membrane damage [26], and this mechanism could explain antimicrobial activity against bacteria.

According to research data [99], the nanoparticle's size is decisive regarding the antibacterial silver properties. It is known that NPs of <10 nm in diameter can attach to the bacteria cell membrane, while larger NPs are not denoted by such a property. The attaching mechanism can be explained as follows: small nanoparticles have a larger surface area to volume ratio for surface interaction of the bacteria cell membrane [104], i.e., the attaching surface area and mass ratio plays the essential role.

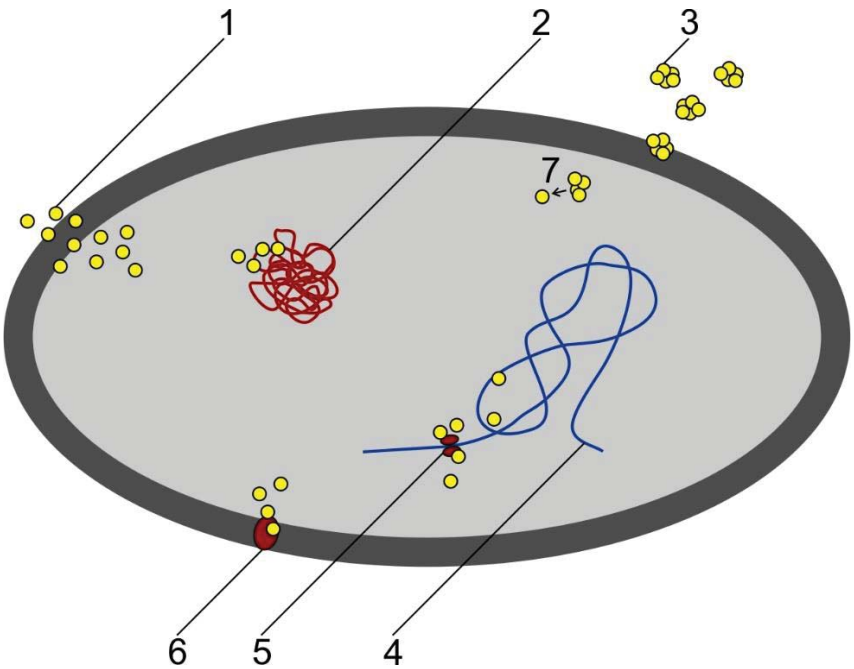

Fig. 2. Antimicrobial action mechanisms of silver ions and NPs [16]: silver ions (1) penetrate the bacterial cell wall or enter through the membrane channels (6) and bind to the DNA (2) molecule, silver ions impair the ability of ribosomes (5) to transcribe the messenger ribosomal RNA (4) and disturb the protein synthesis, silver NPs (3) can cause mechanical damage when entering through the membrane and can release silver ions (7) inside the cell

The mechanism of nanoparticle attraction to the bacteria cell wall may be the electrostatic force initiated by Ag NPs which increases the membrane permeability and results in the cell wall rupture and cytoplasm leakage out [110]. Other studies related with nanoparticle attraction determined that the shape of NPs can play a very important role, for example, study [101] noted that the lattice plane {111} silver NPs configuration had the strongest antimicrobial action compared with spherical and rod-shaped nanoparticles.

Another antimicrobial silver NPs activity *in-vivo*, called *Corona*, was presented; according to this mechanism, Ag NPs in the biological environment can change the surfaces of the adsorption biomolecules such as proteins and lipids which are located on the outer membrane; as a result, the changes of molecules can disturb bacteria cell metabolism and lead to fatal consequences [24].

Many researchers claim that silver NPs can directly interact with the cell walls [91, 92] attach to sulphydryl (sulfhydryl-SH [23, 24]), amino, imidazole, phosphate and carboxyl proteins, denaturate molecules, or inactivate enzymes in the cytoplasm [92]. Yet, in order to cause such effects, the NPs surface should be oxidized to release the Ag ion because NP by itself has no charge which is necessary for molecular connections [92, 102].

When reviewing all the mechanisms (Fig. 2), it can be assumed that silver nanoparticles can do only mechanical damage [99, 106, 109, 110] if the surface of NPs was not oxidized for Ag^+ release. Silver NPs can stick to the cell wall [99] and change the membrane structure [23, 24] or penetrate inside the bacteria [26]. Moreover, silver NPs surfaces in the water media can be oxidized, and silver ions are released inside the cell cytoplasm thereby causing chemical reactions with the respiratory chain [106] ATP, DNR molecules and result in their inactivation [102, 104].

1.3.4 Bacteria resistance mechanism for silver

Bacteria resistance is one of the main problems in the treatment of inflammation in hospitals [111]. Resistance to antimicrobial agents can occur due to the bacterial cell wall chemical composition changes [100]. Composition changes act as a barrier reducing the uptake of antimicrobial compounds from the environment to the cell [40, 106]. Resistance to biocides can also occur due to enzyme synthesis which may cause chemical degradation of the antimicrobial compound [106].

Extensive and uncontrolled usage of Ag containing antimicrobials may result in silver resistance development in bacteria [112]. Furthermore, several studies have shown that bacteria gain resistance against such antimicrobial agents as silver regarding the cell genes and proteins [113] or cell plasmid gens [114] changes. The resistance transfer process for silver to other bacteria cells generation can be carried out via the genetic material of plasmids [97, 112] – self-replicating extra chromosomal DNA. On the other hand, the resistance developing process is slow, and the resistance mechanism development inside the cell is complicated due to the wide range activity of silver ions: it interacts with the membrane [99], ATP and DNA molecules [102, 104], respiratory enzymes; as a result, resistance development

mechanisms are made very complicated [106]. Other studies show that silver resistance can be related with the membrane permeability or cell surface-associated changes [97]. It was determined that the uptake of silver was three to four times lower in the silver-resistant bacteria strain cases comparing with non-resistant strains [115]. The changes of genetic information taking place in silver-resistant bacteria are considered to be unstable, and it is difficult to transfer genetic information mutations for the further bacteria generations [97, 106, 115], and these properties make silver a highly useful antibiotic for extensive applications.

1.3.5 Toxicity of silver NPs and ions

Every antimicrobial agent including silver may involve side effects or can be toxic on the applied concentration. Silver toxicity is directly related to the Ag^{+} amount accumulated or absorbed in the body or in separate organs [116, 40]. Localized silver accumulation and skin-colorization usually appears on the skin areas where silver salts or silver ion rich solutions were applied [97]. The dark blue skin color can slowly disappear depending on the accumulated silver salts concentrations [117]. Large scale silver absorption can appear as silver toxicity or argyria, and, for example, in 1840, the term *argyria* was first mentioned by Fuchs [97, 118]. *Argyria* as a pathology term comes from the Latin word *argentum*. In general, argyria can be caused by overusage of silver ions or particles containing solutions and can result in the accumulation of metallic silver or insoluble silver salts, like silver sulfide, in the skin sub epithelial layer, conjunctiva, nails or gums [47]. Also, the accumulated silver can be found in capillary walls, blood forming elements like macrophages, tissue forming elements – fibroblasts, elastic fibers, eyes, and in nerves [47, 97]. The skin colorasitation effect is a part of the process when soluble silver salts due to reactions with sulphides and chlorides can form insoluble salts which tend to accumulate [97]. Silver accumulation leads to the formation of gray, brown or black granules in the skin tissue – the dermis and cornea layers [47]. These granules can increase the melanization process (when the skin becomes darker), and the accumulated silver granules can result in blue-gray tissue discoloration [97]. Argyria and argyrosis are permanent conditions without any effective therapy [47, 117]. Moreover, such skin reactions as contact dermatitis which is caused by silver are rare for humans, and most cases of silver sensitivity were reported for silver miners and jewelers [117].

Many nanomaterials used in medicine can be potentially harmful, and silver NPs is not an exception [69, 119]. It should be noted that cytotoxicity is one of the main problems of using nanotechnology in such medical devices as bandages [59], and NPs adhesion to the dressing's or bandage's background can prevent the NP migration and toxicity effect for body cells [120]. In another case, silver nanoparticles could activate the complement cascade when entering into the blood systemic circulation, which may lead to wound tissues hypersensitivity reactions and anaphylaxis [121, 122] and may consequently result in a strong allergic reaction. Also, the toxicity of silver NPs may develop due to the ionization of Ag NPs inside the cells; as a result, this process activates ion channels and influences the cell membrane permeability [105]. Membrane permeability can disturb the balance of

potassium and sodium microelements, and, as a result, the apoptosis pathway, involving mitochondria, is induced [79, 97, 123]. On the other hand, there are other possible toxic silver effects for cells, for example, the authors of [124] after obtaining *in-vitro* results, confirmed that keratinocytes and fibroblasts could be damaged by silver sulfide (partly silver selenide) which could be accumulated into the tissues [47], or, according to [11], can induce brain damage, as it was determined with glial cell astrocytes in brain, and these cells were more sensitive to AgNP than neurons after large doses of silver applications.

Silver can be poisonous when too much silver containing water or water based products are consumed, and it is known that silver absorption through the gastrointestinal tract is around 10%, and only 2–4% of the consumed silver can be retained in organs and tissues [117]. On the other hand, it is known that silver does not accumulate in aquatic animals, like other heavy metals (cadmium, lead, mercury) tend to accumulate [97]. It can be assumed that silver toxicity can manifest itself due to the consumption of silver polluted water when the content of silver ions in water and other products can vary depending on the living area, but it is not recommended to intake more than 0.005 mg/kg (of body weight) of silver per day according to the *US Environmental Protection Agency* [97]. On the other hand, it is known that less than 0.5 g in the general population, and, in extreme cases, 100 g of silver can be accumulated in the human body per lifetime [47]. It is being widely discussed, and it is still unclear what could cause silver cytotoxicity: nanoparticles which can migrate and get inserted in the body cells, released silver ions from NPs, or simply Ag ions [125]. Nanosized Ag particles and silver ions can contribute to the toxic effects which are highly toxic to bacteria but are less toxic to human cells because human cells have a nucleus unlike prokaryotic cells [126, 127]. Otherwise, silver can locally accumulate in body fluids and tissues, and also can spread systemically through the body and accumulate in various organs or initiate diseases [95]. AgNPs may affect such organs as lungs, liver, spleen, kidney, and the central nervous system (CNS) [104], and only extreme Ag doses may lead to death [128]. Other studies [119] showed that AgNPs can initiate fragmentation and degeneration processes of mature neurons and inhibit the processes of neuronal branches germination and neurites elongation [128, 129]. Silver can change the gene expression, which can lead to permanent body cell damage, and, as a result, the damaged gens can lead to mutations of various body cells which can be transmitted for further generations [106, 113]. Some studies show that AgNPs of 50 mg/ml in concentration had minimal cytotoxicity for mouse embryo fibroblast cells [111], and 80-nm particles of 12.5 μg/ml concentration had no toxicity [130] effect at all. Larger silver particles are less toxic than small NPs, and it is associated with the smaller silver ions release rate from particles [125]. Yet one of the factors concerning silver is clearly understood – silver ions in very high concentrations can be toxic [59] as well as most chemical elements.

1.4 Diamond like carbon

Diamond like carbon (DLC) material is the amorphous carbon metastable form consisting of sp^2 bonded carbon clusters embedded into the sp^3 bonded carbon

matrix [131]. DLC contains hard carbon solids without hydrogen which possess the hybridized carbon in the nanocrystalline network where atoms are cross-linked in sp^2 and sp^3 configurations [132]. It is known that diamond and graphite are carbon crystalline allotropes, and, in diamond, each carbon atom is covalently bonded to four other atoms and forms (sp^3) hybridization [133]. The crystalline diamond structure has directional complete sp^3 bonding, and these sp^3 bondings can form the extremely strong carbon network developing extraordinary properties like the highest known hardness, unmatched thermal conductivity, chemical inertness, etc. [134]. Otherwise, inside graphite, strong trigonal bonds (sp^2) exist where carbon atoms form the layer by layer structure in the basal plane [135, 136]. Between these layers, a fourth electron, forms a weak van der Waals bond which gives graphite lubricity, a lower density, and soft black material properties [133].

DLC thin film composites contain diamond, graphite and polymeric crystal structures [133]. Due to the unique structure, DLC thin films are atomically smooth amorphous structures and have no open corrosion paths to the substrate [132]. DLC composites have very high densities compared with other hydrocarbons and hydrocarbon polymers, which is caused by the crosslinked structure [133]. Diamond like carbon thin films have also been shown to possess excellent cell compatibility [132] properties which can arise from anions and cations incorporation into the DLC surface [137]. For these properties, DLC can be used for biomedical applications, like arterial stents, surgery needles, medical wires, biosensors, orthopedic applications [132], or for ophthalmic purposes regarding smooth and hard structures [116]. Moreover, due to the absence of resistance for bio fluids, DLC coatings can reduce the risk of bacteria biofilm formation on a coated surface [116, 137].

Research data shows that DLC can be applied for the manufacturing process of corrosion resistant parts for war machines, engines and weaponry [138, 139]. DLC coatings can enhance parts, which are under high mechanical and thermal stress, and where any failure can have lethal consequences [132, 139]. There are other areas of application for coated materials. The authors of [140] experimentally revealed that cotton coated with a DLC thin film can be applied for oil-spill cleanup after accidents in oceans when coated cotton can rapidly absorb petroleum in water, and such enhanced cellulose can be applied for the water cleaning of oil products [140, 141]. Other experiments conducted in [141] determined that DLC coated cotton fabrics exhibit inflammability resistance, and such DLC processed materials can be used as fire-resistant materials.

1.5 DLC manufacturing process

The unbalanced magnetron sputtering (UBMS) technology used for thin layer deposition was first discovered in 1852 and was developed by Window and Savvides [142] in the late 1980s [138]. The unbalanced magnetron became a very useful tool for the sputtering of thin films on various surfaces. Mainly, the UBMS technology can be used for hydrogen-free DLC or DLC doped thin films formation on surfaces [28]. The UBMS operational physical mechanism (Fig. 3) can be explained by atoms relocation, when atoms from the target material surface are ejected and placed on the sputtered surface to form a thin atom layer [143].

Moreover, the sputtering process requires a target or a cathode [28], made from a sputtered material, and pure carbon sources (gas) to manufacture pure DLC films [132]. For the DLC thin film coating formation, the sputtering process requires energy to create sp^2/sp^3 bonds between carbon atoms [133, 144]. The target or the cathode is bombarded by energetic ions generated in glow discharge plasma located in front of the target surface [145, 146]. During the bombardment process, target atoms are ripped off the surface, and, by controlling with a magnetic field, they can be condensed on the substrate's surface [138, 146].

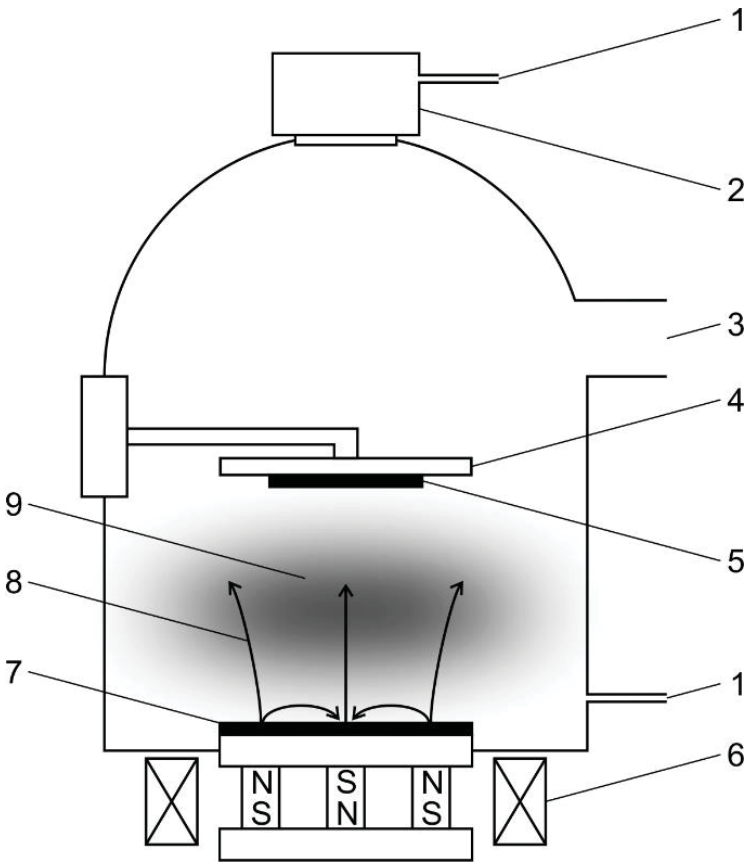

Fig. 3. Scheme of DC unbalanced magnetron: argon gas intake (1), ion beam source (2), gas pump (3), substrate holder (4), substrate (5), excitation coil (6), target (7), magnetic flux (8), plasma glow region (9); and the working principle: ions are generated in plasma and directed at a target, energized ions sputter the target's atoms, and atoms ejected from the target are transported to the substrate surface where atoms condense and form the thin film structure [128] on the substrate surface

The increased target ionization, during the sputtering process, positively influences the sputtering deposition speed rates and the efficiency of the sputtering

process [138]. When growing plain diamond films, sp^3 carbon bonding must be maintained in a dynamic non-equilibrium system with hydrogen, which promotes sp^3 bonding [133]. It is known that a narrow range of ion energies of 100 eV can create sp^3-hybridized C-C bonds between carbon atoms and form DLC layers on the substrate [132]. The increased ionization efficiency allows to maintain the discharge at lower operating pressures (typically, 10^{-3} mbar, compared to 10^{-2} mbar) and at lower operating voltages (typically, 0.5 kV, compared from 2 to 3 kV) [127]. It was determined that an additional magnetron field can extend the plasma ionized region close to the substrate and induce ion bombardment on the growing film, and this process modifies the coating's properties, for example, by releasing the film's internal stress [28, 142].

1.5.1 Doping of DLC thin films

DLC coatings can be mixed with other materials (or DLC doping [116]), such as silver (Ag), nitrogen (N), fluorine (F) and titanium (Ti). Ag-doping has a minor effect for carbon hybridization and the disordering of carbon atoms, but it affects the surface topography [29]. For example, DLC doping experiments with fluorine revealed that when the fluorine content increased, hydrogen incorporation was suppressed, and the optical band gap energy subsequently increased [147]. Moreover, metal dopants are usually responsible for residual stress decrease and the improvement of optical properties [29, 148].

It is known that silver plates or mechanically manufactured silver surfaces have a low mass to surface ratio, and silver nanoparticles could be the best option to increase this ratio and thereby reduce the amount of silver needed to achieve the best silver ion release rate into water and increase the antimicrobial impact [2, 18]. The magnetron sputtering technique is one of the solutions to manufacture thin DLC silver doped coatings without chemical contamination or background damage [149]. During the deposition process, silver particles can form clusters on the deposited surface, or close to the thin film surface [148]. Otherwise, doped metals can improve the desired optical, mechanical or antimicrobial properties, reduce residual stresses, and improve anticorrosion properties [132]. Sputtered graphitic and silver, or other metals, e.g., 5% titanium [133], clusters on the thin film surface improve the mechanical and anti-wear properties [134]. On the other hand, it was determined that the increasing silver concentration into DLC has strong correlation with the increase of graphite-like bonds in an amorphous carbon matrix [32]. The doping of coatings, for example, with silver, has some side effects, e.g., hardness decrease [133, 134]. Otherwise, doping increases the strength of hydrogen-free DLC films but decreases the strength of hydrogenated films [134, 32], and amorphous DLC films may contain up to 50% of hydrogen, which increases the elasticity properties of DLC thin films [133].

1.5.2 Reactive ion etching and thermal-processing of DLCs

DLC thin films can be etched by reactive ion etching for surface structure modifications when using oxygen plasma [150]. The radio frequency oxygen plasma etching method can be used to make such microstructures as micro-groove patterns

onto the DLC surface [151]. Such structures are widely used in sensors and electronics [150] or to remove the DLC layer from DLC:Ag coatings. When oxygen plasma etching processes are used for DLC material processing, oxygen plasma generates CO and CO_2 gases which are pumped out by the vacuum system [151, 152]. The chemical reaction with oxygen plasma can form a silver oxide layer on the DLC:Ag surface and decrease the speed of the etching process [116]. The etching speed decrease can be explained as the oxygen reaction with silver particles, and silver nanoparticles could protect carbon (above NPs) from the oxygen reaction with carbon [116, 29]. What concerns the oxidation of silver particles, DLC films with embedded silver nanoparticles can become more resistant to the oxygen plasma in the etching process [109]. The plasma etching process can remove the thin amorphous carbon layer due to the chemical oxidation processes [29, 109] when reactive oxygen particles break the sp^3/sp^2 bonds and crate new bonds with the carbon atom thereby forming CO and CO_2 gases [116], or they can change the properties of other materials [141].

Some authors claim that hydrogenated [153] or fluorinated [147] diamond like coatings can increase the endothelial cells (cells inside the arteria, vesicles, tube organs) biocompatibility to the implant surface [137].

Another important factor of plasma processing is related to the wettability of DLC-coated cotton fiber. The water static contact angle of the cotton tissue increased to 143±2° after oxygen plasma treatment, while untreated samples had 0° static contact angle, and it should be remarked that extended O_2 plasma treatment can (for 30 min. or longer) damage the cellulose fiber tissue [140] or related organic materials.

DLC:Ag films surface roughness can be increased, and thickness can be decreased by thermal air annealing [153], for example, within the temperature range from 140 to 400 °C**.** [154]. Thermal processing influences the reduction of the sp^3/sp^2 carbon bonds ratio to sp^2, and, as a result, the amount of graphite increases [131]. 400 °C temperature can destroy the DLC matrix, and embedded silver nanoparticles can transform from the spherical form to the prolated form due to the agglomeration process [154]. The treatment process of DLC:Ag films does not cause any chemical reactions, and after thermal processing silver nanoparticles cannot create chemical bonds with carbon; they can only be stabilized by other DLC layers in the thin film [29].

1.6 Disinfection of DLC coatings by applying UV radiation

Surfaces in our environment are covered with dust and bacteria strains, and most manufactured items including DLC:Ag thin film coated nylon fabric textile can be contaminated with bacteria. To kill all microorganisms on surfaces, one of the best methods is UV radiation. UV radiation is one of the most common types of radiation existing in nature, and it is in the range of the electromagnetic spectrum between X-rays (200nm) [155] and the visible light (400nm) [156]. The UV spectrum can be subdivided into short-wave UV (UVC) from 200 to 280nm of wavelengths, medium UV (UVB), from 280 to 320nm of wavelengths, and long-wave UV (UVA) with wavelengths from 320 to 400nm. [157]. The intensity of UV

radiation is expressed as the intensity flux or irradiance (Wm^{-2}), while the radiation dose is expressed as the intensity and time of exposure to a radiant surface (Jm^{-2}) [156, 157].

Short-wave ultraviolet light can strongly reduce the microbial organism population in the air or on hard surfaces, remove organic residues and 'clumps' of bacteria [158] or can eliminate pathogens from water [159].

Larger doses of UV radiation are harmful not only for bacteria but also for body cells [159, 160]. Researches proved that UV radiation has a mutagenic effect for cells because DNA bases can directly absorb incident UVB and UVA photons [161]. The harmful effect of UV radiation can be explained by a biochemical reaction in DNA nucleotide bases, new linkages between adjacent nucleotides in the same DNA molecule can be created and it block replication, which leads to cell death [162].

Extended exposure to UV radiation can damage synthetic organic materials [163], and adequate processing time has to be chosen for the disinfection of hospitals and laboratories solid surfaces from different materials are being processed [164]. UV disinfection has strong advantage comparing with chemical disinfectants. Chemical disinfectants can, for example, reduce the adhesion strength of the applied DLC thin film on textile, and can increase the sheer number of erosion zones on sputtered surfaces [164, 165].

1.7 Antimicrobial properties of DLC and DLC:Ag coating

Antimicrobial properties based on the interaction of silver ions with bacteria are well-known, but DLC antimicrobial properties can be determined not only due to the silver ion activity but also from the physical damage to the cells [166, 167]. These properties can arise from the chemical inertness, and, as a result, they can weaken the chemical interaction process inside the bacteria cell [166, 168]. In other studies, it was determined that hydrogen in C:H and H-free carbon thin film coatings can influence bacteria adhesion properties and their ability to survive [29, 168]. It can be claimed that hydrogen inside thin films can form C–H polar bonds which enhance the Lifshitz – van der Waals force between a bacteria and the polarized surface and induce cell wall damage [168].

The researchers of [167] determined that the silver particle's size plays a very important role in terms of the antimicrobial effectiveness of DLC:Ag thin films. The antimicrobial properties of silver nanoparticles are significantly stronger than those of silver microparticles [125], and silver nanoparticles with a large surface area-to-volume ratio are denoted by great antimicrobial properties and a lower toxicity for body cells [169]. The antimicrobial effect of DLC:Ag thin films could be prolonged by embedding or stabilizing silver NPs into the DLC matrix for higher mechanical resistance, and, as a result, the embedded nanoparticles can slowly release silver ions into the water media and can prolong the antibacterial effect time [15] [96].

Silver has a strong advantage against chemical antibiotics as silver ions can interact with multiple sites of bacteria and are denoted by broad-spectrum activity while chemical antibiotics act to the specific sites of a bacteria cell [170]. What regards the action mechanism of antibiotics, drugs of different chemical

compositions are needed to inactivate different bacteria species. Silver metal ions can act against a wide range of microorganisms, and the most valuable advantage of metal ions is that bacteria cannot gain resistance against metal ions alike that against chemical antibiotics [171]. Yet, on the other hand, not all DLC metal doped coatings are denoted by antimicrobial properties: for example, thin films with cobalt and silver possess bacteria inhibition properties, but DLC with other metal dopants, like indium or zinc, have zero or only minor bacteria inhibition properties [172].

1.8 Summary of the chapter

In this chapter, the main information about wounds, infections and treatment applying silver has been presented. Wound healing is a complex biological process where biochemical pathways and physiological processes control hemostasis after injuries, i.e., the contraction and clogging (with fibrin) of blood vessels [42, 46, 49]. Injury sites usually are not sterile, and bacteria in wounds cause inflammation [34, 35], and the immune system determines the outcome [36, 49, 33]. After the inflammation stage, new tissues and blood vessels proliferate, and, during the maturation stage, the scar formation process begins, i.e., the healing is completed [33, 41, 80].

In clinical cases, wounds infected with methicillin-resistant *Staphylococcus aureus* can become chronic, untreatable, or even mortal [60–62], and a strong antimicrobial agent like silver and its compounds could be applied for treating due to the low toxicity to organism cells and a wide range of antimicrobial activity [63, 91, 102, 106]. Bacteria do not develop resistance against silver due to several mechanisms of antimicrobial action which can be of the mechanical level when silver ions and NPs damage the cell wall and of the molecular level when silver ions block biochemical processes and interact with the synthesis of other biomolecules or with information transfer inside the bacteria cell [24, 93, 98, 102, 105]. Silver in the form of ions or NPs can be successfully applied in bandages [85–87] used in the clinical practice because silver can inactivate bacteria due to several action mechanisms [78, 79, 98]. Yet, on the other hand, silver must be stabilized in a solid or liquid matrix so that to prevent silver toxicity, and one of the most promising methods is silver doped DLC thin films which can sustain silver nanoparticles and release silver ions in water or in a moisture rich environment and sustain as strong antimicrobial properties as those achieved with other pharmaceuticals [31, 85, 87, 90] Silver NPs toxicity depends on the particle's size, the most toxic of those is 10 nm and smaller [104]. NPs toxicity can be reduced to the minimum by stabilizing NPs in the DLC matrix structure, where various sizes of particles can be embedded during the sputtering process by applying unbalanced magnetron and RF plasma etching [150–153] so that to improve its antimicrobial properties.

In the current research work, it is necessary to investigate the antimicrobial p roperties, the action speed and the effectiveness of DLC:Ag thin film coatings with different silver concentrations. In order to create the original bandage prototype (containing a DLC:Ag thin film on textile as a source of silver ions with a silicon structure, filled with gelatin/agar mixture aqueous mass as a silver ion accumulation

layer), silver ion accumulation, ion saturation, silver ion migration and experiments with wounds have to be performed.

2. EXPERIMENTAL TECHNIQUES AND METHODS

The chapter of experimental techniques and methods describes all the materials used in the experiments and lists the experimental details related with all the preparation stages of external usage pharmaceuticals, measurement experiments and the applied techniques.

2.1 Materials

In the current work, Benzylpenicillin (Benzylpenicillinum natricum 1.000.000 International Units (I.U.) in a glass bottle, *Penicillin G. Sandoz*) in microbiology experiments was used. Nylon 6,6 textile (twill weaved fabric, with a weft density of 110 cm^{-1} and a warp density of 100 cm^{-1}), the nylon fabric fiber diameter was 15 μm and the twisted thread was up to 100 μm.

Crystalline silicon wafer was being used in magnetron sputtering processes as the tray; also, sputtered thin films and bacteria biofilms on silicon wafer in SEM analysis were applied.

Mueller Hinton agar (*Thermo Scientific*, Leicestershire, UK) was used as the nutrition media, placed in 94 mm-diameter Petri dishes for bacteria cultivation experiments.

Ar gas in purity of 99.999%, C_2H_2 gas in purity of 99.999%, oxygen of 99.9% purity were used in DLC sputtering and etching processes.

Cellulose fibers (medium, *C6288 Sigma*, *Sigma Aldrich*, St. Louis, MO, USA), gelatin (*53028 FLUKA*, *Sigma Aldrich*) and agar (*A1296 SIGMA*, *Sigma Aldrich*), medical grade silicone elastomer *A-103* (www.factor2.com) contained the SIAL layer of the bandage, which was fixated by braided line *BERKLEY MICRO ICE* 0.006 mm. 96% ethyl alcohol (AB *Stumbras*) was used in the disinfection processes.

Silver nanoparticles (10 nm), 0.02 mg/mL in the aqueous buffer (*Sigma Aldrich*) were applied in experiments with live bacteria strains *in-vitro.*

2.2 Preparation of DLC:Ag thin film contained groups of samples by applying DC unbalanced magnetron sputtering

The sputtering process allows materials to be transferred (evaporated) from the solid state by bombarding their surfaces with energetic ions onto the object's surface. Sputtering starts from a target (the cathode) which is bombarded by high energy ions generated in discharge plasma [142]. Ion bombardment removes atoms from the target and condensates atoms on the surface of the substrate as a thin film layer. Secondary electrons emitted from the target surface play an important role in maintaining the plasma and also serve for increasing the sputtering speed and efficiency [138].

In the current work, coatings (DLC:Ag with various Ag content) on the textile background were deposited (sputtered) by DC-reactive unbalanced magnetron while using a pure silver target in the acetylene atmosphere. The Ag content in DLC

samples was controlled by varying the rates of the feed stock gas flow, the magnetron power and voltage. For the control of the deposition process, crystalline silicon wafer substrates were used in each sputtering process. The argon gas flow into the chamber was 70–80 sccm, acetylene gas: 7.8–21.1. The current in the magnetron was from 0.07 to 0.12 A, voltage from 553 to 741 V.

In the current work, DLC:Ag films were deposited on the nylon fabric surface, and the film thickness was 100 nm. SEM and EDS measurements were performed to identify the carbon and silver concentration ratio in the sputtered coatings on trays. For current experiments, 3 groups of samples on nylon fabric trays with silver concentration (at.%) in DLC: 1) 0.46% 2) 3.12%, 3) 5.31% were prepared

2.2.1 Improvement of DLC:Ag coatings by oxygen plasma

The radio frequency oxygen plasma etching method can be used to make microstructures like micro-groove patterns, to increase roughness and chemical composition of the DLC thin film surface [151]. In the current work, DLC:Ag groups of samples were dry etched by using a *Plasma-600-T* (*JSC Kvartz*) device. The groups of samples were placed inside the processing camera which was etched by radio frequency (RF; 13.56 MHz) oxygen plasma (99.9% purity) under 133 Pa pressure, and 0.3 W/cm² power for 5–30 s was applied.

2.3 Microbiological methods

In the current work, the bacteria (pathogenic and referential) taken from a bacteria bank were used. *S. aureus* (ATCC25923) referential bacteria for control measurements were used. Other pathogenic *S. aureus* bacteria strains were extracted from a pathology substance from infected animals. The *S. aureus* strain (LTSa603), and methicillin-resistant strain (LTSa635) were extracted from healed animals in Lithuanian University of Health Sciences, Dr. L. Kriaučeliūnas Small Animals Clinic. Two strains were isolated from sick humans (LTSaDA01 and LTSaM01).

2.3.1 Disk diffusion method on agar surface in Petri dish

The disk diffusion (Fig. 4) tests were used for testing the antimicrobial properties of silver NP contained samples. The current method is one of the oldest and most widely used antimicrobial testing methods for antimicrobial susceptibility. It is suitable for testing various bacterial pathogens [173]. Also, the disk diffusion method is widely used to detect methicillin resistance in *S. aureus* bacteria [174].

This method contains several steps: the preparation of nutrition media (various agar media like *Mueller Hinton* with additives are used) which should be poured hot in Petri dishes when bacteria cultivation on the agar surface can be performed. The application of samples on the agar surface is the final step before placing the Petri dishes into a thermostat for incubation (16–20 h). In the current experiments, the prepared agar media was poured into Petri dishes and stored until hardening. The bacteria cultivation process on the agar surface was performed in a laminar box. The bacteria culture must be pure and live, and, for better performance, all the bacteria strains taken from the bacteria bank were recultivated on nutrition media, and, after this procedure, the bacteria substance was prepared for the experiments. The

prepared inoculum was placed (by using a loop or a swab) on the agar surface, the testing material was placed (moistened and sticked) onto the agar surface with the maximum possible contact surface, and Petri dishes were placed upside down in a thermostat for 16–20 h. The steps of the procedure were no longer than 15 min. until placing the samples inside the thermostat, as indicated in EUCAST recommendations [175].

The evaluation process of the inhibition zones was performed after 16–20 h. If bacteria colonies could be observed as individual colony forming units (CFU), the inoculum was too light, and the experiments had to be repeated with a better inoculum, recommended 0.5 McFarland units, according to the Clinical and Laboratory Standards Institute [176].

The inhibition zones were measured from the sample's side to the nearest millimeter by using a ruler, or else the automated zone reader can be used [173]. Specific inhibition zone reading instructions can be found in the EUCAST disk diffusion test manual [175].

In the current work, several bacteria species (and several bacteria Mf concentrations) have been used. The bacterial suspension in the test tube was prepared for inoculation experiments. The swab was rinsed in a prepared bacteria suspension, and, in next step (moving swab on all the agar surface in the Petri dish), the bacteria suspension was transferred onto the agar surface. In 5 min, the samples were placed onto the agar surface. For better adhesion, a small amount of purified water was applied on nylon fabric samples to moisten them. Petri dishes with all the samples were incubated for 20 h at 35 °C in a thermostat.

The larger concentration (1 McFarland) was chosen due to the better CFU density on the agar surface, and for a more efficient evaluation process of the antimicrobial effects.

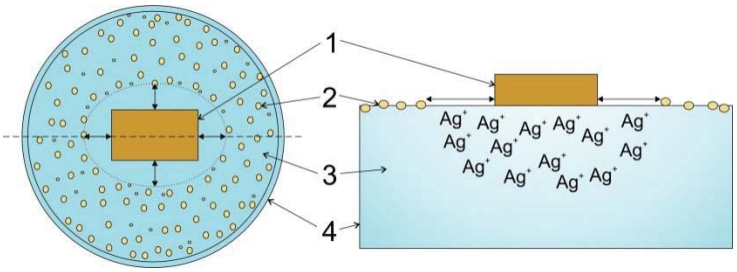

Fig. 4. Disc diffusion method and silver ions working mechanism: Petri dish fundus (4) was completely covered with agar media (3), and on the agar surface, DLC:Ag sample (1) was placed on the surface, bacteria colonies (2) demonstrated growth on silver ion free zones, silver ion saturated area was free from bacteria CFU, and inhibition zone appeared after 16–20 h.

The current experiments with all the groups of samples with different silver concentrations were repeated 4 times (on the first day and after the 1st, 2nd and 3rd weeks) within a one-month period. The experimental results were processed by

using computer programmes for calculations (*Microsoft Excel 2016*), graphic information processing was performed with *Corel* draw. For fitting the data results, *OriginPro* (*OriginLab*, Northampton, MA, USA) and the exponential law of Levenberg Marquardt with the text formula $y=y_0+A\cdot\exp(R_0\cdot x)$ was applied.

2.3.2 Serial dilution method

The method is used for dense culture reduction into a less and less dense culture so that to get a more usable concentration of CFU on a Petri dish. When applying this method, each dilution reduces the bacteria concentration 10-fold. For example (Fig. 5), from 10 ml of the primary bacterial culture, 1 ml is taken and poured into a second 9 ml volume test tube with a nutrition solution or sterile water [177]. After each dilution, the suspension of bacteria is diluted 10 times, and the experiments can be continued till the required bacteria concentration is achieved, and the bacteria CFU are detected on inoculated agar media.

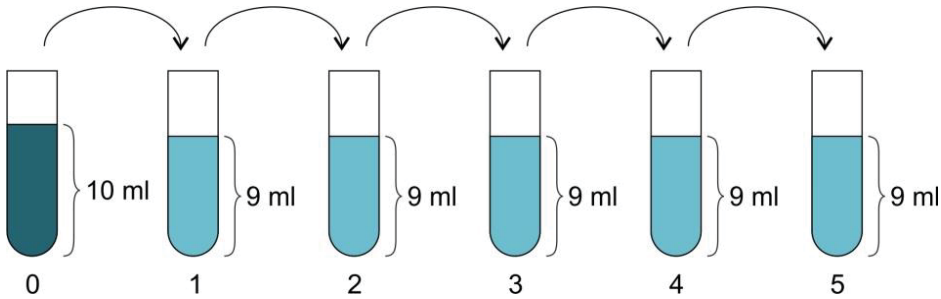

Fig. 5. Workflow of serial dilution method: one milliliter of bacteria suspension (undiluted) from test tube (0) is taken and placed into the first test tube (marked as 1), mixed, and the same (1 ml) volume of diluted (10^{-1}) bacteria suspension is transferred to the second test tube (2) where the dilution number becomes (10^{-2}); the dilution procedure can be repeated until live CFU can be found on agar surface in Petri dish after inoculation

In the current work, the serial dilution method was applied as shown in (Fig. 5). 6 tubes containing 9 ml of distilled water were diluted by using a pipette, 1 ml of bacteria suspension (0 test tube, Fig. 5) was poured into 9 ml of a saline solution and stirred. From the stirred solution, 1 ml of a diluted suspension was poured into the second tube with distilled water; hence, the second tube is diluted at 10^{-2}. The procedure can be continued until the value of 10^{-6} or more when live CFU can be found on the agar surface after inoculation on the agar surface.

2.3.3 Spread plate method

The spread plate is the method (Fig. 6) used to place bacteria on the agar surface in a Petri dish after the serial dilution method experiments. This method enables to calculate isolated bacteria colonies distributed on the agar surface. This method was applied for the isolation and identification of a variety of microbes and for the estimation of the CFU number. After the dilution experiments, 0.1 ml of the

bacteria suspension from the final test tube (the primary suspension was diluted at 10^3 to 10^5 depending on specific experiments) were inoculated on the agar surface, and Petri dishes were placed in the thermostat.

The Petri dishes were incubated in a thermostat for 16–20 h [178]. For faster growth, the sample can be incubated at 37 °C [175, 179]. After the incubation in a thermostat, bacteria colonies on the agar surface in Petri dishes were calculated. Each surviving bacteria gives a single colony forming unit (CFU) on the agar surface in a Petri dish.

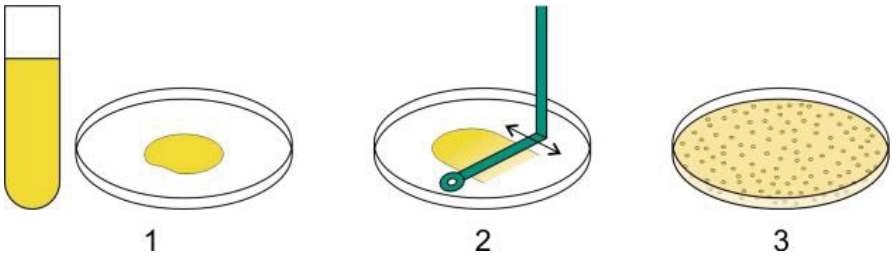

Fig. 6. Visualization of the spread plate method: a drop of bacteria suspension (1) on agar media is spread by using bent microbiological loop (2) through agar surface; after incubation period in the thermostat, the live bacteria CFU are calculated on agar (3) surface

After the calculation, the number of live bacteria in the researched sample can be calculated by using the formula: CFU/ml = (number of colonies x the dilution factor) / the volume of the culture plate [178]. The experiments were repeated 3–4 times for statistical reliability.

2.4 Detection of (CFU) number in suspension

A densitometer (measuring the optical density of semi-transparent or opaque materials) can also be used for bacteria cell concentration measurements, sensitivity to antibiotics determination, or for the estimation of quantitative concentration; it can also measure the light absorption of color solution at a specific wavelength. It is possible to measure the turbidity of a solution across a wider range (up to 15.0 McFarland units), but it is usually used to measure the turbidity in the range of 0.3–5.0 McFarland units, which is equal to (100×10^6 – 150×10^7 cells/ml) [180].

Table 1. Bacterial cells (CFU/ml) suspension density [181] according to McFarland turbidity standard

McFarland turbidity standard No.	**0.5**	**1**	**2**	**3**	**4**
1% barium chloride (ml)	0.05	0.1	0.2	0.3	0.4
1% sulphuric acid (ml)	9.95	9.9	9.8	9.7	9.6
Approx. cell density ($1x10^8$ CFU/ml)	1.5	3	6	9	12

McFarland Standards are used for the determination of an approximate bacteria number in a solution suspension. The measurements working principle is

the use of the McFarland densitometer where 600 nm of the wavelength of a light beam measures the optical density of an opaque bacteria solution. These measurements (data of the McFarland number) are compared with the McFarland turbidity standards (Table 1), and the bacteria CFU value of cells/ml can be subsequently calculated [182].

For microbiology experiments, a densitometer (*Grant bio DEN-1*) was applied for the current work measurements, and the solution for apparatus calibration was prepared by using McFarland turbidity standards by mixing various volumes of 1% of sulphuric acid and 1% of barium chloride (Table 1). The McFarland turbidity standard provides an optical density comparable to the density of a bacterial suspension [183].

2.5 S. aureus bacteria morphology changes after penicillin treatment

S. aureus (ATCC25923) penicillin sensitive bacteria were used for all measurements. Bacteria suspension of $2.1 \times 10^9 ml^{-1}$ of CFU in the saline solution (0.9%) was prepared for the current experiments. The CFU number was determined by the McFarland densitometer measurements, and the calculations were performed according to the McFarland turbidity standards, respectively (Table 1).

The antimicrobial agent for the current experiments was prepared by injecting 2 ml of 0.9% saline solution into a benzylpenicillin drug bottle and mixing well until the benzylpenicillin powder dissolved. The prepared antimicrobial agent solution contained 500,000 I.U. (International Units) per 1 ml of benzylpenicillin (BP), and it was used in all experiments.

During the experiments, after 1–3 minutes after BP application, a small drop of the solution from the test tube was taken out and placed on silicon wafer pieces for SEM analysis. Control samples and treated with BP bacteria samples were prepared for the SEM analysis by applying the fixed-by-heat method [184]. Dried at room temperature silicon wafer pieces were held for short time (several times for a few seconds, wafer bottom) above a flame and cooled down [184, 185]. After the fixing procedure, the samples were rinsed in distilled water so that to wash out the antibiotic residuals and sodium chloride crystals. The BP effect for the bacteria cell walls was observed by employing a *FEI Quanta 200 FEG* scanning electron microscope in the low vacuum mode.

2.6 Scanning electron microscopy (SEM) and energy dispersive X-ray spectroscopy

Scanning electron microscopy is a highly useful tool for the observation of objects and structures in the nanosize diameter [186]. For example, *S. aureus* bacteria is about 1 μm of diameter [187], and optical microscopes do not provide high-resolution pictures; hence, only SEM is the perfect tool for analyzing bacteria cells and cell wall changes [188]. The SEM working principle can be explained as follows: electrons in the tube from the field-emission cathode between the cathode and the anode are accelerated from 0.1 keV to 50 keV energy, and primary electrons in SEM are focused into the electron probe (a small-diameter beam) which is moving across the specimen (in two perpendicular (x and y) directions) for the

detection of surface unevenness, and this delivers the sample image after data processing has been completed [189]. The electron probe is controlled by electrostatic or magnetic fields which change the direction of the electron beam in two directions (raster scanning) [189, 190]. A modern SEM typically provides an image resolution between 1 and 10 nm [190], and the apparatus can be equipped with an energy-dispersive lithium drifted silicon detector for the detection of X-ray lines (which are specific for the element) in the resolution of ΔE≈100–200 eV [189] for energy dispersive X-ray spectroscopy.

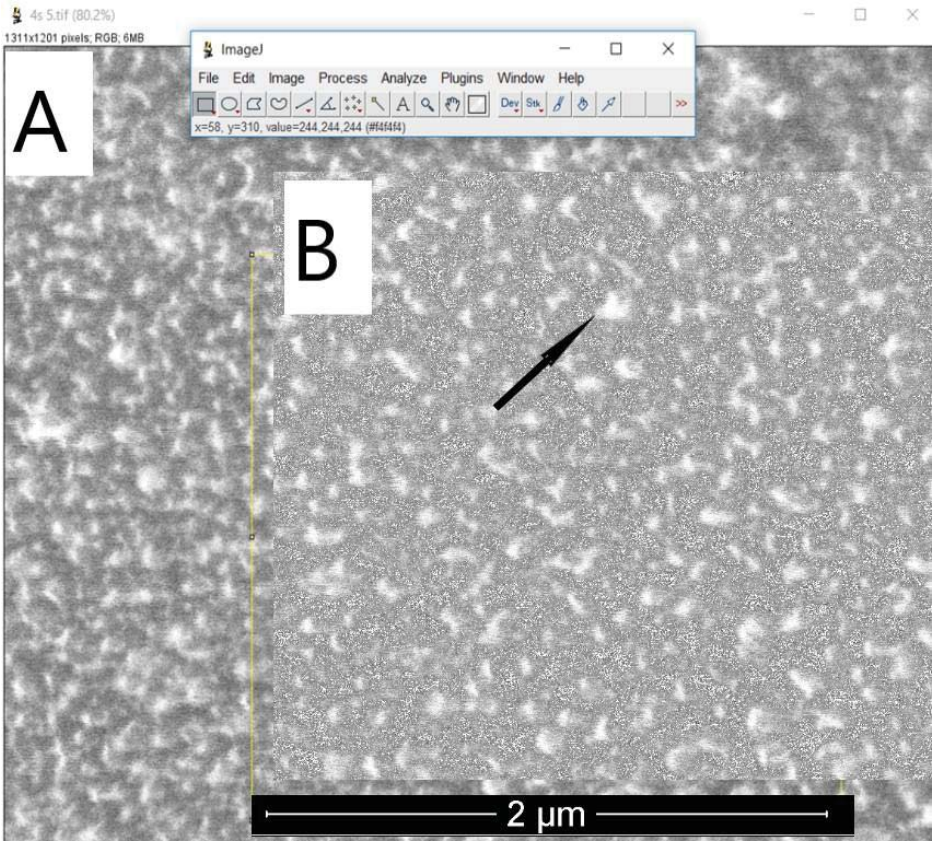

Fig 7. SEM photo analysis with *Image J*, original photo (A) and its version after filtration and processing with software (B), the arrow marks the silver nano cluster

In this work, a *SEM FEI Quanta 200 FEG* with an energy dispersive X-ray spectrometer (EDS) was used; the unit was manufactured by *Bruker Quantax*. EDS measurements for the silver content detection in the samples sputtered on nylon fabric and silicon wafer were performed at 5-keV of accelerating voltage so that to minimize Si K peak excitation. NPs size and distribution analysis in sputtered coating (by using SEM pictures) was done by using the *Image J* (NIH) open code

software and the custom *MATLAB* (*MathWorks*) code. *Image J* software was used for SEM picture analysis according to the instructions of [191], and silver nanoparticles (their size and distribution) were investigated, i.e., the software calculated the white spots in the picture which were identified as silver nanoparticles (Fig. 7).

2.7 Atomic absorption spectroscopy

The atomic absorption (AA) phenomenon first was observed in 1802 with the discovery of the Fraunhofer lines in the sun's spectrum [192]. In 1953, Australian physicist Sir Alan Walsh demonstrated that atomic absorption could be used as a quantitative analytical tool [192, 193]. Atomic absorption spectrometry is a universal analytical method for the determination of metallic elements in very low and major concentrations [194, 193].

The working principle of AAS can be explained as follows: a liquid sample is introduced into a flame (see Fig. 8. (3)) where the sample solution is dispersed into a spray which is desolvated into salt particles and subsequently vaporized into neutral atoms, ionic species and molecular species [194]. A light beam (see Fig. 8 (1)) passes through the flame (3) (where the analyte is vaporized into neutral atoms) into the monochromator (4). Every atom of the material has its own distinct wavelength patterns; atoms can absorb energy regarding the unique configuration of electrons in their outer shell [153]. The transmitted light radiation at the specified wavelength travels from the monochromator into the detector (5). The detector measures the beam light intensity which is reduced due to the absence of metal in the solution. The detector detects the reduction of light intensity and evaluates these changes as the light absorption by specific metal ions. Finally, the absorption results are shown (7), and the concentration of the analyzed solution can be detected [194].

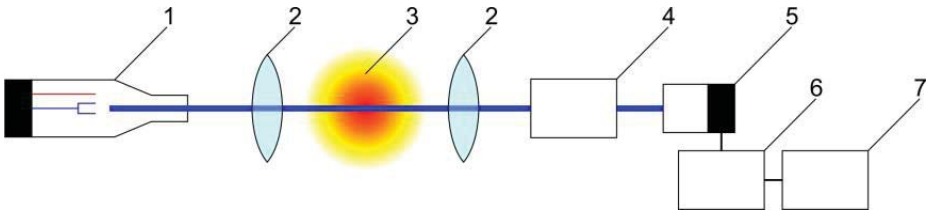

Fig. 8. Atomic absorption spectroscopy scheme: (1) hollow cathode lamp, (2) lens, (3) atomized sample, (4) monochromator, (5) detector, (6) amplifier, (7) readout device, material atoms (in transit of light) can absorb some light from the light beam, and the absorbance of the light energy directly depends on the concentration of metal ions in analyte

An atomic absorption spectrometer (*Perkin Elmer Model 403*) was used to detect the silver ion concentration in distilled water. The distilled water for the measurement experiments was prepared after the rinsing procedures. Nylon fabric DLC:Ag coated samples were rinsed in distilled water for various time intervals (from 20 min to 48 h.) in different test tubes. After the procedure, water was filtrated

and prepared for AAS measurements. AAS spectroscopy was applied with the aim to determine ion migration from the coatings to purified water.

2.8 Tests with laboratory animals

Animal testing experiments were performed according to the State Food and Veterinary Service permission (2015-05-15 Nr. G2-30). Laboratory animals (guinea pigs) were placed in special cages (2 in one cage) with full food (dry special food for lab animals) and water accessibility, also, special small shelters to hide were installed in cages as well. The cages were stored in a lab with daylight accessibility (not in direct sunlight).

The fur on the dorsal area was shaved, and the skin was disinfected with 70% ethyl alcohol. Then, the skin epidermis (not all the skin) layer was cut by using the tip of a scalpel. The bandage samples were sticked to the skin by using medical duct tape. For better fixation, the special waistcoat for animals was used to prevent the removal of the testing material. Every 3 hours, the condition and behavior of the lab animals was observed after the bandage application (except for night), and the treatment effect (wound observation) was evaluated after 24 h. The same bandage was used for 4 days, until the wound contracted.

For the infected wound experiments, the wounds were infected by using the pathogenic bacteria of *S. aureus*. The drop of bacteria suspension was applied in the wound, and, after that, bandages were applied for healing.

During the wound healing evaluation experiments, microbiological samples from the healing wound tissues (by using a swab) were taken every day to investigate the bacterial CFU number inside. All the guinea pigs survived and were left in the vivarium after the experiments.

3. EXPERIMENTAL RESULTS AND DISCUSSION

The chapter of experimental results and discussion describes the results of all the experiments with the stages of preparation of external usage pharmaceuticals, tests with bacteria, measurement experiments and early stage experimental data with the animal model.

3.1 Preparation of DLC:Ag coated groups of samples on nylon fabric

3 groups of samples (GoS) of DLC:Ag coatings with different silver concentrations from 0.46 to 5.31 at. % (Table 2) were manufactured by using DC unbalanced magnetron sputtering on nylon fabric.

Table 2. Chemical composition of groups of samples (GoS) after EDS analysis

GoS No	Carbon (at. %)	Silver (at. %)
1	99.54	0.46
2	96.88	3.12
3	94.69	5.31

It was determined that the sputtering parameters (Table 2) performed an important role in the thin film formation process [138] and that the DLC:Ag properties in the sputtering process can be controlled by changing acetylene, argon gas flux ratio and the sputtering time, respectively [195]. During the magnetron sputtering experiments, the first group of samples (containing 0.46 at. % of Ag) was prepared according to the following parameters: the sputtering duration was 520 s; the argon gas flow was 70 standard cubic centimeters per minute (sccm) sccm, acetylene gas 21.1 sccm flow, respectively (see Table 3). The second group of samples contained 3.12 at. % of Ag in the DLC matrix which was prepared by applying the same parameters of gases, but the sputtering time was decreased from 520 s to 235 s, and the magnetron voltage and the current were increased. The increased magnetron current and voltage parameters also influenced the larger deposition content of silver, as determined in [96, 196, 197].

Table 3. Parameters of DC unbalanced magnetron sputtering process

Sample No.	Sputtering duration (s)	Ar gas flow (sccm)	C_2H_2 gas flow (sccm)	Magnetron voltage (V)	Magnetron current (A)
1	520	70	21.1	553–625	0.07–0.12
2	235	70	21.1	568–741	0.07–0.22
3	200	80	7.8	625–656	0.10–0.11

The group of samples containing the largest silver 5.31 at. % concentration was prepared by applying the shortest sputtering time (200 s) and by increasing the Ar gas flow to 80 sccm and decreasing to 7.8 sccm acetylene gas flow into the

magnetron chamber. It is known that a small gas ratio increase can determine the changes of structural properties of DLC coatings [198] and can strongly influence the silver concentration changes in the deposited thin films [195]. The required effect was obtained in the sputtering process when manufacturing the group of samples with 5.31 at. % of Ag where minimal changes of the Ar gas flow and acetylene gas flow decrease increased the silver deposition into DLC coatings, as it also was determined in experiments by other authors [148, 195, 197]. Otherwise, the magnetron sputtering experiments when preparing GoS with 3.12 and 5.31 at. % of Ag showed that the sputtering time duration defines the thin film deposition into the DLC matrix when the gas ratio is the same, but the sputtering time and the magnetron voltage/current parameters are different. Experiments of other authors [198, 199] also confirmed that minor changes of the time parameters changed the chemical structure of DLC:Ag coatings. Our experiments showed that not only the gas ratio changes can determine the silver content in coatings, but also other physical parameters play an important role in the thin film deposition process [195, 200].

3.1.1 EDS chemical analysis of RF plasma etched samples

Unetched GoS exhibited minor or no antimicrobial properties at all. For the improvement of the silver ion release properties, i.e., the antimicrobial activity, RF plasma etching was applied. When analyzing O_2 plasma etched coatings from EDS measurements, data can be obtained that after 5 and 20 seconds of etching, the concentration of carbon decreases and silver increases, respectively (see Fig. 9). After 20 seconds of plasma etching, the silver concentration ratio in all the three groups of samples was 0.9, 3.4 and 6.9 at. % (rounded), respectively. The changes of chemical elements are presented in Fig. 8. From the plasma etching results and the chemical elements concentration ratio changes, it can be determined that the first group of samples had major concentration ratio changes when comparing with the other groups of samples. These major concentration changes, according to sources [109, 201], occurred due to the large chemically active surface area and the chemical reaction between oxygen and carbon during the oxygen plasma processing experiments. In the plasma etching process, the carbon structures were more reactive than the silver clusters, and oxygen destroyed the graphite rings to create more C-O bonds on the DLC surface [109]. During this process, not all of the carbon atoms were ripped out from the DLC matrix as CO and CO_2 gases (as determined in [109, 201] some carbon atoms created C-O bonds in coating surface. On the other hand, the measurements of all the groups of samples were done after one-year exposure in the atmosphere, and the surface adsorption processes could interfere with the reliability of measurements, i.e., oxygen concentration changes of sputtered thin films on nylon fabrics were possible. Groups 2 and 3 of the samples had less oxygen in DLC:Ag thin films due to the lower carbon concentration on the surface [2, 46] where silver clusters after the magnetron sputtering process covered a larger surface area, and, according to sources [140, 202], prevented DLC from e chemical reactions with oxygen. Silver is less reactive than carbon, and silver nanoclusters in

DLC coatings worked as a shield for carbon structures [2, 46] and consequently reduced the corrosive effect of oxygen plasma.

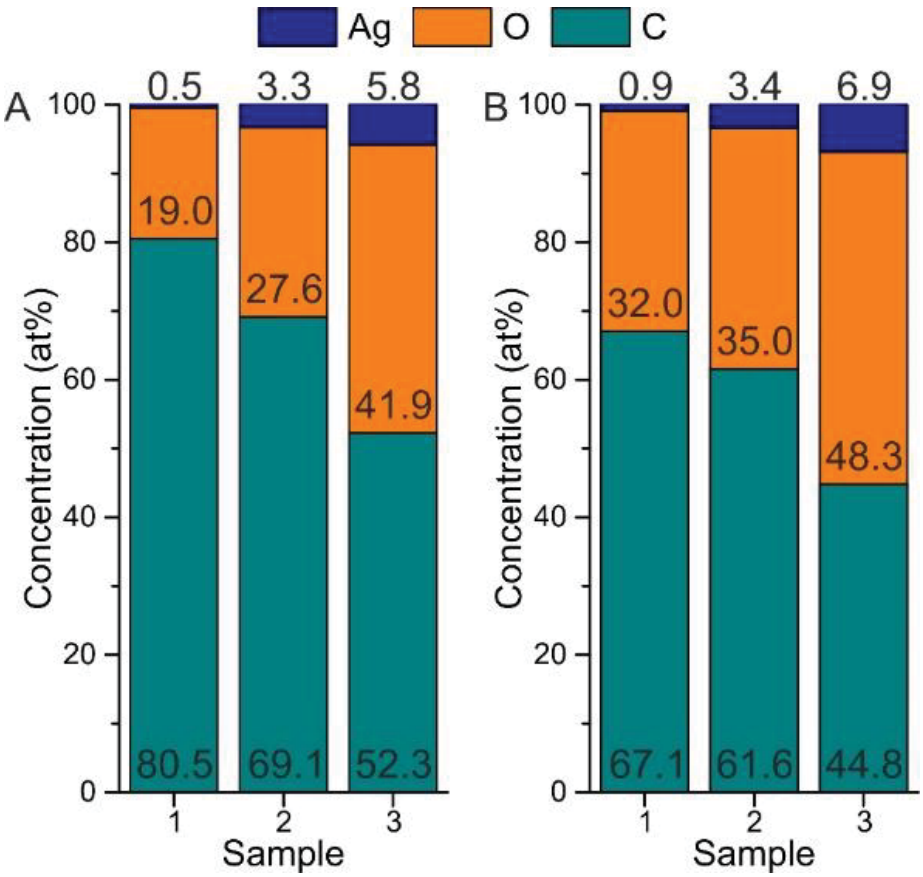

Fig. 9. Chemical composition of DLC:Ag thin films on nylon fabric: after 5 s (A) and after 20 s (B)

On the other hand, the highest reduction of carbon concentration in thin films had the positive effect for the silver concentration ratio changes in the first GoS, whereas the opposite effect was obtained in the third GoS.

RF oxygen plasma etching reduced carbon and increased the silver and oxygen concentration in all of the three groups of samples, and the ratio of chemical elements correlated well with the metallic silver content in the DLC matrix. The plasma etching effect can be explained according to [145, 146, 203, 204] as the removal of the thin amorphous DLC carbon layer from the surface.

3.1.2 SEM analysis of prepared samples with DLC:Ag coatings

The groups of samples after the sputtering process were investigated by applying SEM microscopy with EDS spectroscopy for visual and silver

concentration evaluation. One of the most challenging aspects in the DLC:Ag deposition process was to disperse nanoparticles homogeneously inside the DLC matrix [109] on the nylon fabric fibers.

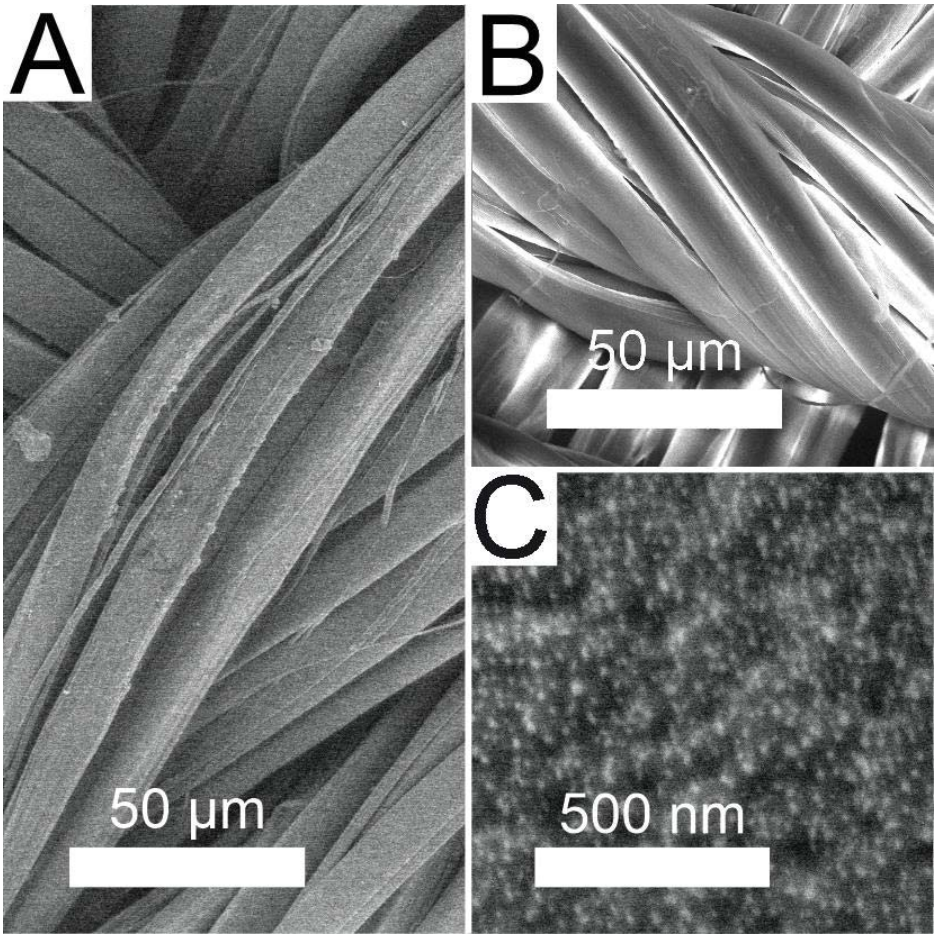

Fig. 10. Nylon fabric fibers in SEM image: sputtered fibers (A), unprocessed nylon fibers – (B), and thin DLC:Ag film on silk fiber (C)

Nylon fabric thin film coatings were investigated by applying SEM microscopy for morphological analysis after the DLC:Ag deposition process and after the treatment of oxygen plasma. Uncoated (with DLC:Ag thin film) nylon fabric had fibers with a smooth surface (Fig. 10 (B)) DLC:Ag thin film was sputtered on the fabric's surface (Fig. 10, A) as a thin (up to 100 nm) layer film, which was a typical DLC:Ag thin film, as presented in (Fig. 10, C).

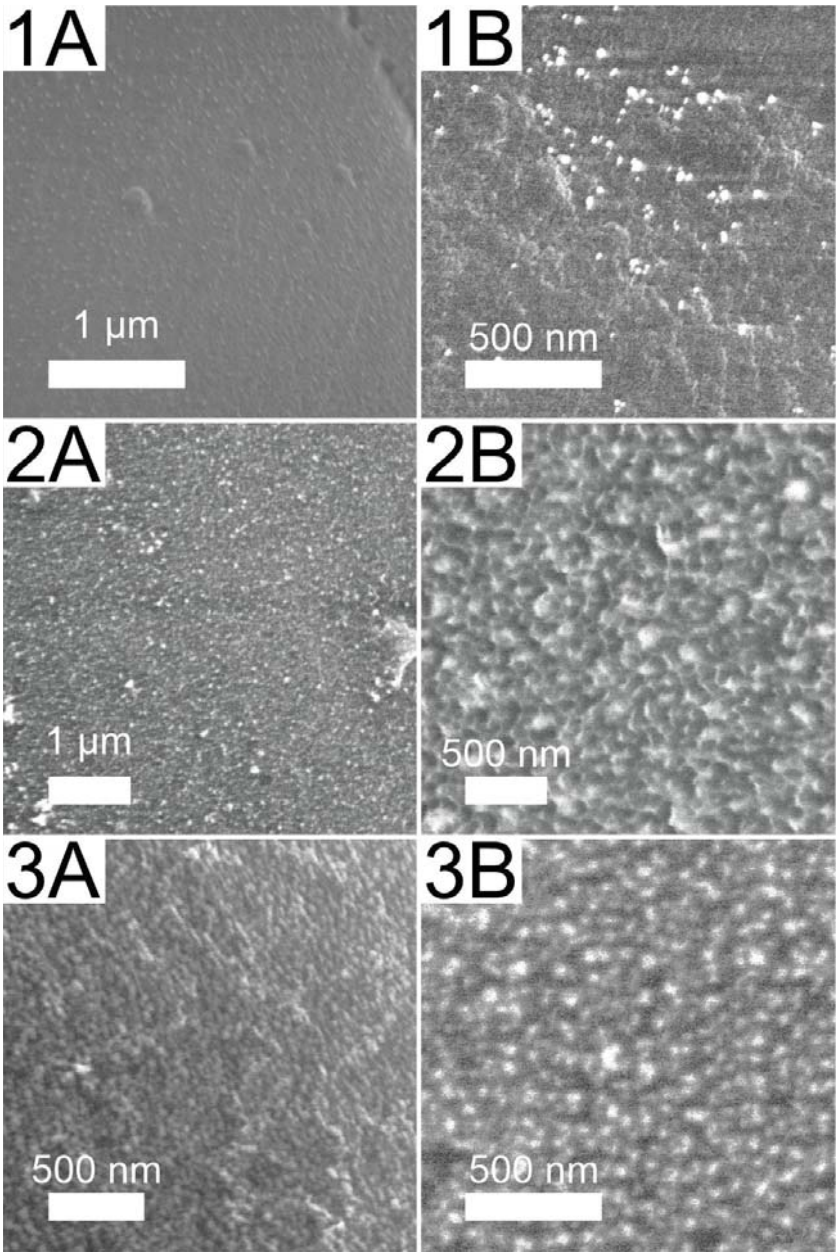

Fig. 11. SEM analysis of groups of samples: before (A) and after (B) 20 (s) of etching: first group of samples (1A and 1B), second group of samples (2A and 2B), third group of samples (3A and 3 B)

SEM photos showed that nylon fabric fibers were not damaged during the magnetron sputtering process, and it was determined that fibers were successfully coated with DLC:Ag thin film, and the surfaces of the prepared coatings had

different visual surface morphology (see Fig. 11), i.e., these morphological differences correlated with the silver concentrations in GoS.

The DLC:Ag thin film was smooth in the first group of samples where the silver concentration was 0.5 at.% (Fig. 11, 1A) and visually rough in the second and third groups of samples (Fig. 11, 2A and 3A).

Such DLC:Ag coatings, according to [203], have features which are characteristic for DLC:Ag. The authors of [205] discovered that silver doped DLC coatings exhibit a decrease of the characteristic C-H stretching region due to the increase of the silver concentration in the thin films, and carbon atoms in films are bonded in the sp^3 configuration. In the thin films of DLC, the C-H bonds play an important role in the sputtering process when a DLC:Ag thin film is growing on the tray substance like on a nylon fabric [79, 206].

Based on the research data, good adhesion between the nylon fabric and DLC coatings was observed. After etching and long storage periods (3–12 months), DLC thin films were strongly adhered onto the nylon fabric, and no clean or decayed areas were found. It was determined that DLC hardness and the internal stress decrease [116] when the sp^2/sp^3 ratio in the deposited coatings increases [170]. According to the author of [148], DLC:Ag coatings with a silver concentration of 3.6 at. % exhibited residual stress reduction without substantial hardness degradation. Groups of samples contained 3.12 at. % and 5.31 at. % after a one-year period were investigated, and no structural changes were found. Moreover, it was determined by the authors of [195] that metal doping of DLC coatings, when the doping materials are used in low percentage values, can improve the carbon structure and provide the important friction and wear properties.

Otherwise, it was determined that increasing the silver concentration by more than 11 at. % correlates with the decrease of hardness and residual stress [148] and the reduction of the total surface free energy [29]. Based on other authors' [29, 148] researches, the silver concentration has to be less than 11 at. % so that to ensure the optimal properties of DLC silver doped thin films. In the current research, the silver concentration did not reach more than 6.9 at. % in the DLC matrix after 20 s of etching (see Fig. 8), and the coated silk samples were stable after several treatments with oxygen plasma within one-year period.

After the data analysis, it was determined that the DLC carbon matrix was deposited uniformly on the filaments, and that silver NPs after the magnetron sputtering process were embedded into the DLC matrix as it was determined in works [79, 207], and that nanoparticles were homogeneously located all over the surface (see Fig. 11 and Fig. 13). To compare the research data, analysis of DLC:Ag coatings deposited on silicon wafer and on a nylon fabric tissue was performed. SEM analysis revealed that DLC:Ag coatings can be successfully sputtered on both silicon wafer and nylon fabric .

From the results of the current experiments, it follows that plasma etching changed the chemical and morphological structure of the deposited thin films, as it was found in [151, 198, 205]. Amorphous carbon reduction appeared due to the oxygen plasma chemical reactions which induced morphology changes – small pits were etched on NP-free areas (Fig. 11, 2B). It was found out that DLC:Ag thin film

structure changes were obtained only after RF plasma etching procedures when the groups of samples without oxygen plasma etching had a smoother surface (Fig. 11, 1A–3A). It was found out that the etching process revealed silver nanoclusters in all groups of samples (1–3). A longer exposure time in oxygen plasma had a strong effect for the surface of the deposited films, for example, after 20 s of etching, the thin film surface was rough, and nanoparticles were revealed on top of the DLC matrix, as similarly obtained in [29, 45].

Surface processing with O_2 plasma can cause chemical reactions with carbon materials like DLC [109], where plasma destructs graphite rings and can etch away non-diamond carbon [208]. The oxidation process can increase the number of single carbon chains, and it was determined that aliphatic carbon atoms can be the predominant carbon form in the plasma processed coatings [141, 204]. From the experiments conducted in the current work, it was determined that plasma treatment made the surface rougher [109, 146], and, according to [109, 209], the DLC surface was more desorbed and superhydrophilic after the treatment. As a result, the DLC:Ag thin film superhydrophilic surface improved silver ion diffusion [148, 210] from the deposited surface to the wet agar media regarding good water contact with NPs.

3.1.2.1 Silver nanoparticles in DLC:Ag thin film matrix

The DC reactive magnetron sputtering technology can be used for the production of silver nanoclusters or nanoparticles embedded into the DLC matrix during the sputtering process [15, 211]. By applying the *Image J* software for the analysis of SEM photos [191] of 20 s etched of all groups of samples, the sizes of silver nanoparticles and their distribution on the coating's surface were investigated. The results are presented in (Fig. 12). In the current work, it was determined that the average nanoparticle size in 1–3 GoS was from 16.1 nm to 28.8 nm, and the particles were distributed uniformly onto the DLC:Ag surface. The size of silver nanoparticles varied in range from 3 to 63 nm. At the low silver concentration of GoS, the low dimension silver nanoparticles prevailed, whereas in the larger concentration, the larger diameter was predominant.

After the analysis of SEM photos, it was determined that nanoparticles in the DLC matrix were embedded during the sputtering process, and the particle sizes and their distribution are presented as follows:

In the first group of samples, the silver concentration after 20 s of plasma etching was 0.9 at. %, dominated with nanoparticles in diameters of 9–12 nm (15.9%), 6–9 nm (14.4%) and 12–15 nm (12.8%), and the average size of the particles was 16.1 nm (±5.8 nm).

In the second group of samples (3.4 at. % of silver), silver nanoparticles in diameters of 12–15 nm contained 16.8%, and 15–18 nm made up 14.1%. Nanoparticles in sizes of 18–21 nm and 33–36 nm were distributed at 13% and 13.2% respectively. The average size of all particles was 23.7 nm (±9.6 nm).

In the third group of samples with 6.9 at. % Ag, the nanoparticles in the diameter of 27–30 nm dominated in the coating structure and constituted the 18.2% share, another group of larger particles of 42–45 nm made up 12.9%, whereas

smaller particles of 6–9 nm and 12–15 nm of size constituted 10.4% and 10.3%, respectively. The average particle size was 28.8 nm (±12.6 nm). After the analysis of SEM pictures, strong NPs size and silver concentration correlations were determined for DLC:Ag films. The collected data showed that the group of samples with the lowest silver concentration had the smallest nanoparticles (dominated by 9–12 nm and 6–9 nm sizes), and the average particle size was 16.1 nm. The GoS with the highest concentration of silver showed the opposite correlation – it was dominated by nanoparticles in the range of 27–30 nm, and the average NPs size was 28.8 nm (see Fig. 12). From the experimental data, it follows that the increased silver content in the DLC matrix defined the formation of a larger cluster diameter during the sputtering process [127, 201] and led to the increase of DLC:Ag film roughness. The results of the first GoS showed that the raw (untreated plasma) samples had a smooth surface, and silver nanoparticles were hardly visible on the analyzed surface (Fig. 11, 1A). After RF oxygen plasma etching, the surface roughness increased, and, consequently, nanoparticles became more visible comparing with the non-etched GoS (Fig. 11, 1B), but, on the other hand, plasma etching can change the size of the primary sputtered silver nanoclusters or their shape, or induce fall-outs of particles and the carbon matrix reduction [136] as it was determined in the current GoS analysis. From the researches of the author of [205], it follows that thin films with less than 5 at. % of silver clusters had minimal structural changes after various durations of etching [29, 195]. In the current research, nylon fabric coated GoS (2 and 3) after etching had no significant surface structure changes, but NPs fall-out and drop out from DLC areas was observed more frequently when comparing with GoS etched for less than 20 s (see Fig. 13).

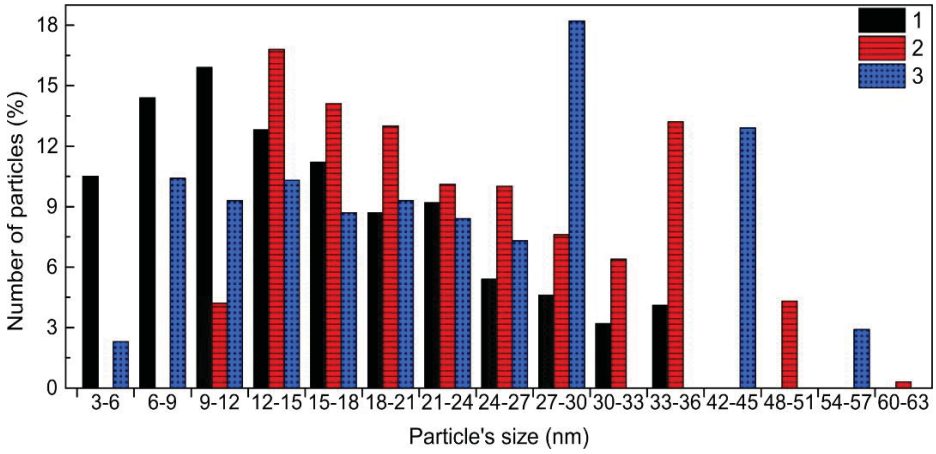

Fig. 12. Silver nanoparticle size and distribution in DLC coatings: NPs in groups of samples (1–3) are presented in 3–63 nm range

Oxygen plasma contains high energy reactive oxygen particles [140, 151, 152] which can form the oxide layer on silver nanoparticles embedded in the DLC matrix [109, 168]. Silver nanoparticles with the bonded oxygen layer on the surface reduce

the energy barrier to break Ag-Ag bonds [205] and increase the rate of the Ostwald ripening process [205, 212]. In the coatings of a higher silver concentration, the bleaching of the silver nanoparticle system [213] could be obtained, but, in the current work, no changes of NPs size were observed after 20–30 seconds of the etching process, and small silver clusters did not form larger clusters.

The author of [148] noted that DLC samples with Ag of 3.55 at. % featured the granular structure with similar particle sizes, and, when larger concentration films were prepared, large-size islands were obtained. The granular type structures were obtained in GoS (2–3), but the structures were distributed in various regions of the sputtered samples, i.e., not uniformly. On the other hand, the samples etched for 20 –30 seconds did not show clustering [150], but the etched DLC surface with a partially removed layer of amorphous carbon revealed silver NP on the thin film surface as shown in [150, 170, 197]. Yet, the etching of GoS for more than 25 s removed the DLC matrix which worked as a stabilizing agent for silver nanoparticles, and thus more fall out areas were detected (Fig. 13). This effect could be attributed to the ion beam irradiation-induced 'ripening process' of nanoparticles [205, 212], and it was observed in the case of the etching of DLC:Ag nanocomposites. Other authors revealed in their research data that longer etching can cause very low NP oxidation, and these nanoparticles can fall out from the DLC matrix [168].

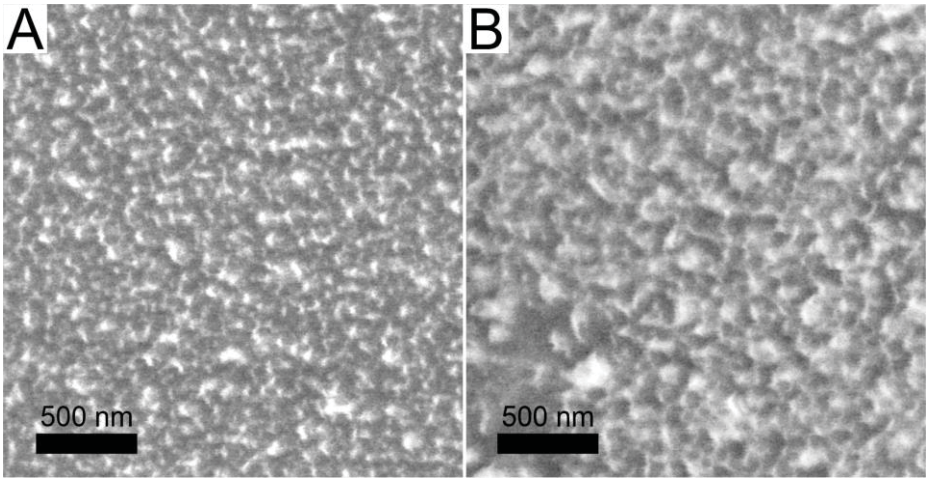

Fig. 13. SEM photo of the second group of samples: after 5 s of etching (A), after 30 s (B)

The decreasing number of small nanoparticles in coatings can strongly reduce the silver ion release process [17, 212] comparing with the less etched samples (for 20 s in the current research), when small NPs are less oxidized, and are still embedded in the DLC matrix and can thereby ensure the optimum silver ion release performance, as it was obtained in the test results of GoS containing more than 3 at. % Ag after 20–30 s of etching.

3.2 Silver ion release kinetics

DLC thin films were alloyed with silver to provide antimicrobial properties which were determined by the silver ion release rate from the thin film surface to water media. The silver ion release process starts when the aqueous media reaches the particle's surface [45, 214]. In the current work, the silver ion release studies were performed by applying the equally etched (for 20 s) 6 cm^2-sized groups of samples placed in purified water from 20 to 1440 min. AAS measurements were performed to identify the silver ion release amount (ppm) from 6 cm^2 nylon fabric groups of the samples into 1 ml of purified water. After analysis of the data provided by the current experiments (see Fig. 14), it was found out that the plasma treated groups of samples had different silver ion release speed properties from all of GoS to water media, and the results of the three groups of DLC:Ag samples are presented as follows:

After 20 minutes, the first group of samples containing silver of 0.9 at. % released very small amounts of silver ions (see Fig. 14), the concentration was less than 0.1 ppm after 60 min. After 180 min, the silver ion concentration reached 0.3 ppm, and after 24 hours of exposure time, the value was 0.5 ppm.

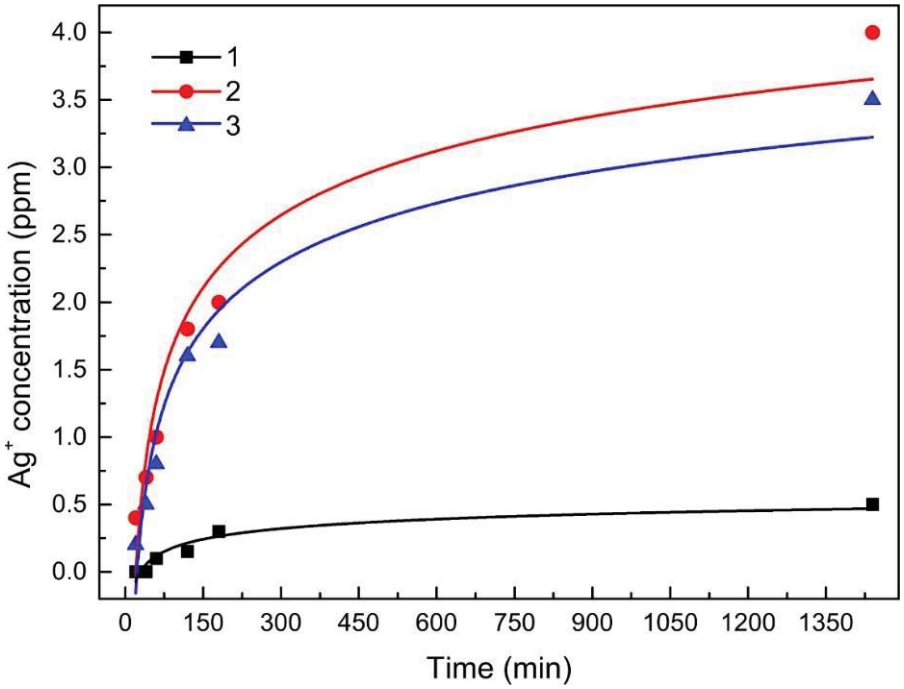

Fig. 14. Silver ion release results of DLC:Ag groups of samples: 1st – 0.9%; 2nd – 3.4%; 3rd – 6.9 at.% Ag, while the contact surface area ratio to water volume was 6 cm^2 to 1 ml, the exposure time was from 20 min to 1440 min

The test results with the second group of samples containing 3.4 at. % Ag revealed that, after 60 min, the concentration of silver ions reached 1 ppm, after 3

hours, it was 2 ppm, and the concentration peak was achieved after 24 hours at 4 ppm.

The test results with the third group of samples containing 6.9 at. % of Ag after 20 s of RF plasma etching showed that, after 1 hour, Ag ion concentration was 0.8 ppm, after 2–3 hours, it was less than 2 ppm, after 24 hours, the concentration was 3.5 ppm, respectively. It is known that heavy metal NPs have superb advantages due to the high specific surface area, which increases the ability to release ions comparing with metal plates or fabrics [215]. The plasma etched surface of DLC:Ag had partially embedded silver nanoparticles into the DLC matrix, and the efficiency of the silver ion migration from all the groups of samples depended on the silver NPs size and the silver content. It was found out that the silver ion concentration in purified water at 35 °C was from 0.0 to 4.0 ppm.

The efficiency of Ag^+ ions release to the aqueous media tended to increase further after RF oxygen plasma etching [79, 214], and the silver ion concentration was below the toxic level (up to 13.5 μg/mL) [79] for organism cells, but it was toxic for bacteria. During the experiments, it was determined that the concentration of silver ions in purified water rapidly increased during the initial 180 min and reached the saturation limit after 1440 min. The saturation effect was also obtained in [215], and the saturation of silver ions to 4 ppm can be explained by a well-established balance between silver ions in the water and the surface of solid nanoparticles partially embedded in the DLC matrix. In terms of this balance, the fast silver ion release effect during the initial hours was achieved due to silver ion migration into the water media from high silver ion concentration areas which were close to the NPs surface to the low silver ion saturated zones [2, 216] or where greater distances among nanoparticles were present. After the time when the silver ion saturation level reached 4 ppm, part of silver ions came back onto the NPs surface or were reduced to small NPs [215, 217], or else, as explained by other authors [215], the silver ion concentration in the aqueous media is determined by the balance of the solid body and the dissolved ions. A similar result was obtained in work [207], when DLC:Ag samples (4.5 at. %) demonstrated less than 4 ppm silver ion concentration after 24 hours; exactly as it was determined in the current chapter experiments. The surface structure of prepared DLC:Ag and the active surface of silver nanoparticles, particle distribution and film thickness [214] are the main factors for good silver ion release properties in the water media [218, 219]. Experiments showed that a higher silver concentration in the deposited films (such as the 3rd GoS) does not ensure the best silver ion release performance. Otherwise, larger silver concentration in coatings leads to a larger reservoir of silver ions and can extend the beneficial Ag ion release properties [93]. From the results of the current work, it follows that the silver ion release rate from the second group of samples containing 3.4 at. % of Ag was the highest comparing with the group of samples containing 6.9 at. % of Ag, where the silver concentration in the thin film was larger than in the second group. Similar results were obtained in [201] when the silver ion release effectiveness decreased with an increase of the Ag content in thin DLC:Ag films.

Moreover, the NPs oxidation process in water can start from the surfaces of small nanoparticles; instead, and a higher number of large NPs in coatings can reduce the silver ion release speed [169]. This explains the silver ion release differences between GoS 2 of more than 3 at.% Ag and GoS 3 of more than 6 at. % Ag. After conducting AAS analysis, a very low silver ion release rate was detected in the first group of samples (0.9 at. % Ag after 20 s of etching) when, after 24 hours of exposure in purified water, only 0.5 ppm of silver ions was released, which is less than needed for the antimicrobial properties to be manifested [220]. The second group of samples (3.4 at. % of Ag after 20 s of etching) showed better silver ion release properties than the third group of samples with 6.9 at. % of silver after 20 s of RF plasma etching.

The released silver ions reached 1 ppm concentration which is necessary to achieve antimicrobial properties after 60 min. From the other authors' findings, it is known that antibacterial activity against *S. aureus* starts from 1 ppm of silver ions concentration in the media [220], and GoS 3 (6.9 at. % Ag) reached this concentration after more than one hour, and GoS 3 was not as efficient for the ion release as the second group of the samples. The silver ion release efficiency from the second group of samples (3.4 at. % Ag) can be explained by the particle mass and the active surface ratio [216, 221]. Larger diameter silver nanoparticles have a smaller surface area which acts as a silver ion donor in oxidative dissolution [96], but only offers low efficiency. According to [125], Ag NP of up to 30 nm in diameter released the highest levels of Ag ions [222], and, from the NPs analysis results, it can be seen that, in the second GoS, nanoparticles of 12–18 nm dominated. It was determined that very small NPs (about 2 nm) of a very low mass contained only several hundred atoms; they had a large bioactive surface area and could release more silver ions comparing with heavy nanoparticles [169]; moreover, the largest silver contact surface area with water ensures high silver ion release rates [28, 24]. Silver NPs after contact with water release ions into the media, and, as a result, they can lose the primary structure and fall out from the matrix. The authors of [169] note that silver ion extraction from the nanoparticle surfaces can influence the nanocomposite morphology changes. Morphology changes can occur due to low NPs oxidation and size reduction, which influences the decrease of the nanoparticle amount after immersion into water [214, 169], and, as a result of NPs oxidation, pits or other surface defects can reduce the silver ion release properties as determined after a longer (30 s) etching time. Based on the current experiment data and the findings of other authors [214], the silver concentration in thin films has less influence for the results, and it could be claimed that the silver release rate could be at a low level, independently from the Ag concentration in films where silver NPs are hidden in the DLC matrix and have no direct contact with water [148, 51]. The direct contact of silver NPs with water can be reduced due to the oxide layer on the DLC:Ag thin film surface, as it determined in [146, 205], after the plasma etching process, which can also increase the fall outs and the NPs number reduction. NPs fall outs, which were determined during SEM analysis, negatively affected the silver ion release results, as also shown in [109, 209], and the Ag ions kinetic model [96,

223] explains that the ion release rate increases with the amount of silver NPs on the surface, and, based on the results of experimental data, the optimum etching time was determined as 20–25 s (see Fig. 16) for all the groups of samples.

3.3 Antimicrobial effect of DLC:Ag coated GoS for bacteria cultivated on agar surface

In the current chapter, antimicrobial experiments with *S. aureus* strains applying nylon fabric trays sputtered with DLC:Ag thin films were performed. Three groups of samples containing silver in DLC were tested. The groups of samples were untreated and later etched by RF oxygen plasma for 5-15-20-25-30 seconds so that to determine the optimum plasma etching time for the maximum antimicrobial activity, and, in order to obtain this effect, the disc diffusion method was applied (see Fig. 15).

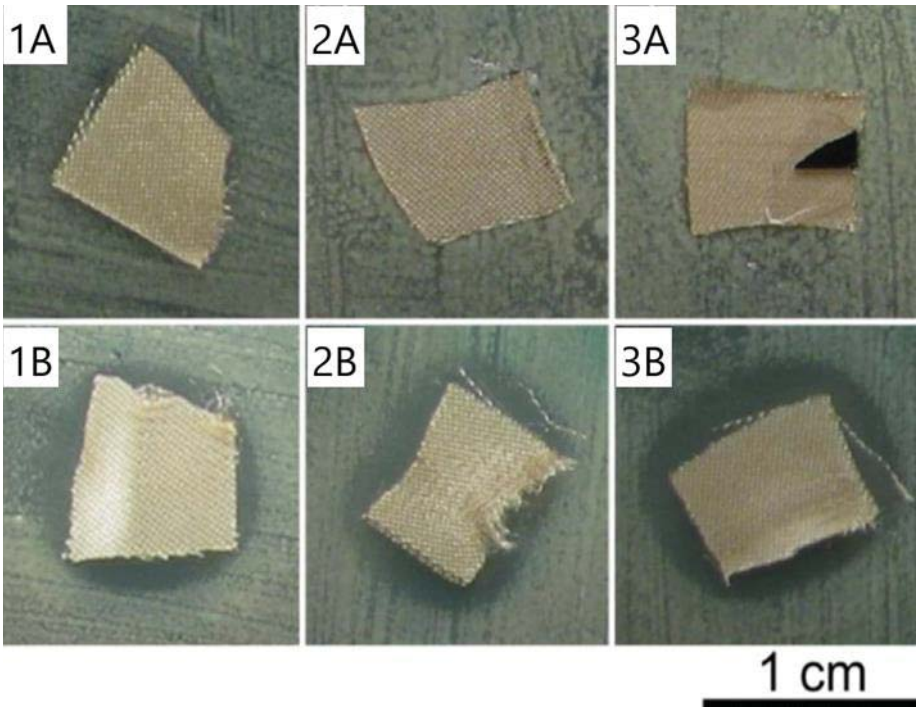

Fig. 15. Antimicrobial properties of prepared DLC:Ag etched and untreated group of samples (GoS) on nylon fabric tray: *S. aureus* LTSaM01 bacteria cultivated in Petri dish on agar and GoS 1–3 (A) plasma unetched and 1–3 (B) plasma etched for 20 s was glued with water on agar surface, placed in thermostat, and the results were evaluated next day

During the experiments, it was found out that the untreated plasma DLC:Ag coated samples had minor or no antimicrobial properties for *S. aureus* bacteria. The tests revealed that even large silver concentration containing (oxygen plasma untreated) coatings only showed a minor antimicrobial effect which is related with

the NPs active surface and volume ratio [31, 221], or, as was determined in [93, 214], silver nanoparticles did not contact with the wet agar surface, which resulted in undetectable diffusion of ions.

The oxygen RF plasma processed groups of samples had a measurable antimicrobial effect. The first GoS after 5 seconds of etching showed no antimicrobial properties. The positive antimicrobial activity can be identified when the inhibition zone is larger than 1 mm., whereas it was insufficient when the bacteria totally colonized the area around the sample without any clear zone [26], or when bacteria could colonize the sample's surface without silver nanoparticles [126, 224]. The results of such tests were obtained due to the insufficient silver ion concentration around the sample when it was sticked onto the agar surface, and the required concentration of 1 ppm of silver ions ultimately was not achieved [220]. After 15 s of etching, the first GoS had a 0.5 mm inhibition zone (for a clear zone around the sample on agar surface, see Fig. 16) for all the tested bacteria strains. After 20 s of the oxygen plasma processing time, the inhibition zone for bacteria LTSaDA01, LTSaM01 strains were 1.5 mm.

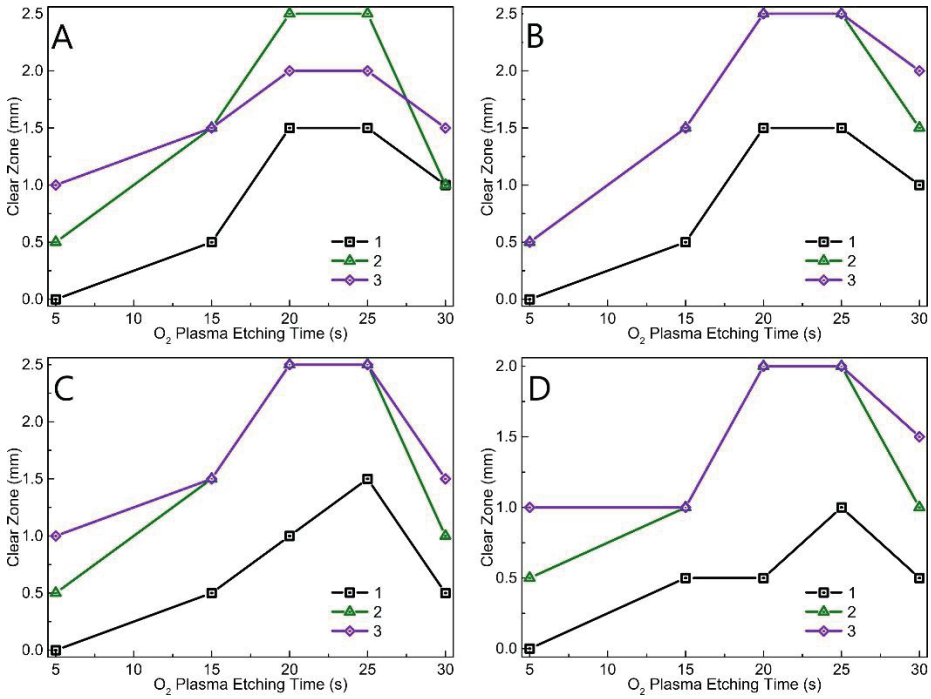

Fig. 16. Disk diffusion method test results of DLC:Ag RF oxygen plasma etched nylon fabric GoS (1–3): samples were etched for 5-15-20-25-30 s (X axis), and clear zone on agar surface with cultivated *S. aureus* bacteria (A) LTSaDA01; (B) LTSaM01; (C) LTSa635 and (D) LTSa603 strains (Y axis)

For other strains – LTSa635 and LTSa603 – the inhibition zone was 0.5 and 1 mm, respectively. The optimum etching time was 25 s, and the microbiology test

showed 1.5 mm clear zones for the three bacteria strains, except for LTSa603, and only 1 mm clear zone on the agar surface was obtained.

Tests with the second group of samples (untreated) showed that, after 5 s of plasma etching, the clear zone in all Petri dishes with all bacteria strains was 0.5 mm After 15 s of etching, the antimicrobial properties increased, and the inhibition zone diameter of bacteria strains LTSaDA01, LTSaM01, LTSa635 was 1.5 mm except for bacteria strain LTSa603 whose inhibition zone was only 1 mm GoS processed with RF oxygen plasma for 20 and 25 s (see Fig. 16) had the same antimicrobial results. The inhibition zones of 2.5 mm were obtained for LTSaDA01, LTSaM01, LTSa635 *S. aureus* bacteria strains, and a 2 mm clear zone around the sample in a Petri dish was found with LTSa603 bacteria. The etching for 30 s reduced the antimicrobial activity for all bacteria strains, and the inhibition zones were from 1 mm to 1.5 mm. The third group of samples had the largest silver concentration, and, after 5 s of the plasma processing time, they showed the best antimicrobial results comparing with all the groups of samples etched for an equal amount of time. After 15 s of plasma treatment, the antimicrobial results were identical for GoS 2 dominated by 1.5 mm inhibition zones except for LTSa603 where 1 mm inhibition zones were obtained. After 20–30 seconds of plasma etching, the antimicrobial results were similar to the results of the second group of samples, and only 0.5 mm difference for some bacteria strains was obtained (see Fig. 16).

After microbiology testing (the disk diffusion method – see Fig. 16), it was found out that DLC thin film coated samples with a low silver content showed no antimicrobial activity. Yet, some scientific researches [206] show that DLC has the antimicrobial properties when applied on textile without silver, and it killed bacteria after 18 hours. What regards current research, it was found out that, by applying the disk diffusion method, even the low silver concentration RF plasma treated samples had no antimicrobial properties. Moreover, other authors [109, 172] revealed that the plasma treatment of DLC thin films did not increase the antimicrobial effect. A possible explanation of the DLC antimicrobial action, according to research [206], could be the DLC mechanical bacteria cell wall damage which can be induced by the DLC surface [109], and, hence, the increased surface roughness has no correlation with the antimicrobial properties. It should be noted that the authors of [206] in their research applied bacteria directly onto the coating surface with minimum nutrition media. Other authors, e.g., [168], discovered that the coating structure plays an important role for bacteria adhesion, and the rough surface can determine the bacteria biofilm formation on the surface [12, 16, 162]. For example, rough structures on the surface can disrupt the bacteria colonization and biofilm formation process [111], but, in this research, after plasma etching, the roughness of all groups of samples strongly increased, and, according to authors of [17, 168, 53], the antimicrobial properties might be developed not only due to silver ion release but also due to the structural properties of the surface. Such structures might work for antimicrobial clothes but are not suitable for wound dressings where nutrition media for bacteria growth is available in the wound bed and tissues [33, 64]. On the other hand, silver treated materials, such as antimicrobial cotton [120, 46, 226],

synthesized by reduction of silver salts [105, 225, 227], can be used as antimicrobial materials without DLC:Ag coatings [46, 218, 226].

According to the data of our experiment, the best group of samples for the bandage prototype was elected, and it was found out that the first group of samples had the weakest antimicrobial properties, compared with GoS 2 and 3. The silver ion antimicrobial effect can be obtained on the wet surface because, for the silver ion migration process (diffusion from the solid body (NPs) to water), a liquid transport system is needed, such as water, to transfer silver ions to bacteria [228]. In other cases, silver ions do not reach the target (bacteria), and their antimicrobial properties are eliminated [93, 229] as based on the currently available results of antimicrobial research. It was determined that RF plasma etching improved the Ag release rate as shown in [93]. The silver ion kinetics [88, 125] (silver ion diffusion from the sample's thin film surface to a water rich media) performed the essential role for antimicrobial activity [88, 229]. It was found out that silver NPs in the DLC thin film matrix without good contact with a water rich media had zero or only very weak antimicrobial properties as presented in [40, 120]. Only the coatings with exposed silver nanoparticles can release silver ions and are denoted by the possession of antimicrobial properties [214]. After analysis of the obtained results, it was determined that the surface morphology changes, induced by the etching process, strongly increased the antimicrobial properties [141, 135] due to the exposure of Ag NPs from the DLC matrix to the thin film surface, as presented in other authors' works [16, 92, 170, 202]. This effect can be explained as the chemical composition changes inside the thin films and after plasma treatment, i.e., small-sized nanoparticles were revealed on the surface as observed in [27, 96, 153]; experimental data demonstrated that the plasma treatment process (20–25 s.) enhanced the samples and increased the antimicrobial properties. Otherwise, the coatings containing more silver NPs on the DLC surface can be damaged if the duration of the plasma treatment procedure is excessive [109, 140], for example, 30 s. Groups (1–3) of samples showed weaker antimicrobial properties after 30 s of etching (comparing with 20 s etched GoS), and the inhibition zone (or the clear zone around the samples) decreased (see Fig. 16). The experiment results suggest that plasma etching formed the oxygen atoms (oxide) layer on the NPs surface and reduced the silver ion migration from the NPs surface to water [109].

Based on the results of other authors [16, 93], DLC or DLC:Ag coatings, when Ag NPs are not exposed (without RF plasma etching) on the film surface, exhibit no antimicrobial properties, but oxygen plasma processed DLC:Ag coatings gain cytotoxic properties for bacteria, and they could potentially be used for the traditional antibacterial therapy [79, 202**]** or in external use pharmaceuticals as proposed in the current dissertation.

3.4 Antimicrobial properties of DLC:Ag samples *in-vitro*

DLC silver doped coatings have silver NPs in their carbon matrix, and the silver antimicrobial action mechanism is related with the silver ion diffusion rate [27, 116]. In the current chapter, the correlation between the silver ion concentration in the water media and the changes of the bakteria colony forming units (CFU)

numbers are presented. As the silver ions source, for the current experiments, DLC:Ag 20 s etched groups of samples were selected according to the best antimicrobial results presented in Fig. 16. For the testing of antimicrobial properties, groups of samples were immersed into a solution with bacteria strains.

Table 4. Microbiological test results with referential *S. aureus* bacteria

Time (min)	CFU	CFU %	Ag^+ conc. (ppm)
Control samples			
20–300	488–505	100	0
Group of samples 1 (0.9 at. % Ag)			
20	481	98.6	0
40	478	97.2	0
60	475	96.3	0.1
120	468	92.9	0.15
180	454	90.8	0.2
240	436	87.2	0.2
300	420	84	0.25
Group of samples 2 (3.4 at. % Ag)			
20	412	84.4	0.4
40	356	74.2	0.7
60	146	29.6	1.0
120	86	17.1	1.8
180	52	10.4	2
240	28	5.6	2.2
300	6	1.2	2.5
Group of samples 3 (6.9 at. % Ag)			
20	464	95.1	0.2
40	384	78	0.5
60	238	48.3	0.85
120	113	22.4	1.6
180	92	18.4	1.8
240	72	14.4	1.9
300	30	6	2

Dilution of bacteria suspension was 10^{-5}, active contact surface was $6cm^2/ml$, GoS etching time was 20 s

The experiments were performed based on the methodology and findings outlined in [215, 230]. The bacteria solution of 0.5 Mf was used in our experiments, and groups of DLC:Ag coated samples (GoS 1–3) were immersed into the test tube with the referential bacteria suspension for different time intervals. The test tubes were placed in a thermostat at 35 °C and were taken out for inoculation experiments only. The serial dilution method was used for bacteria CFU dilution before the inoculation procedure on the agar surface. The silver ion release detection experiment was performed by applying DLC:Ag groups of samples in test tubes with purified water, without bacteria, for 20–120 min intervals. AAS measurements were performed to determine silver ion concentrations at different time intervals.

The test results show that CFU in the control test tube slightly increased (multiplied), from 488 to 504 during 120 min. The first group of samples (0.9 at. % Ag), applied in the test tube, had a weak antimicrobial effect for *S. aureus* bacteria. After 20 min, the bacteria CFU number decreased by 1.4%, and, after 120 min, it decreased by 7.1% (see Table 4). Silver ions in water were detected after 60 min, and their concentration reached 0.1 ppm; after 120 min, it was 0.15 ppm, and after 300 min, it reached 0.25 ppm; 16% reduction of the bacteria CFU was registered. The second group of samples with 3.4 at. % of silver had stronger antimicrobial properties than the first group of samples.

The tests showed that, after 20 min, the bacteria CFU was reduced by 15.6%, and the silver concentration in water reached 0.4 ppm. After 40 min, the silver ion concentration was 0.7 ppm, and the bacteria CFU number decreased by 25.8%. After 60 min, the strongest effect was obtained when the silver concentration achieved 1 ppm – the CFU number was reduced by 70.4 %. After 300 min., the silver ion concentration reached 2.5 ppm, and 98.8% bacteria CFU was killed by silver ions.

The third group of samples containing 6.9 at. % of silver showed weaker antimicrobial activity comparing with GoS 2, and the silver ion release rate into distilled water was lower than that of the second group of the samples. The experiment data showed that, after 20 min, the CFU number decreased by 4.9%, and, after 40 min 22% respectively. The silver ion release speed was slower than for the second group of samples, and the bacteria CFU reduction number rate was slower after 60 and 120 min, the values of 51.7% and 77.6% were obtained. After 300 min, 94% of the bacteria colony forming units (CFU) was inactivated, and the silver ion concentration was 2 ppm.

From the test results, it can be determined that the silver ion concentration correlated with the antimicrobial properties and was related with the silver ion kinetics as noted in [93, 125]. Also, silver ions showed antimicrobial activity at a very low level, as discovered during the experiments with the first group of samples (see Table 4). The etched GoS had silver NPs exposed on the thin film surface, and silver nanoparticles could be oxidized in water (silver atoms were ripped off from the nanoparticle surface) and became silver ions [215]. Based on the research data, it was found out that the group of samples with the largest silver concentration after etching (6.9 at. %) had a lower ion release rate and a weaker antimicrobial activity level comparing with the second group of samples (3.4 at. % Ag). The current experiments showed that the silver nanoparticle size (the active surface ratio) and the direct contact with water are essential factors for antimicrobial properties as determined in [51, 96, 153].

3.5 Antimicrobial properties of silver ion saturated distilled water

The current experiments were performed to investigate the silver ion action effectiveness inside a bandage and in the wound's bed by applying the *in-vitro* model. Silver ion saturated water in various concentrations was used for bacteria treatment, i.e., the bacteria suspension was diluted with silver ion saturated water to kill the bacteria.

The experiment time intervals were from 20 to 340 min, and 2, 6 and 8 ppm concentration of silver ion saturated water was applied to the bacteria suspension in order to dilute the primary suspension to 0.5 Mf level, and 1, 3, 4 ppm of Ag^+ conc. was sustained inside the test tubes (with bacteria); as a result, the bacteria of 0.5 Mf concentration was affected by 1-3-4 ppm of silver ions, and the results (see Fig. 17) can be presented as follows:

Distilled water with silver ion concentration of 1 ppm. had some antimicrobial properties, but the bacteria CFU number decrease in the time scale was minor. After 20 min., the bacteria CFU decreased by 12.7%, and, after 60 min., the CFU decreased by 30.3%. After 340 min., the bacteria CFU reduced by 45.6% (see Fig. 17, 1), i.e. the slower silver ion antimicrobial action effect to the bacteria was obtained.

3 ppm of silver ions showed better antimicrobial results than the 1 ppm concentration. The larger concentration of silver ions increased the bacteria CFU inactivation speed and the efficiency, as it was determined in [126, 170]. After 20 min, the CFU number decreased by 14.5%, whereas, after 120 min, decreased by 53.5% (see Fig. 17, 2). After 340 min., the CFU number decreased by 67.8%, and it was greater than in the experimental results with 1 ppm Ag^+ concentration.

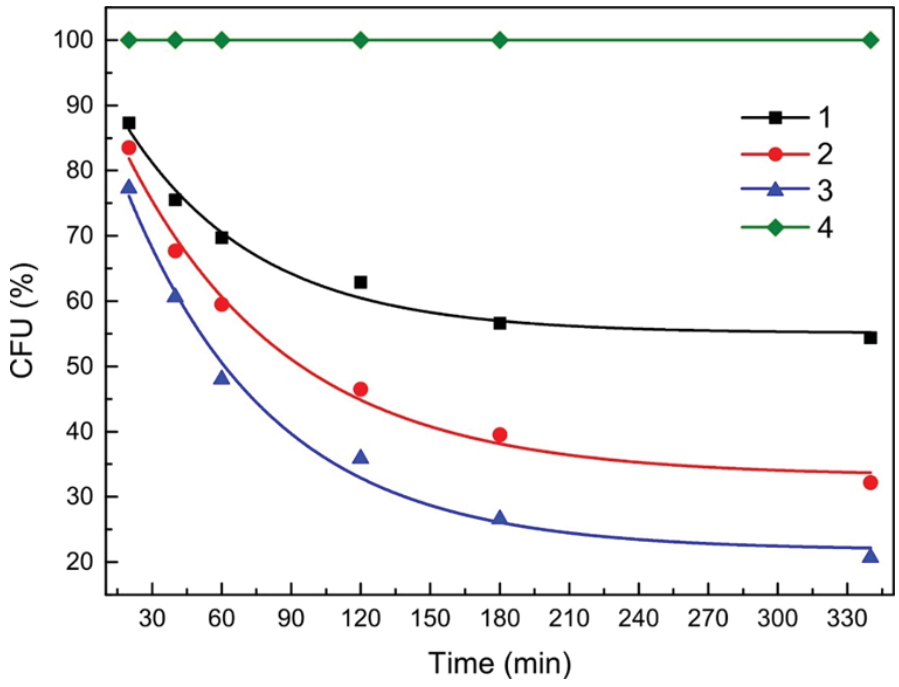

Fig. 17. Correlation of silver ion concentration (1–4 ppm) and CFU (0.5 Mf) reduction in-time scale: 1 – (1 ppm), 2 – (3 ppm), 3 – (4 ppm) Ag+ concentration and 4 – bacteria control tests (without silver ions) are presented

The largest silver ion concentration induced the fastest antimicrobial effect comparing with the other concentrations as expected. After 20 min, the bacteria CFU (0.5 Mf CFU placed into 4 ppm of silver solution) reduced the CFU number by 22.7%, and, after 120 min, this number decreased by 64.1%. The surviving number of CFU after 340 min was 20.7%, i.e., the total killed bacteria CFU number was 79.3% (see Fig. 17, 3).

In the experiments of the current chapter, direct silver ion antimicrobial action and its efficiency were determined. The authors of [97] provided a method to calculate the silver ion count which could affect one CFU (or bacterium). The silver ion count in 1 ml (in 1, 3, 4 ppm. concentration) of Ag^+ solution for one CFU was calculated according to the formula:

$$\frac{x\ ppm \times 10^{-6}}{1\ mL} \times \frac{N_A}{mole\ Ag} = \frac{4 \times 10^{-6}}{1} \times \frac{6.02 \times 10^{23}}{107.86} = 2.23 \times 10^{16} \quad (1)$$

where N_A –Avogadro constant (6.02×10^{23} mol^{-1}), Ag mole mass – 107.86, ppm – silver concentration parts per million (4 ppm)

One milliliter of 4 ppm Ag^+ saturated water contained 2.23×10^{16} silver ions, and 0.5 Mf of bacteria suspension contained 1.5×10^8 colony forming units (or CFU).

According to Equation (1), the number of silver ions which could affect one bacterium is: 1 ppm. (conc.) – 3.72×10^7 (Ag^+) affected one bacterium; 3 ppm. (conc.) – 1.11×10^8 Ag^+ / bacterium and 4 ppm (conc.) – 1.49×10^8 Ag^+, respectively.

It was determined that 1 ppm concentration of Ag ions showed antimicrobial properties, and, according to our calculations, the efficient silver ion number for one bacteria cell is 3.72×10^7. A greater concentration of Ag ions showed better antimicrobial activity. According to the research data of [10, 218], the antimicrobial effect was obtained at a few ppm concentration of Ag^+ or lower concentrations than 1 ppm [97, 231], but the current research data demonstrated that a higher silver ion concentration level in a bacteria rich watery medium resulted in faster and stronger antimicrobial activity comparing with a low Ag^+ concentration. Other researches (with such microorganisms as trypansomes and yeasts) determined that the antimicrobial action for these microorganisms appeared from 10^5 to 10^7 of silver ions per cell [97] as also determined in the current experiments.

3.5.1 Effect of antimicrobial agents for bacteria morphology

The current experiments were performed with the objective to investigate the silver ion and NPs antimicrobial efficiency for the *S. aureus* bacteria cell wall, and the results were compared with the well known antibiotic benzylpenicillin.

The silver antimicrobial mechanism for *S. aureus* bacteria was determined by applying 4 ppm concentration of silver ions in 0.5 Mf bacteria test solution, and the identical experiment was performed with silver NPs of 4 ppm in a bacterial solution. After 300 min, bacteria inoculation experiments were performed, and it was found out that silver ions reduced the bacteria population by 76%, and silver nanoparticles achieved the score of 80%, respectively. Ag^+ was directly responsible for the

antibacterial effect as determined in [93, 96]. For the SEM analysis, one drop of a bacteria suspension with Ag^+ and NPs containing solution was placed on silicon wafer, dried out, fixed by heat, and rinsed in distilled water to remove NaCl crystals.

The experimental data showed that silver ions had a visible effect on the bacteria cell wall (see Fig. 18, B). Most bacteria showed cell wall changes, cell morphology pathologies, and lysed cells were found, see (Fig. 18, B; as marked with arrows). It was determined that a lot of spots and cases of cytoplasm leakage appeared on the bacteria surface whereas in the control photo no bacteria wall changes were observed (Fig. 18, A).

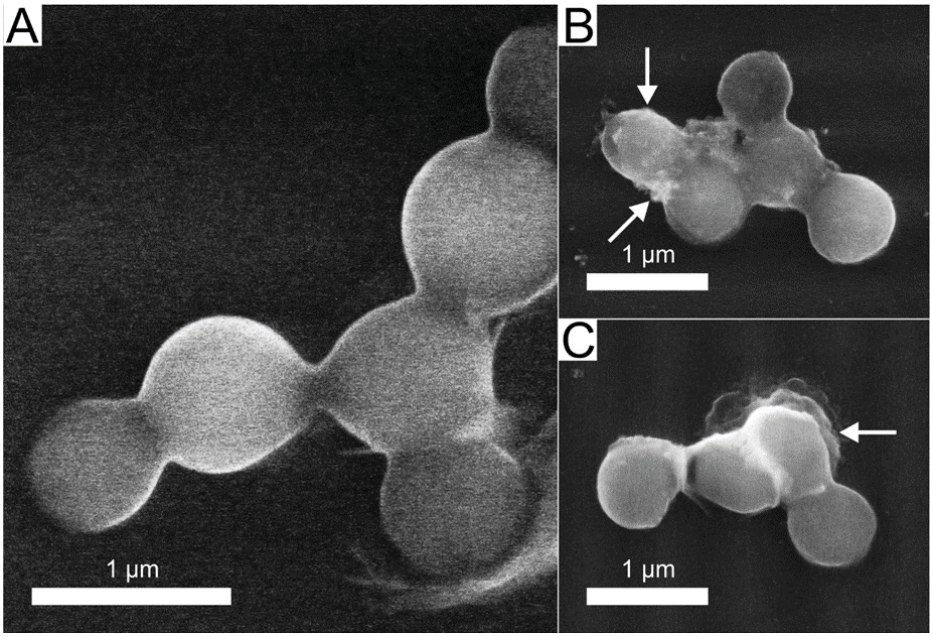

Fig. 18. Microphotographs of silver treated and untreated bacteria: (A) – control, (B) – bacteria treated with silver ions, and treated with 10 nm silver NPs (C), damaged cell wall is marked with arrows

This effect could be explained based on the findings of [34, 36], that a bacteria cell wall the negative charge can interact with positively charged Ag ions accumulated at the cell membrane [98]. According to the authors of [100, 101], the bacteria after interactions with silver ions were affected, and the irregularly shaped pits on the bacteria surface were observed, as determined in the current research. Moreover, the authors of [107] also claim that Ag^+ ions can suppress the bacteria growth (76% in our experiment) in small Ag^+ concentrations or rupture the cell wall when Ag ions merge to the negatively charged cell wall, as was also observed during SEM photo analysis, but only a few cell-disrupting bacteria were found. Silver ions have the ability to access the inside of the bacteria cell by using general bacteria poirins [105] and can block the activity of cytoplasmic proteins, thereby stopping the ATP functions [104] as well as DNA normal chain replication and transcription processes [105], thus leading to death. But, on the other hand, after the data analysis

of the current experiments, it was determined that a lot of bacteria cells had surface changes, and the silver antimicrobial effect might be caused by the mechanical and molecular level damages, respectively [79, 216].

After the SEM photo analysis of bacteria, when 10 nm of silver NPs was applied, the cells with partially damaged or completely disrupted cell walls were found, see (Fig. 18, C). The experiment results suggest that NPs of <10 nm in diameter can easily attach to the membrane surface compared to the larger NPs [99]. It can be postulated that small Ag nanoparticles have a larger surface area to volume ratio, and can thus easier attach to the cell wall [104, 111]. The nanoparticle attraction mechanism to the bacteria cell wall may be electrostatic attraction which increases the membrane permeability. This results in the rupture, and the cytoplasm leaks out [17, 110, 232]. The authors of [92] claim that Ag NPs have no direct effect for DNA and proteins, but, on the other hand, silver NPs can result in the formation of pits (permanent cell wall damages [15, 216] leading to permeability loss and bacteria death [92]).

After obtaining test results when *S. aureus* bacteria were treated, it can be claimed that silver ions and silver nanoparticles are denoted by the antimicrobial effect, as it was determined in the current experiments. When comparing the antimicrobial effect, it should be noted that silver nanoparticles can directly interact with the cell walls [91], generate free radicals and release silver ions from NPs as the secondary slow process to sustain the antimicrobial effect so that to achieve a stronger antimicrobial effect [92], as obtained in the current experiment (80%) comparing with distilled water saturated with silver ions (76%).

In the experiments with benzylpenicillin (BP) and *S. aureus* bacteria, after SEM analysis, it was determined that biological reactions between BP and *S. aureus* cell wall triggered morphological changes (see Fig. 19). BP as an antimicrobial agent interacted with the *S. aureus* bacteria cell wall, damaged the cell wall integrity, and the result was the destruction of the cell wall [233].

Table 5. Microbiology tests results after BP application

Benzylpenicillin (ml)	0	0.1	0.2	0.3	0.4
No. of live CFU	61	7	5	1	0
Killed CFU (%)	0	88.5	91.8	98.4	100

The test results with the control sample confirmed the growth of unaffected bacteria of BP. After the first BP of 0.1 ml injection, 88.5% of bacteria CFU were inactivated, and these results can be explained [see 234] as the BP action speed and the efficiency of the bactericidal action, since it is not proportional to the antibiotic concentration. Rapidly dividing cells and bacteria cells in the resting stage are not proportionally affected [236]. Minor cell wall changes were observed after 0.1 ml application, and, compared with the control sample in SEM microphotographs (see Fig. 19, A and B). The benzylpenicillin molecule creates a covalent bond with the target molecules on the cell wall surface between the beta-lactam ring carbonyl group and an unidentified group on the penicillin-binding components [235], and low BP concentration has a minor effect on the cell wall morphology. As it was

determined, the insufficient concentration of BP can induce only minor cell wall changes, but, on the other hand, it inactivates bacteria growth (see Table 4).

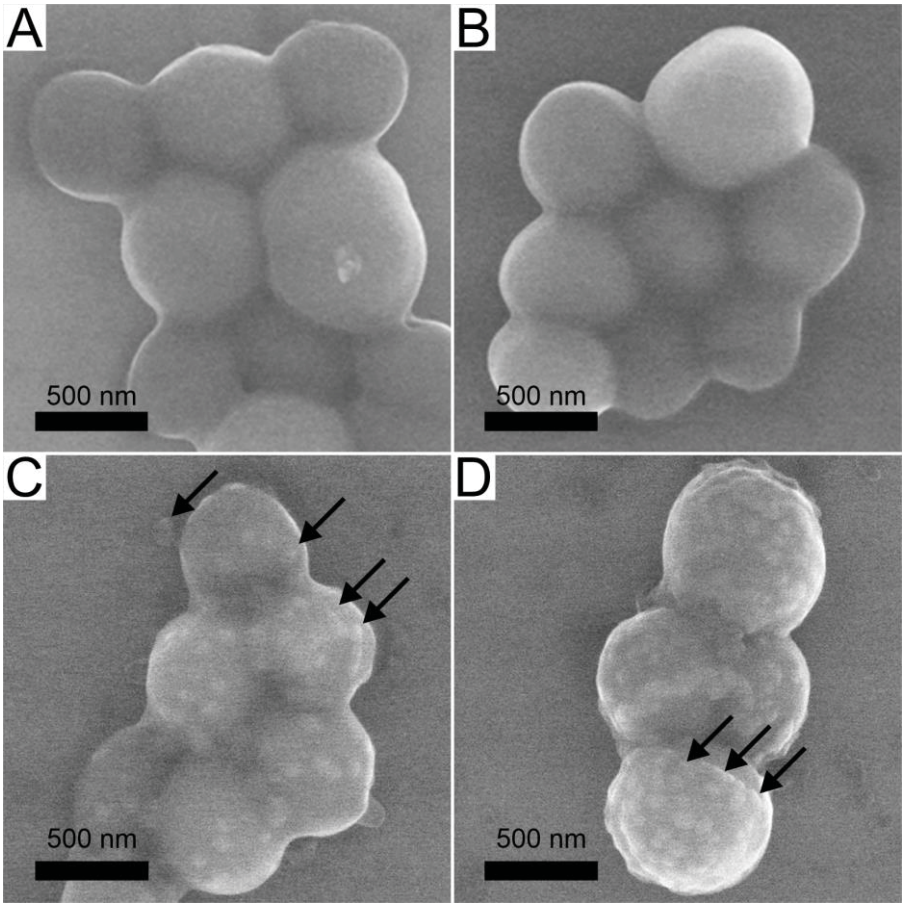

Fig. 19. Induced bacterial cell wall changes after the application of benzylpenicillin: A – control, B – after 0.1 ml, C – 0.2 ml and after 5 min 0.2 ml, D – one injection of 0.4 ml of benzylpenicillin into bacterial suspension

Moreover, it is known that penicillin group antibiotics produce their effect due to the BP specific action mechanism, and the survival effect of bacteria can be explained as follows: bacteria with a defective or damaged cell wall due to the spheroplast activity can synthesize the new cell wall and restore the BP caused damage, and this effect can be obtained only in conditions of insufficient BP concentration [233]. After 0.4 ml or 200000 I.U. injection, all of the bacteria CFU were killed (see Table 4). When continuing researches, it were found out that, after two separate sequential 0.2 ml of BP solution injections (total 0.4 ml), the cell wall was strongly damaged (Fig. 19, C). On the other hand, one injection in one action of the same amount (0.4 ml) of BP had the strongest effect for the bacteria cell wall. BP-caused damage was observed as spots on the entire cell wall surface, damaged

zones (Fig. 19, D) of cell walls and membrane leak outs appeared. These morphology changes were identified as denatured proteins and lipids or surface pits [126, 227].

From the SEM data analysis, it can be determined that bacteria cells have a different cell wall morphology it was observed as structural changes of a cell wall, which correlated with different BP volume application (and conc.) during experiments [237].

3.6 Bandage materials testing and prototype assembly

In the current chapter, we apply the selected group of samples for the bandage prototype as the background, and the results are presented. GoS 2 with silver concentration of 3.4 at. %, after 20 s of RF oxygen plasma etching was selected as the source of silver ions for two types of prepared bandage prototypes. After the performed tests, construction improvements serving the objective to increase the antimicrobial activity and efficiency were made. Two types of bandage prototypes, their construction properties, the proposed working mechanism, as well as their antimicrobial properties are presented.

In the preparation process of the first bandage prototype (see Fig. 20), DLC:Ag coatings were sputtered on the substrate (nylon fabric) by using a DC unbalanced magnetron.

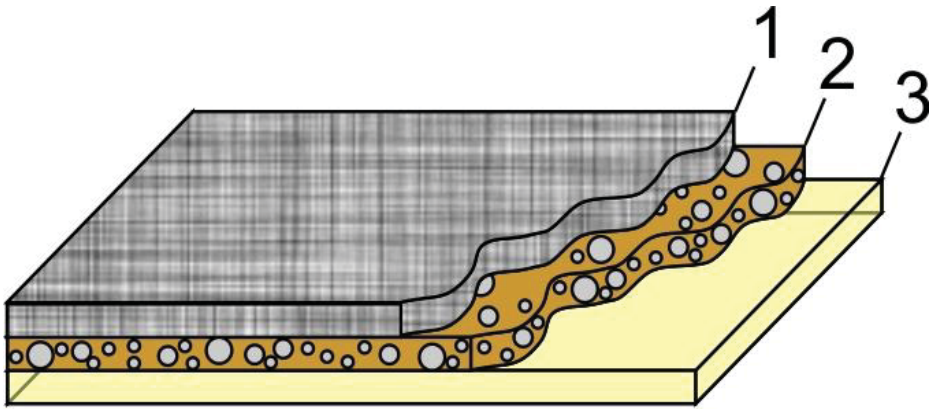

Fig. 20. First bandage prototype: 1 – nylon fabric coated with DLC:Ag thin film (3.46 at. % Ag), 2 – thin cellulose layer, 3 – thin gelatin/agar layer

According to the idea of the prototype, a bandage containing DLC silver doped coatings in water media should release portions of Ag ions [79, 102, 238] as we pursue to implement the following objectives: a very hydrophilic and permeable layer barrier is needed to ensure the best silver ion performance in the bandage [214], which leads to a fast antimicrobial effect during the early hours [10, 238]. The second group of samples (3.4 at. %) for the first bandage prototype was disinfected by using a UV irradiation emitting lamp in a laminar box. After the disinfection procedures, the prepared nylon fabric samples were coated with a thin layer of

cellulose fibers mixed with gelatin and rolled while using a 50 mm stainless steel roller so that to remove water and gelatin excess, thereby forming 0.01–0.02 mm of a thin layer of cellulose. DLC:Ag coated nylon fabric cannot be applied on the wound surface directly due to possible contamination with debris [79, 140], and a thin layer on DLC:Ag coatings is necessary to solve the problem. The silver ion accumulation layer was prepared by applying a warm (38–40 °C) suspension of gelatin and agar (at 90%/10% ratio). The warm gelatin was poured onto the coated nylon fabric surface (DLC:Ag GoS 3.4 at. % Ag) which had been covered with a thin cellulose layer in advance. The excess of the warm suspension was removed by using a spin coater at a low speed (120 rpm), and the silver ion accumulation layer of 1 mm of thickness was manufactured. The gelatin and agar layer had very good water absorption abilities, as presented in [239, 240], and agar gelatin can increase the antimicrobial efficiency of DLC:Ag coated surfaces.

This effect can be achieved when dissolving a layer of gelatin-agar we spread silver ions rapidly into the aqueous media [51, 211]. The silver ion accumulation layer of 1 mm of thickness was selected based on microbiology data. It was found out that the effective silver ion migration distance in agar was up to 2–2.5 mm. The microbiology tests and experiments with lab animals showed the technology advances and disadvantages, and the necessary improvements were implemented in the second bandage prototype.

The second bandage prototype (see Fig. 21) was prepared based on microbiology, silver ion kinetics and the data of tests involving experiments with animals. During the researches, we found out the necessary conditions for silver ions to accumulate, as obtained in [40, 136, 211]. Moreover, it was found out that the fast and large concentration of silver ions released into the bacteria suspension provides the best antimicrobial results (see Fig. 22) in the time scale as also obtained determined in other scientific experiments [71, 126, 216]. Finally, the silver ion concentration sustainability (due to the DLC:Ag thin film) in the media can provide a sustainable and long-term antimicrobial effect against all bacteria [92, 126].

All the manufacturing procedures and improvements were implemented according to our test results produced for the current dissertation, and the bandage manufacturing process can be divided into steps: DLC:Ag thin film sputtering on nylon fabric, DLC:Ag film etching for 20 s, UV disinfection, formation of a protective layer, formation of the silicone 3D net structure, and formation of the silver ion accumulation layer. The assembled bandage was fastened to a sticky medical film, and it was ready to use for experiments with animals.

DLC:Ag thin film sputtering on the nylon fabric was performed by using a DC unbalanced magnetron, nylon fabric coated with DLC:Ag film (GoS 2, 3.4 at. % Ag) was etched for 20 seconds to yield silver nanoparticles hidden inside the DLC matrix. Samples were disinfected by using a UV irradiation emitting lamp in a laminar box for 4 hours. The samples were stored in plastic Petri dishes so that to avoid any additional contamination. After UV disinfection, the prepared nylon fabric samples of a size of 20x40 mm were coated with a thin layer of cellulose fibers, mixed with gelatin and rolled by using 50 mm diameter stainless steel roller while using a pressure of 5 kg/cm^2 so that to remove water and gelatin excess. After the

rolling process, a 0.01–0.02 mm thin layer of cellulose was formed on the coated DLC:Ag surface. The layer was formed to prevent DLC:Ag from falling out from the silk surface, and the layer worked as a membrane to sustain any residues close to the DLC:Ag sputtered nylon fabric surface. The silver ion accumulation layer (SIAL) was improved by the 3D silicone net structure which was manufactured like a honeycomb mesh (one element size: 2 mm x 2mm) in squares (see Fig. 21, 4), the thickness of the partitions was 0.3 mm, and the thickness of the entire net was 2 mm.

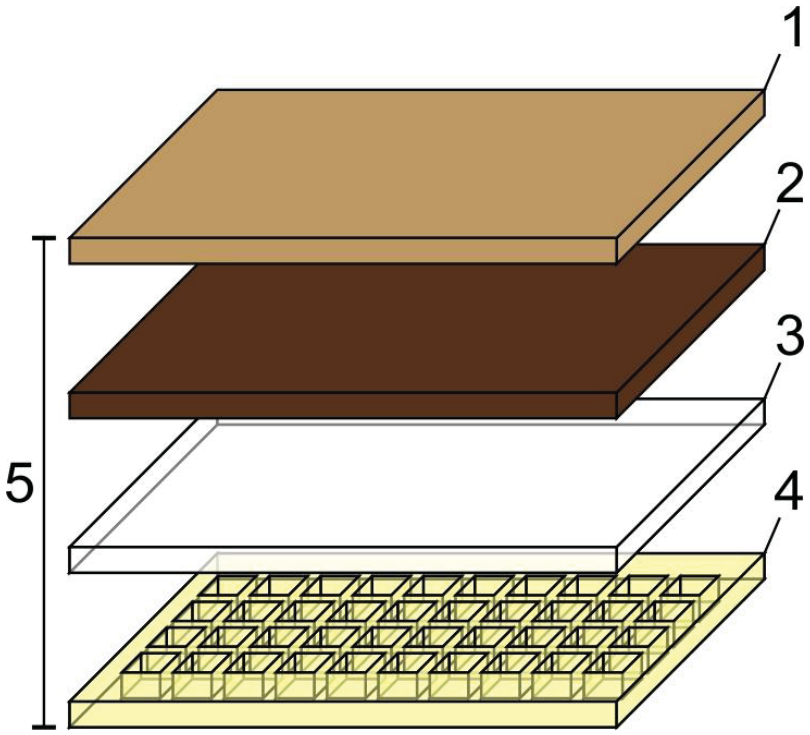

Fig. 21. Advanced bandage prototype (5) contains the following layers: sticky medical film (1), DLC:Ag coated nylon fabric (3.4 at. % Ag) (2), cellulose layer (3), silver ion accumulation layer (4) (SIAL)

The 3D silicone net was manufactured from two-component medical grade silicone. Silicone was poured into a special mold made from epoxy resin and left at room temperature for 48 h. After 48 h, the silicone net was removed from the mold, washed with ethyl alcohol, dried out and prepared for the next stage. The silver ion accumulation layer was prepared by using a mix of gelatin and agar (at 90%/10% ratio) warm suspension (40–45 °C) which was poured into a Petri dish with the already manufactured 3D silicone net. The silicon net was placed on the bottom in the Petri dish, and the gelatin-agar mix was poured up to 2 mm level (to fully cover the silicone net). After several hours, gelatin-agar became hard, and the 3D silicon net, filled with gelatin-agar, was re-placed from the Petri dish onto the DLC:Ag group of samples containing 3.4 at. % Ag, coated with 0.01–0.02 mm of the thin

layer of cellulose. For a better contact, a few drops of warm (38–40 °C) gelatin were applied as a glue. Such a silver ion accumulation layer preparation technique allowed avoiding air burbles formation inside the 3D net cavities.

The silicon honeycomb structure was manufactured as the final layer and was filled with the agar/gelatin water-based mass. The small area of the direct contact of the silicone net structure to the wound surface provided antistick properties, and the silicone net partitions were responsible for liquid gelatin mass restriction on the treated area. The assembly process of the bandage was performed in a laminar box to ensure sterility. Finally, the bandage was assembled on a sticky medical film with microholes, the sandwiched layers (DLC:Ag on silk, protective and Ag^+ accumulation layers) were sewn up (through all layers) by using a 0.006 mm sterile braided line to the sticky film.

3.6.1 Antimicrobial effect of SIAL layer integrated in bandage prototype

The effectiveness of the silver ion accumulation layer was evaluated by applying microbiology tests with the referential bacteria (see Fig. 22) and pathogenic bacteria (see Fig. 23). In order to compare SIAL layer effectiveness, first of all, the DLC:Ag group of samples (without SIAL) containing 3.4 at. % Ag of 6 cm^2 was immersed into 1 ml of volume of purified water and sustained in thermostat for 35 °C in order to observe the silver ion migration process into distilled water. The prepared prototype with SIAL had an even stronger and faster effect than the nylon fabric coated with DLC:Ag (see Fig. 22 and Fig. 23). After prototype application into the bacteria suspension at 35 °C, the SIAL layer dissolved and spread out the accumulated silver ions, and a strong antimicrobial effect was obtained. After 20 min, the bacteria population was reduced by 70.7%, whereas, after 120 min, the CFU number was reduced by 92.6%, and, after 340 min, the CFU number decreased by 99.6% in the samples with the referential bacteria (see Fig. 22).

The results of microbiological experiments when applying GoS 2 containing Ag of 3.4 at. % and the bandage prototype (with the SIAL layer) involving highly pathogenic *S. aureus* bacteria strains LTSa635 (MRSA), LTSaDA01, LTSaM01 and LTSa603 are presented in (Fig. 23). After microbiology experiments with GoS 2 and the bandage prototype, the results are presented as follows:

Antimicrobial tests with bacteria strains LTSaDA01, LTSaM01 and LTSa603 showed that, after 20 min of exposure time, GoS 2 with DLC:Ag-coated nylon fabric affected (killed) 10%–15% of *S. aureus* bacteria CFU when the prototype with the SIAL layer killed 63%–65%, respectively. Tests with methicillin resistant (MRSA) *S. aureus* strain (LTSa635) exposed for the same duration showed the antimicrobial effect efficiencies of 9% and 55%, respectively. After 60 min of treatment time when applying the group of samples containing 3.4 at. % of silver, the bacteria CFU (LTSaDA01, LTSaM01, LTSa603) number decrease was more than 60%. A stronger antibacterial effect was obtained with the bandage prototype improved with the SIAL layer. After 60 min of experiment time, the bacteria CFU number decreased by about 80%. MRSA (LTSa635) strain was more resistant to silver ions than other bacteria strains, and the group of samples with the thin film of

DLC:Ag 3.4 at. % Ag reduced the bacteria LTSa635 CFU number by 47%, and the proposed bandage prototype with SIAL was able to reduce the CFU number by about 80%, respectively. The tests data revealed, that after an hour of testing time, the prototype with SIAL equally affected all bacteria strains, even MRSA. After 2 hours of soaking the group of samples (3.4 at. % Ag) in test tubes with bacteria strains, more than 92% of CFU were inactivated, whereas the prototype with SIAL was able to inactivate more than 95% of all bacteria strains, including MRSA (see Fig. 23, C). Antimicrobial testing results after the longest exposure time (320 min.) revealed that the group of samples with 3.4% Ag (at.%) and the proposed prototype had a similar antimicrobial effect – more than 99% of all bacteria CFU were killed, and the spread plate method results revealed that only a few bacteria CFU grew on the agar surface.

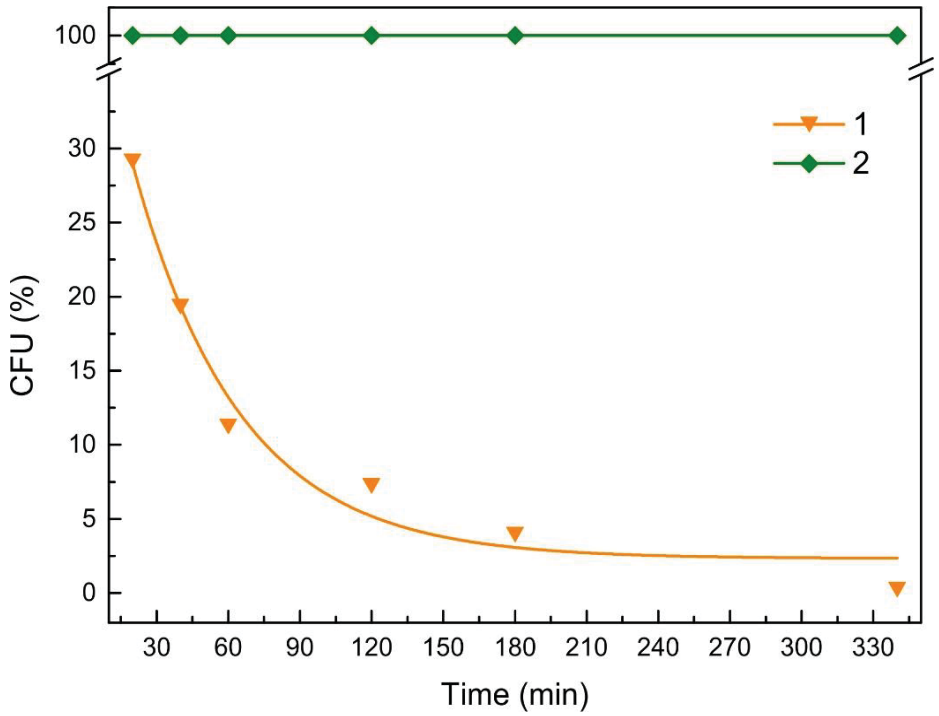

Fig. 22. Antimicrobial results (with referential bacteria 0.5 Mf) of the bandage prototype: SIAL layer (1), control measurements (2), the prepared prototype was soaked in bacteria suspension which was placed in thermostat at 35 °C temperature

The results of antimicrobial tests confirmed that the RF plasma etched group of samples with DLC:Ag (3.4 at. % Ag) showed antimicrobial properties against the pathogenic bacteria, and therefore it can be used for wound treatment. According to the experimental results, the bacteria can be killed at more than 99% of efficiency by using DLC:Ag (3.4 at. % Ag) thin film coatings on the nylon fabric, or by using the proposed prototype. The main difference between these samples (GoS 2 and the

bandage prototype) is the antimicrobial effect action time or the bacteria killing speed. Similar studies performed in [15] with silver doped DLC coatings showed similar antimicrobial properties with other bacteria species. It was found out that the amount of bacteria (specifically, *Clostridium jejuni* and *Listeria monocytogenes*) was strongly reduced after 15 min. of exposure time, and, after 24 h, bacteria CFU was below the detection level [15]. Other authors obtained results which showed that the Ag ions release speed was fast during the initial 24 h, and the sustained release continued for several days [210, 215]. According to these research results, it can be claimed that silver ions can be accumulated into the SIAL layer, and, after layer dissolution, the silver ions can diffuse (from DLC:Ag layer in bandage) into bacterial suspension, while sustaining the silver ion concentration necessary for the antimicrobial effect for more than 24 h. Other authors in their studies with silver NPs of 300 ppm. concentration confirmed that a large concentration of silver still cannot kill all bacteria to count zero after 30 min, while such results can be achieved after 48 hours [241].

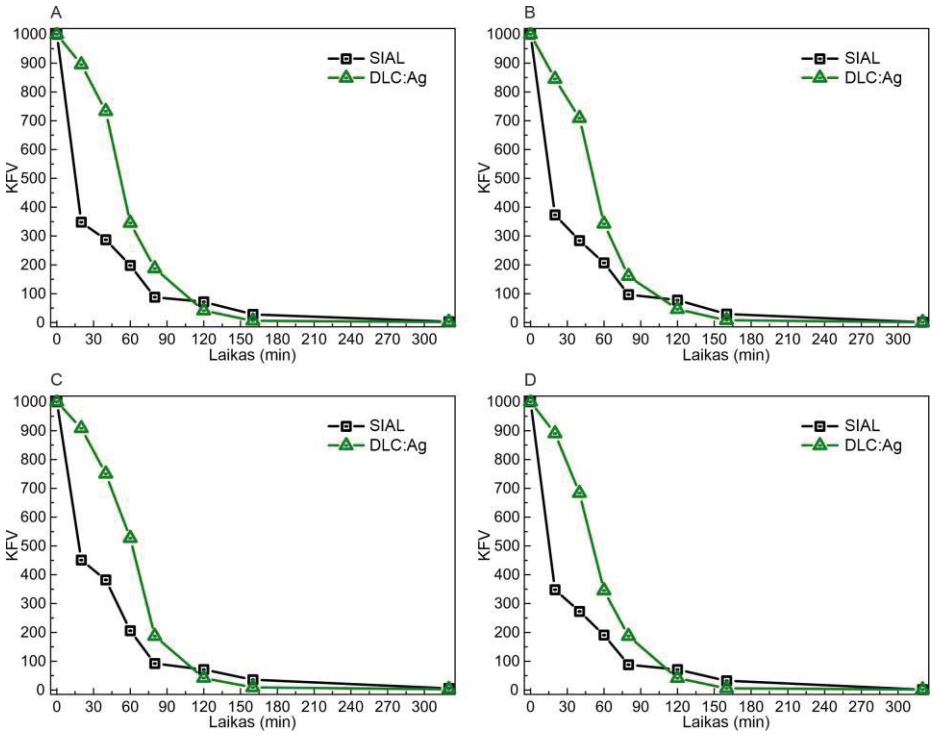

Fig. 23. Antibacterial test results with *S. aureus* bacteria strains: (A) LTSaDA01; (B) LTSaM01; (C) LTSa635 (MRSA) and (D) LTSa603, bacteria concentration: 1 Mf = $3x10^8$ CFU, dilution 10^{-5} and DLC:Ag is the background of bandage, SIAL: DLC:Ag coated silk with cellulose and gelatin/agar layers (for the first bandage prototype, see Fig. 20)

On the other hand, research [242] showed that 100% antimicrobial effect can be achieved after 72 h of contact of silver nanoparticles in a bacteria culture media. According to the experimental data of the current work, 100% efficiency was not achieved, and the maximum antimicrobial efficiency of 99.9% with bacteria LTSaM01 were obtained by employing the second group of samples with 3.4 at.% Ag and the bandage prototype with GoS 2 and the SIAL layer, respectively. The explanation why 100% antimicrobial efficiency was not achieved could be the bacteria Stationary Phase [169] and the condition of non-replicating bacterial persistence [243]. For the maximum antimicrobial effect, other research [78, 97] works suggest employing larger concentrations of silver ions for pathogenic bacteria. The author of [97] suggests 8–80 ppm concentration of Ag ions for *Staphylococcus aureus* for 10^5–10^7 (CFU)/ml concentration.

Moreover, most pathogenic organisms (including *S. aureus*) can be killed at silver ion concentrations of 5–40 ppm [78, 97]. Other authors in their research works found out that 15 ppm of the concentration of ionic silver can inhibit the oxidation of glucose, glycerol, fumarate, succinate, D-lactate, L-Lactate, and other endogenous substances in *E. coli* bacteria strains [97]. On the other hand, high doses of silver can be toxic for all live organisms, not only for bacteria [47, 97, 118], and the proposed bandage which can create 4 ppm silver ion concentration in the aqueous media, as presented in the current work, can be used as a safe bandage for an organism due to its good antimicrobial properties.

To sum up, the prepared bandage prototype with SIAL had stronger antimicrobial properties and offered faster antibacterial action speed comparing with DLC:Ag coated GoS (3.4 at. % Ag). According to the experimental results, it was determined that silver nanoparticles play an important role for silver ion transmission and accumulation processes into a gel-like structure (SIAL) which can dissolve and release all the accumulated silver ions instantly. Our results showed that such a technology could be applied for wound dressings whenever time plays an important role, and bacteria have to be inactivated within a short period so that to prevent efficient multiplication of CFU in the affected tissues [59, 244].

3.6.2 Bandage prototype stability tests

Before tests with animals, stability tests were performed. The bandage was stored in a laboratory, at room temperature, packed in a vacuum polyethylene bag for 6 months. There were no visible changes after this period. No changes of antimicrobial properties were registered throughout the entire testing period. Antimicrobial activity tests (the spread plate method) showed good results, and there were no indications registered of any reduced antimicrobial activity. Tests for the skin reaction after 6 months of storage (allergic tests) were conducted with guinea pigs. They showed no redness or inflammation signs. According to the test results, the bandage prototype could be deemed safe for application on a wound after 6 months of storage.

For such a bandage, strong silver NPs adherence to the supporting surface, such as DLC coatings, is essential for the practical use [81] because the silver release properties depend on the contact of water molecules with the surface of

active nanoparticles [16, 93, 108]. When barriers (a thin cellulose layer in the current bandage prototype) are used for stabilizing the coating's surface, the silver ion release properties can be reduced due to lack of water uptake which should be sufficient for high Ag^+ release [225]. In the current case, the thin cellulose layer inside the bandage was able to transmit easily silver ions through the membrane, and reduction of antimicrobial properties was not detected during the testing period. It is known that, for optimal antimicrobial activity [92, 240], the stability of Ag nanoclusters plays an important role because aggregating particles decrease the contact surface and the Ag^+ release rate [169].

In addition to the efficient antimicrobial properties, the current bandage with the SIAL layer featuring the nylon fabric skeleton ensured good mechanical properties, ant the cellulose layer, serving as the membrane, detained particles and debris [105, 245] inside the bandage, in the proximity to the DLC:Ag surface. Moreover, it passed the silver ions from the NPs surface to the SIAL layer, and the bandage was stable without undergoing any changes of its microbiology properties for more than 6 months.

3.7 Bandage prototype pilot study with lab animals

In the current chapter, the bandage prototype along with control bandages were tested on lab animals. Small injuries (up to 34 mm) were made for our wound healing experiments, one group of wounds was uninfected, whereas the second group was infected with *S. aureus* (MRSA). The bacteria suspension of 0.5 Mf of 20 µl was applied into the wound on day 0, and the CFU number in the wound's fluids after days 1–3 was determined by applying microbiology methods – i.e., samples were taken with a cotton swab from the wound's bed, and later were rinsed, mixed in a test tube, then diluted to 10^{-2} and inoculated on the agar surface. The experiments were conducted by using 8 lab animals per one experiment (n = 8).

3.7.1 Cotton bandage testing

For pharmaceutical evaluation (with lab animals), tests with wounds were performed. In the testing procedure, several parameters were observed: the wound's inflammation signs, redness, tissue regeneration, and bacterial pollution inside the wound. The lab animals – guinea pigs – were selected for experiments so that to define all the healing process during a shorter period of time, such as several days, rather than a week if comparing with humans [246]. In the current experiment, a wound was defined as *healed* when 90% or more of the wound's surface was reepithelialized [249] on the wound healing area.

In the course of the first experiment, an ordinary cotton bandage was applied on the lab animal's wound. The next day, a cotton bandage was sticked to the wound due to scab formation which was removed during the wound observation process. The sticking of the cotton bandage to the soft wound tissues had unwanted consequences. During the process of removal, a part of the healing soft tissues was damaged in the process of investigation [247]. Due to scab formation, the healing process was too complicated for the evaluation of the treatment effect (see Table 6, bandage 0). The wound exudate (with lymphocytes and proteins) reacted with the

biomaterials applied on the wound surface and caused inflammation [38, 39]. It is well known that the wound itself can create excellent conditions for microorganisms to grow [31, 33, 61], which can delay the healing process and lead to an infection [50, 107], as determined in bandage testing. These processes are unwanted because mammalian wounding responses may result in nonfunctional fibrotic tissue formation [19, 248] which can be referred to as the scar tissue [33, 37], which is exactly what was observed in tests with the control bandage. On the other hand, animals can restore wounded tissues or organs to a varying degree, according to the species and the developmental stage [35, 247], and thus not all animals can be used for the testing of pharmaceuticals which will be used on people.

The purpose of healing is to recover the skin functions [44], and this physiological process involves coagulation, inflammation, proliferation, matrix and tissue remodeling stages [46, 249]; these healing stages were monitored and registered during the bandage testing experiments. The wound tissue repair starts immediately after employing various growth factors [33, 40, 46] which involve all skin cell types responsible for all wound healing stages [19, 33, 35]. The surface of cotton bandages can be absorbed by proteins like albumin with fibrinogen and can elicit foreign body reactions by increasing the inflammatory response and prolonging the wound healing process [104]. This effect was observed in the cotton bandage testing; then, the wound healing continues more than 5–7 days. The adhered dressings had a negative effect on repairing the tissues due to the epithelial layer disruption during the dressing removal procedure as observed in the current experiments as well as in other authors' experiments [36, 42, 44].

3.7.2 Tests with control bandage

The control bandages were prepared by using nylon fabric without DLC:Ag thin film, with cellulose and an agar-gelatin layer, without a 3D silicone net (Table 6, No. 1), and an identical bandage with a 3D silicone net with agar-gelatin inside the cavities (Table 6, No. 1A) was also used. The aim of the current experiment was to investigate the SIAL effect on a wound without silver ions being involved, and to compare the wound healing outcomes with the bandage prototype containing a DLC:Ag coated film featuring 3.4% Ag (at. %). In the current research, the control bandage (Table 6, No. 1) was applied on an MRSA infected wound in order to determine the healing effects. After the experiments, the bandage yielded better healing properties [42, 249] comparing with the cotton bandage; on the other hand, a disadvantage was observed that the prototype got stuck to the wound's surface. The sticking effect was caused by the outflow of the agar-gelatin layer, where gel remains were dried out thereby causing the issue of sticking; also, the bandage became hard and inflexible when the gelatin/agar layer was outflowed and dried out. Due to that reason, a small scab was observed on the wound's surface throughout the entire 3 days, and the contraction of the wound's length was from 30 to 25 mm. Tests with wounds infected with MRSA bacteria after 24 h showed wound tissue inflammation signs, such as redness and/or tissue swelling during the control bandage testing time (Fig. 24). A sample for microbiology analysis was taken on days 1–2, and bacteria CFU were found: on the first day184 CFU were found, and,

on second day, the CFU number was reduced to up to 128 CFU (see Table 6, No.1). The reduction of CFU was induced by the strong immune system of the guinea pig [37, 42, 128], and, on day 3, the CFU number was reduced to 78. The immune system activity of the guinea pig was observed by the healing analysis throughout the 2 days, the swollen areas were reduced, and healing process started, but, on the other hand, the wound's soft tissues were of dark red color, and a scab was formed. The healing process continued up to day 5, when the scar tissue formed, and the wound's soft tissues were regenerated [33, 99]. The tests with the bandage (Table 6, No. 1A) with SIAL in which the 3D silicone net cavities were filled with the agar-gelatin mass (without silver ions) offered better healing properties, the scab was not formed on the wound's surface, and the CFU number decreased from 172 to 64 from day 1 to day 3.

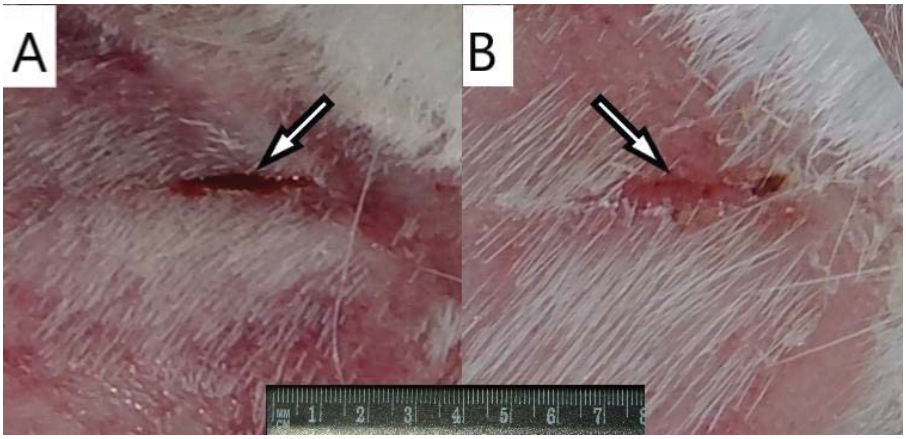

Fig. 24. MRSA infected wound treatment with control bandage: (without silver, No. 1); after 2 days: A, after 4 days of treatment: B, wounds are marked with arrows

The reduction of the CFU effect occurred due to the strong immune system, it positively influenced the healing effect, i.e., such blood cells as neutrophils were the first defense barrier against the bacteria [31, 250]. In the liquid fluids of the wound, mixed with the agar-gelatin mass, blood cells can migrate towards the bacteria and eliminate it by phagocytosis, by releasing proteinases which initiate the bacteria inactivation process in the wounded tissues [37, 250].

3.7.3 Wound treatment with bandage prototype

The bandage prototype containing DLC:Ag 3.4 at. % Ag thin film, cellulose and SIAL (see Fig. 21) was applied on MRSA bacteria infected (Table 6, No. 2) and uninfected (Table 6, No. 3) wounds so that to compare the healing effect.

The experimental data with the MRSA bacteria infected wounds and the bandage prototype after the first day of treatment showed that the wound tissue healing process was good: the tissues were of the pink color, minimal swelling was observed comparing with the control tests (see Fig. 25). The microbiology results

showed, after one day the live bacteria CFU number reduced from 184 to 91 after the application of the bandage prototype if comparing with the control tests (Table 6, No. 2). After the second day, the CFU number was reduced from 91 to 54, and the healing process was evaluated as good. The action time of silver ions was essential for the bandage's strong antimicrobial effect [93, 216] when it was being applied on the infected wound. On day 3, the wound morphology analysis showed that the edges of the wound were sharp, and no visible inflammation signs were observed.

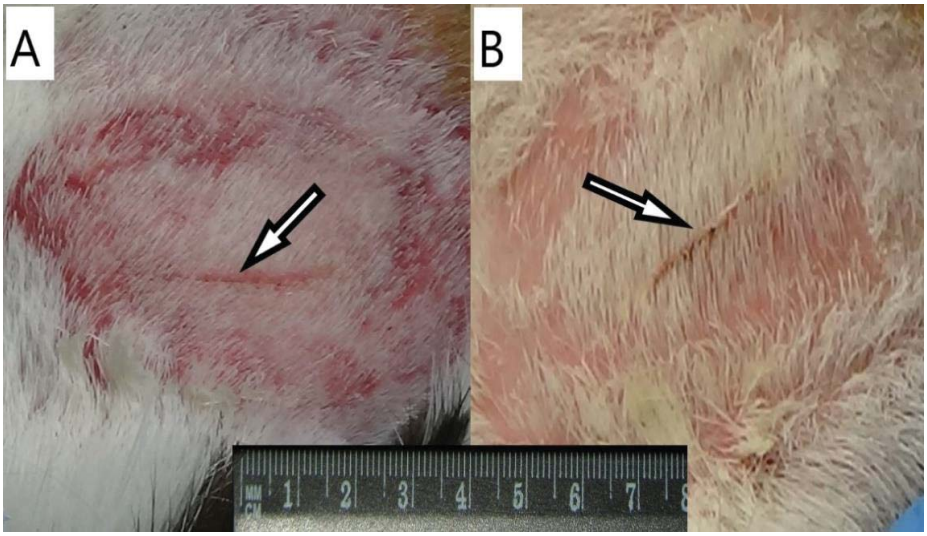

Fig. 25. MRSA infected wound treatment with bandage prototype: A: after 2 days, B: 4 days after treatment

The regeneration process of the wound tissues was clearly visible, and the wound's length/depth ratio was reduced. No bacteria CFU was found inside the wound tissues after the microbiology testing procedures, and the wound contracted. It was found out that silver can reduce the amount of MRSA bacteria in chronic wounds after silver bandage application [59], and it is known that chronic wounds can sustain more bacteria with different resistance [19, 36, 61]. A long-lasting bandage with a high silver ion concentration level is needed to achieve the best healing effect as determined in the current tests. The anti-inflammatory effect of silver (due to bacteria activity) can occur due to the suppression of the complement activity, and these physiological properties can influence the results of positive healing as presented in [46, 224]. Moreover, the authors of [45, 215] observed the correlation between the bacteria adhesion to the skin or wound tissues and the effectiveness of treatment. Adhesion can involve reversible bacterial association during the early hours, i.e., after post-implantation, it can be followed by stronger bacterial adhesion to the surface [171], and, after 24 h, bacteria can form a biofilm [2] which is resistant to systemic antibiotic treatment. This effect can appear regarding the host defense mechanism, when bacteria at the margins of the colony protect the bacteria in the inner zones [17, 127]. According to these wound healing properties, the fast silver ion release from the SIAL layer can protect the wound

surface from the biofilm formation and kill a large scale of bacteria in the wound bed as it was presented in the current research. But, on the other hand, the silver action *in-vitro* can be different, comparing with the experiments *in-vivo*, as determined by [27, 47, 116]. These differences can be induced by the silver ion interaction with organic molecules, proteinaceous exudate or inorganic ions such as sulfates, phosphates or chloride, which can react with silver and form AgCl salt of very low solubility; as a result, reduction of the number of free silver ions in the wound's bed was achieved [59]. When such a bandage (without the SIAL layer) is directly applied on the wound's surface, the chemical reaction between the silver ions and sodium chloride [40, 219] (in the blood plasma) can induce the negative effect for the Ag^+ release rate. Silver chloride is almost insoluble salt [40, 102, 218] and can reduce the amount of free silver ions to minimum and cover silver NPs with the chloride layer thereby reducing the Ag ion release rate [251]. In the current research, the SIAL layer can sustain a higher release rate of silver ions and maintain the process for a longer period of time, and thin films or membranes between the NPs layer and the wound fluids can protect silver NPs from the chemical reaction with Cl ions [40, 211]. The SIAL layer can reduce the chemical reactions with silver nanoparticles [93, 99] and sustain the strong antimicrobial activity [249] close to the wound's surface inside the gelatin/agar liquid gel. Otherwise, the slow release kinetics of silver ions results in slow silver depletion, and this feature minimizes the potential toxicity; thus, the coatings can be effective for a longer period [96].

It is known that antimicrobial properties are directly related with the concentration of silver ions in a bacteria rich media [252] like in the MRSA polluted wound, as presented in the current research. A wound dressing (without SIAL) containing silver NPs can release only 0.6 ppm of silver per 24 h as determined by [251], while the DLC:Ag coated and SIAL layer improved bandage can release up to 4 ppm, respectively. This effect may be explained as silver NPs exposure by Cl ions [251]. On the other hand, the local pH reduction [95] in wound fluids and aerobic environment changes [104] may enhance the silver release rate from the coatings to the water rich media. Otherwise, according to [253], approximately 39% more silver was released into alkaline sweat (pH 8.0), as compared to acidic sweat (pH 5.5). Healthy skin pH is slightly acidic, at the level between 4–6 pH [254], while, for an infected wound, its pH usually moves to a neutral or a slightly alkali pH value [253, 254], and a wound infection in lab animals might increase the Ag ion release and the healing speed, respectively. The authors of [46] established that, for example, Ag NPs not only increased the healing speed of the wound, or had the repairing effect for the dermal tissue, but also improved the cosmetic appearance in the animal model [169]. After the application of the current bandage prototype, only the mark of injury (Fig. 25, B) was observed in the epidermis layer. This good healing effect occurred due to the suppression of inflammatory cytokines and induced apoptosis of the inflammatory cells [29, 244]. The reduced inflammatory process can suppress the scar formation process [31, 46], which leads to minor marks [33] of injury after the healing procedure. After the conducted tests with the bandage prototype (Table 6, No. 2), the healing process without any strong inflammation signs was observed.

The wound tissues were of the light pink color, and small growing blood vessels were observed at the wound's edges and its bottom.

Table 6. Wound healing observation of lab animals*

No. / d	Cut length (1-3 d) mm			Capillary net growth			Swelling			Redness			Scab			Bacteria CFU		
	1	**2**	**3**	**1**	**2**	**3**	**1**	**2**	**3**	**1**	**2**	**3**	**1**	**2**	**3**	**1**	**2**	**3**
0	31	30	28	n	p	p	p	p	p	p	p	p	p	p	p	-	-	-
1	30	28	25	n	p	n	p	n	n	p	p	n	p	p	p	184	128	76
1A	29	27	25	p	p	n	p	n	n	p	n	n	n	n	n	172	106	64
2	32	30	29	p	p	n	n	n	n	n	n	n	n	n	n	91	54	0
3	26	22	18	p	p	n	n	n	n	n	n	n	n	n	n	-	-	-

Legend of the Table: p – positive, n – negative effect. Several different types of bandages were tested; 0 – cotton bandage on uninfected wound; 1 – control: agar-gelatin spincoated bandage prototype without DLC:Ag, applied on infected wound, 1A – nylon fabric (without DLC:Ag) with SIAL on infected wound, 2 – bandage prototype with DLC:Ag and SIAL layer applied on infected wound, 3 – bandage prototype with DLC:Ag and SIAL layer applied on uninfected wound

On the second day, the tissues were of the darker pink color due to capillary net regeneration, and the wound was less deep in comparison with the first day. The length of the wound decreased, and the good healing effect can be explained as follows: the bandage applied on the uninfected wound's surface warmed up, and the gel in SIAL melted quickly thus releasing the accumulated silver ions into the wound's bed. The silver ions worked as 'healing promoters' [2, 10, 16, 19] and were replaced by tissue fluids; the silver ions diffused from the bandage to sustain the silver ion concentration [41]. Moreover, serum albumins in the wound's bed or inside the bandage can enhance the silver ion release process [40, 95]. This effect is based on the formation of silver chemical complexes on the molecule's surface of blood plasma proteins, when silver detaches from the molecule surface and strongly increases the amount of Ag^+ ions [95]. On the other hand, the molecular complex formation can depress the Ag release [94, 107], and the bandage structure in which the layers are incorporated can eliminate this factor. Moreover, silver can speed up the healing effect according to [224, 247] due to the increase of the collagen fibers accumulation in the extracellular matrix and differentiation process of keratinocytes. In the current research, the wound healing process was observed every 24 h during the investigation of bandage application. After closer analysis of the wound tissue, no swelling or strong redness were observed. The bandage was not sticked to the wound surface the way it happened with cotton and control bandages (Table 6, No. 0 and 1, respectively), and it was removed without resistance and without any soft wound tissue damage. The bandage SIAL layer with silicone partitions (Table 6, No. 1A) was able to sustain the melted agar-gelatin mass on the wound surface, and no scab formation process was observed. It was confirmed that the liquid agar-gelatin

mass reduced the scab formation process and increased the healing speed from 5 days to 3 days.

From the data obtained in the current experiments, the most prominent healing effect was observed with uninfected, i.e., bacteria free wounds as the wound contracted faster comparing with MRSA infected wounds. After 5 days of treatment, almost no signs of the wound were found in cases of infected and uninfected wounds, respectively. These results confirmed that silver applied on wounds can increase the healing speed as it was determined in [169], and it reduced the residual effects of the injury due to the suppression of the inflammatory process [46, 244]. Other authors [59] claim that nanocrystalline silver dressings can reduce the total amount of proteases in wounds while encouraging optimal patterns of healing and reducing the inflammation process in tissues [40, 80]; as a result, minor scar signs were observed in the current experiments when wound healing was being monitored. Similar tests with lab rats [124] revealed that nanocrystalline wound dressings, when applied on burned wounds, can increase the number of the surviving lab animals [88, 247].

But, on the other hand, silver-based products should be used with caution when wounds with donor cells are treated, similarly to the case of wounds after burns, because silver (silver ions and NPs) may do harm for rapidly proliferating cells [124, 125]. In the current bandage prototype, the cellulose layer and the SIAL structure were used to avoid Ag NPs migration, and, in the second bandage prototype, the silver ion concentration reached a level of up to 4 ppm. The authors of [17, 169] suggested to control the silver ion release rate for tissue safety and for antimicrobial efficiency reasons, the way it was being done when applying the cellulose and SIAL layers in the current bandage prototypes. In order to ensure the silver ion release control, the SIAL layer performed the essential role for the accumulation of silver ions up to the saturation level and for high speed distribution of Ag ions inside the wound tissues, respectively. The minimum silver ion concentration for *S. aureus* bacteria starts from 1 ppm [220], although other authors [40, 94, 255] found out that larger concentrations are needed. For example, it was determined [18, 72] that the inhibitory concentrations for all bacteria are between 3.37 and 13.5 ppm, which inflicts no significant cytotoxic activity for organism.

In the current research, no harmful effect of the bandage prototypes was observed comparing with the cotton bandage and the bandage without DLC:Ag. The large doses of silver applied for guinea pigs may cause histopathological abnormalities in the skin, liver and spleen [128], but, in the case current study, no animal death or signs of toxicity were observed, exactly as in other authors' researches [252].

The toxic dose of 300 mg of Ag Np for lab rats was discovered, and such a dose induced slight liver damage; also, dose-dependent accumulation in all the tissues was observed [99]. Smaller silver doses (ranging from 10 to 100 mg/L) can be tolerated by mammalian body cells [229]; such doses are toxic for bacteria. Such doses of silver were not reached in the bandage prototype, only 4 ppm of silver ions can be released to the skin surface. Moreover, the DLC thin films which are used in the bandage have no toxic effect as determined in [132], and they can be applied

safely for body cells. DLC is a chemicals-free coating, and, unlike nanocrystalline silver containing wound dressings, no chemical remains after NPs synthesis were found [82]. Chemical remains could induce such side effects as wound surface overhydration and maceration of the surrounding healthy skin [59]. In the current work, the tested bandage showed no visible toxic effect for the animals. No skin color, tissue and/or animal behavior changes were observed. All of the lab animals successfully healed, and no cases of death were registered.

3.8 Working mechanism of bandage prototype

The purposes of wound dressings are to increase the healing effect, reduce the pain and bacteria-initiated inflammation [44, 107, 249], and the ideal wound-dressing could be described as follows: wound site protection from any environmental impact, wound moisture maintenance, gas diffusion, temperature and pH control, easiness to remove without pain [107]. Extensive discussion about silver as an antimicrobial agent can be found in various medical fields, including infectiology, surgery with burns and wound treatment, etc. Usually, surfaces contaminated with bacteria can be sterilized by applying disinfectans with the alcohol base, but wound tissues can be damaged; in this case, other antiseptics are used. What concerns wound treatment, especially open wounds, for example, after burns, a questions arises: (a) what type of medical device can be applied; (b) what will the side effect(s) be; (c) will it be effective? When answering these questions, a hypothesis was raised about the bandage working mechanism: bacteria multiply and produce toxins in a moisture rich environment. In this context, the antimicrobial agent has to be delivered to bacteria with effective concentration, also, the antimicrobial agent has to be less toxic to the organism cells than to the bacteria. As a result, the NPs concentration and Ag ions concentration has to be selected properly, and, finally, the device construction and the working mechanism could be recreated by copying the burn blister formation physiology process after burns of second degree. In this case, regenerating wound tissues have no mechanical contact, the exudate inside the blister is sterile and ensures the ideal condition for the cell regeneration and wound healing. While implementing the research, the proper silver ion source was selected, and the bandage structure was created which imitated the artificial sterile segmented blister with an antimicrobial filler inside which can be placed onto the damaged skin area.

Before the experiments, several questions were raised: (i) what is the silver ion concentration which is necessary for antimicrobial activity; (ii) what is the antimicrobial effect difference between silver ion saturated water and silver NPs coated surface; (iii) what is the optimal silver ion concentration for the efficient antimicrobial action so that to avoid organism cells intoxication? The silver ion release mechanism was determined by applying several tests, including disc diffusion, silver ion saturation of distilled water, silver ion saturated water and rinsed DLC:Ag coated surface antimicrobial effect in the time scale.

The working mechanism (see Fig. 26) of the patch was determined after data analysis of the conducted tests. The current bandage with the DLC:Ag coated nylon fabric skeleton and the SIAL layer ensured good mechanical properties for the

prepared patch prototype, and the cellulose layer, as a membrane between the DLC:Ag thin film and SIAL, sustained particles and debris on the thin film sputtered nylon fabric, i.e., inside the patch. The silver ion release properties and the antimicrobial activity of the prepared DLC:Ag (3.4 at. %) sample and the prepared prototype with SIAL was investigated. Data analysis showed that the SIAL layer worked slower comparing with 4 ppm saturated distilled water, the antimicrobial delay effect was related with the dissolving time of the SIAL layer. The DLC:Ag thin film coated sample exhibited a strong and long-lasting antimicrobial effect, while 4 ppm saturated water demonstrated a strong but short-timed effect. The experimental results showed that the prepared prototype with DLC:Ag (3.4 at. % Ag) had more than 99% antimicrobial efficiency per 340 min (referential *S. aureus*), and 100% of MRSA CFU were killed in the wound after 72 h.

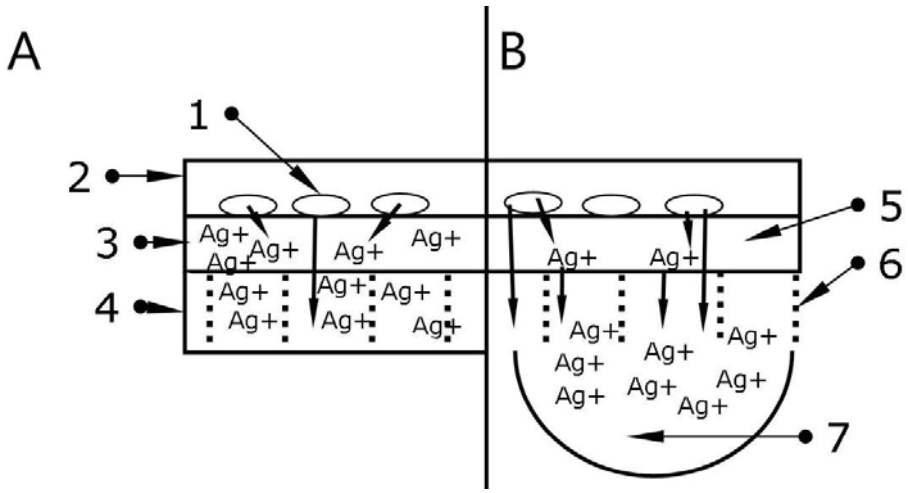

Fig. 26. Bandage prototype (A) working mechanism: silver ions start to migrate from silver NPs (1) to low silver ion concentration zones (5) through the cellulose membrane (3) to agar/gelatin layer (4) (SIAL); when bandage is placed on wounded skin (B), the gelatin/agar (gel) in SIAL layer warms up, gel in cavities (between silicone partitions (6)) melts and can move towards the wound's tissues (7) and transport and release all accumulated silver ions close to the bacteria contaminated areas

Accumulated silver ions spread out from gelatin to the solution after application on the warm skin surface or after immersion into a warm (35 °C) bacteria suspension, as presented in our experiments results. The SIAL layer with gelatin/agar became liquid after warming up to 35 °C, and it can be diluted with bacteria suspension or blood plasma. The dilution of the silver ion saturated gelatin/agar melted mass can induce the strong antimicrobial effect because the gelatin/agar with the accumulated silver ions dissolves and can spread throughout the entire bacteria rich media as determined by our bandage prototype antimicrobial testing results. On top of that, it was determined that the free silver ion concentration

in the bacteria suspension decreased, and this result correlated with reducing antimicrobial properties, and a similar effect was received in [126]. This effect can be explained as the sublethal binding process of Ag ions to bacteria [126], i.e., silver ions are 'consumed' [40, 126] by bacteria, and the concentration of active silver ions decreases. To solve the problem of the reduction of silver ions and the decrease of antimicrobial properties, nylon fabric coated with the DLC:Ag thin film layer with the silver concentration of 3.4 at. % was integrated inside the bandage prototype as the source of silver ions. After SIAL dissolution into the warm bacteria suspension, the silver ion concentration decreases, and the Ag^+ release (migration) process begins from the surface of silver NPs embedded into the DLC:Ag matrix (see Fig. 26). This mechanism can restore the silver ion concentration in the diluted gelatin/agar layer (SIAL) or in the wound's fluids and sustain the antimicrobial activity [71, 256].

The high silver ion concentration ensured not only the rapid CFU number decrease rate, but also the long-term antimicrobial effect, as it was also determined in [40, 96, 127]. In this double silver ion release system when silver ions can be accumulated until the saturation level of 4 ppm, and when the saturation level decreases due to the dissolution into the watery media, silver nanoparticles can restore the Ag^+ concentration and continue the releasing process of Ag ions from silver NPs embedded into the DLC matrix to the liquid media. Moreover, the prepared bandage prototype had the antistick properties which were tested and proven during the experiments with animals, and the antistick properties were developed after silicon 3D net installation into the SIAL layer, since the low contact surface (between the net partitions and the wound tissues) reduced the ability to stick to the surface, and the melted gelatin/agar gel enhanced these properties even more. It was determined [10, 249] the wet bandages, like those made from hydrogels, featured antistick properties, and dressings with a more adherent contact to the wound surface did not offer such good results as those obtained in our tests with the first bandage prototype and the tested commercial cotton bandage.

Silver ions can interact with organic molecules as well as with inorganic ions like sulfates, phosphates or chloride, which can react with silver and form the insoluble AgCl salt – thereby reducing the concentration of free silver ions [59] and negatively influencing the test results. Silver chloride is an almost insoluble salt [40, 102, 218], and it can reduce the free silver concentration to the minimum and cover silver NPs with a silver chloride layer, thus strongly reducing the Ag ion release rate [251] from the sputtered surface. Moreover, it was determined that the molecular complex formation can depress Ag release [94, 107] when direct contact with NPs is available. Liquid gel and other membranous structures, installed in the prototype, can reduce this effect. SIAL can sustain a higher and longer release rate of silver ions. It works as a protective layer, obstructs the direct contact of NPs with blood, and can protect silver NPs from chemical reaction with Cl ions [40, 211], sustain the strong antimicrobial activity [249] close to wound's surface as well as inside the gelatin/agar liquid gel which was located inside silicon honeycomb cavities. Otherwise, the slower kinetics of silver ions release, which was obsrved in

experiments, influence the slow silver depletion, and this property minimizes the potential toxicity; also, coatings can be effective for a longer period [96].

Bacteria biofilm formation (in 60% of cases of chronic wounds) [257] is one of the factors in the process of wound transitioning into the chronic state, and the bandage in the current research was created with the objective to avoid chronic cases by reducing the bacteria CFU within a short period of time. The bandage applied on a wound had a contact with the soft wound tissues where the exudate and nutrients from blood can increase the bacteria biofilm formation and cause serious infection [250, 257]. The presented prototype with the SIAL layer of the bandage prototype saturated the wound's fluids with silver ions and sustained antimicrobial environment in the wound's bed for optimum healing.

4. CONCLUSIONS

1. The prepared 3 groups of samples with DLC:Ag thin films on the nylon fabric deposited by the DC unbalanced magnetron sputtering were processed by RF oxygen plasma etching (0.3 W/cm², 20 s); the silver concentration in the first group of samples increased from 0.46 to 0.93 at. %, in the second group from 3.12 to 3.4 at. %, and in the third group from 5.31 to the 6.9 at. %). Silver NPs size was found to be dependent on Ag concentration and varied from 3 to 63 nm, (the average size of silver NPs in the first group of samples was 16.1 nm, in the second – 23.7, and in the third – 28.8 nm, respectively).
2. RF oxygen plasma etching for 20–25 s was found to be efficient in terms of the increase of the silver ion release, and the second GoS demonstrated the best silver ion release properties, i.e., up to 4 ppm per 24 hours after 20–25 s of RF plasma processing time.
3. Effective silver ion concentration against *S. aureus* bacteria (0.5 Mf) was found to be less than 1 ppm, and the strongest antimicrobial activity was obtained with 4 ppm. The best antimicrobial properties against all *S. aureus* bacteria strains on the agar surface and *in-vitro* (killing 83% bacteria within 120 min) were demonstrated by the second group of samples (3.4 at.% Ag).
4. Silver ions and nanoparticles *in-vitro* induce cell wall changes for *S. aureus* bacteria, and it was determined that silver ions and silver NPs damaged the bacteria cell's walls in a similar way to penicillin. After treatment with silver ions and silver NPs, the bacteria were inactivated (killed) at a rate of 76% and 80%, respectively.
5. The bandage prototype was successfully prepared by applying the DLC:Ag (3.4 at. % Ag) thin film coated nylon fabric (GoS 2), cellulose membrane and silver ion accumulation layer with a gelatin and agar mix. The bandage construction was up to 50% more efficient for bacteria in suspension than DLC:Ag nylon fabric coated samples after 20 min. The main advantages of such a bandage structure are the antimicrobial action speed during the initial 60 min and the property of anti-sticking to the wound (as confirmed by tests with animals).
6. According to our test results with lab animals, it was confirmed that the bandage prototype increased the healing speed by 40% and killed 100% of the bacteria inside the wound on the third day. The bandage reduced scar marks. No allergy reactions or residual phenomena on the skin surface were observed, and no deaths of lab animals were registered.

SANTRAUKA

Parengtoje disertacijoje yra aprašomi deimanto tipo anglies dangų bei deimanto tipo anglies nanokompozitų sintezė ant nailono audinių ir taikymai kuriant išorinio poveikio vaistines formas, skirtas gydyti mikroorganizmais užterštas žaizdas. Buvo nustatyta, kad sidabru legiruotos deimanto tipo anglies dangos yra tinkama medžiaga kuriant išorinio poveikio vaistinę formą arba pleistrą, kuris dėl dangų panaudojimo įgyja antimikrobinių savybių ir yra tinkamas naudoti žaizdoms gydyti (nesukeliant šalutinio poveikio).

Atlikus tyrimus buvo nustatyta, kad sidabro jonai ir sidabro nanodalelės pažeidžia bakterijų ląstelių sieneles ir jas nužudo. Veikimo mechanizmai ir morfologiniai pakitimai, atsiradę dėl sidabro ir antibiotiko benzilpenicilino panaudojimo, buvo nustatyti atlikus skenuojančią elektroninę mikroskopiją.

Kuriant bandomuosius pleistrus buvo užgarintos deimanto tipo anglies dangos su sidabru (100 nm) ant silicio plokštelių ir nailono audinio, naudojant nuolatinės srovės nesubalansuotą magnetroną. Magnetroninio dulkinimo metu buvo naudojamas grynas sidabro taikinys acetileno dujų aplinkoje, kontroliuojant magnetrono galią, įtampą bei dujų srauto greitį į magnetrono kamerą, buvo kontroliuojamas dangos storis, cheminė sudėtis, struktūra. Užneštos dangos buvo analizuojamos naudojant skenuojantį elektroninį mikroskopą, rentgeno spindulių energijos dispersijos spektroskopiją. Sidabro jonų (išsiskyrusių iš dangų) tirpale nustatymui – atominės absorbcijos spektroskopiją. Užneštų dangų savybių gerinimui buvo atliekamas radijo dažnio (13,56 MHz) dangų paviršiaus ėsdinimas deguonies plazma. Ėsdintos dangos turėjo šiurkštesnį paviršių bei geresnes antimikrobines savybes dėl geresnės sidabro jonų difuzijos iš dangos į vandeningas terpes, lyginant su neėsdintomis. Antimikrobinio dangų poveikio tyrimai buvo atliekami Lietuvos sveikatos mokslų universiteto Mikrobiologijos ir virusologijos institute, naudojant standartinius mikrobiologinius testus: diskų difuzijos metodą, paskleidimo ant lėkštutės bei serijinių praskiedimų metodą.

Remiantis eksperimentų duomenimis, buvo atrinktos bandinių grupės su 3,4 % sidabro koncentracija, užnešta ant nailono audinio, kuris buvo naudojamas gaminant išorinės vaistinės formos (pleistro) prototipą. Sidabro jonų kaupimui panaudotas vandeninis želatinos ir agaro mišinys, kuris plonu sluoksniu buvo užneštas ant danga užgarinto ir deguonies plazma ėsdinto audinio. Pritaikius tokį sprendimą antimikrobinis poveikis buvo iki 50 % greitesnis, lyginant su pleistru be želatinos ir agaro sluoksnio.

Atlikus bandymus su laboratoriniais gyvūnais, buvo nustatyta, kad po 72 valandų bakterijų žaizdoje nebuvo aptikta, o gijimo laikas buvo 40 % trumpesnis, lyginant su paprastu medvilniniu pleistru be sidabro. Atlikus bandinių su bakterijomis SEM analizę buvo nustatyta, kad sidabro jonai sukelia pokyčius *in vitro* bakterijų ląstelių sienelėse kaip ir benzilpenicilinas.

ĮVADAS

Šis mokslinis darbas susijęs su infekuotų žaizdų gydymu ir tikslas – sukurti pleistrą su sidabro jonais, kurie bus veiklioji antimikrobinė medžiaga ir užtikrins geras gydomąsias savybes.

Gyvybei pavojingos bakterijos egzistuoja mūsų aplinkoje, yra randamos ant dažnai naudojamų buitinių prietaisų, mobiliųjų telefonų, raktų ir pan. Būdami aplinkoje, pilnoje įvairiausių bakterijų, mes rizikuojame susirgti arba dėl infekcijos žaizdoje netekti galūnės ar net mirti [1, 2]. Viena pavojingiausių bakterijų yra *Staphyloccocus aureus*, meticilinui atspari padermė, sukeltą infekciją gydyti labai sunku naudojant antibiotikus, todėl komplikacijos dažnai baigiasi galūnių amputacija ar net mirtimi dėl sepsio [3].

Prieš penicilino atradimą (Aleksandras Flemingas 1929 m [4]) žmonės mirdavo dėl įvairių sužeidimų, kurie komplikuodavosi į sepsį [5]. Bet vėliau dėl didelio penicilino naudojimo, nuo septintojo XX a. dešimtmečio *S. aureus* bakterijos sukeltų infekcijų gydymas tapo komplikuotas dėl atsiradusio atsparumo šiam antibiotikui. *S. aureus* bakterijos atsparumas galimai išsivystė dėl perteklinio naudojimo gyvulininkystėje, kur jis buvo naudojamas kaip pašarų priedas [6], taip pat dėl besaikio naudojimo ligoninėse ar nesilaikant antibiotikų vartojimo rekomendacijų, t. y. kai gydymo kurso antibiotikais nebūdavo laikomasi [7]. Taip pat buvo nustatyta, kad musės gali pernešti meticilinui atsparias bakterijas iš fermų į ligonines ir kitas gyvenamąsias vietas ir taip didina tikimybę susižeidus buityje užkrėsti žaizdą šia bakterija [8, 9]. Skaičiuojama, kad apie 65 % *S. aureus* bakterijų sukeltų infekcijų yra meticilinui atspari padermė [5], todėl plačiai naudojami antibiotikai tapo neveiksmingi ir žaizdų gydymas virto dideliu iššūkiu gydytojams.

Šiandien žaizdų gydymas tampa didžiuliu iššūkiu, todėl kyla naujų efektyvių vaistinių produktų poreikis ir vienas iš daugiausiai žadančių – sidabro nanodalelėmis bei sidabro jonais praturtinti gaminiai [10]. Sidabro panaudojimas gydymui turi ilgą istoriją, pavyzdžiui, 1884 m. vokiečių gydytojas naudojo 1 % sidabro nitrato tirpalą naujagimių aklumui gydyti po atsiradusių akių infekcijų [18], vėliau, įsitikinus sidabro gydomosiomis savybėmis, Jungtinių valstijų Maisto ir vaistų administracija aprobavo gydymui skirtą koloidinį sidabro tirpalą. Šiuo metu klinikinėje praktikoje yra naudojami vandens ir sidabro jonų prisotinti preparatai, hidrogeliai, putos, kremai, įvairūs tinkleliai ir polimeriniai audiniai, kurie neprilimpa prie gydomų audinių [21, 22].

Kuriant pleistrus, skirtus žaizdoms gydyti, sidabro nanodalelės turi būti susintetintos ir patalpintos pleistro pagrinde, nes sidabro nanodalelės vandeningoje terpėje (putose, kremuose) gali sulipti ir prarasti savo savybes. Vienas švariausių metodų gaminant sidabro nanodaleles ir jas stabilizuojant pagrinde yra reaktyvus magnetroninis dulkinimas [28]. Tyrimų metu buvo pagamintas pleistro prototipas panaudojant DTAD su sidabro nanodalelėmis, ant kurio buvo uždėti sluoksniai su želatina ir agaru, siekiant išvengti dangos tiesioginio kontakto su žaizdos audiniais, užtikrinti ilgalaikes antimikrobines savybes, neprikibimą prie žaizdos audinių ir geras gydomąsias savybes.

Tiriamajame darbe visi tikslai buvo įgyvendinti, prototipas sukurtas, atlikus eksperimentus buvo nustatyta, kad pleistras sutrumpino žaizdų gijimą iki 40 % bei per tris dienas sunaikino visas patogenines *S. aureus* bakterijas žaizdoje.

Darbo tikslas

Darbo tikslas – sukurti išorinio poveikio vaistinę formą (pleistrą) naudojant DTAD ir sidabro nanokompozitų dangas. Šios dangos būtų sidabro jonų šaltinis pleistre, taip pat sidabro jonai pleistre atliktų antimikrobinių vaistų vaidmenį. Farmakologinis įvertinimas yra kitas svarbus žingsnis kuriant ankstyvos stadijos pleistro prototipą, todėl būtina įvertinti antimikrobines savybes ir poveikį laboratoriniams gyvūnams.

Darbo uždaviniai

1. Ištirti deimanto tipo amorfinių anglies dangų, legiruotų sidabru (DTAD:Ag), cheminės sudėties, paviršiaus morfologijos pokyčius ir nanodalelių dydžių pasiskirstymą dangos paviršiuje po ėsdinimo radijo dažnio (RD) deguonies plazma.
2. Nustatyti optimalų DTAD:Ag paviršių RD ėsdinimo deguonies plazma laiką ir bandinių ėsdinimo laiko įtaką sidabro jonų difuzijai į vandenį.
3. Atlikti mikrobiologinius tyrimus, nustatyti mažiausią efektyvią sidabro jonų koncentraciją vandenyje, kuri turi antimikrobinių savybių, ir atrinkti bandinių grupę pleistro prototipui kurti.
4. Nustatyti sidabro jonų ir sidabro nanodalelių bei benzilpenicilino sukeltus bakterijų sienelių vizualinių pokyčių panašumus ir skirtumus.
5. Paruošti išorinio poveikio vaistinę formą – pleistrą – panaudojant DTAD:Ag ir atlikti sidabro jonų difuzijos į vandenį eksperimentus ir mikrobiologinius bandymus *in vitro.*
6. Įvertinti pleistro farmakologinį efektą naudojant laboratorinius gyvūnus ir nustatyti antimikrobinį poveikį *in vivo*.

Mokslinis naujumas

1. Sukurta metodika, kaip pagaminti DTAD:Ag dangas ant nailono (poliamidas 6.6) audinio ir kaip naudojant ėsdinimo deguonies plazma technologiją pagerinti ilgalaikį antimikrobinį poveikį, kuris išlieka daugiau kaip 2 metus.
2. Atliktas detalus sidabro jonų ir nanodalelių antimikrobinio poveikio bakterijų sienelėms tyrimas ir nustatyta optimali sidabro jonų koncentracija, reikalinga užtikrinti geras antimikrobines savybes.
3. Buvo sukurtas pleistro prototipas, kurio unikali struktūra patentuota Lietuvoje, taip pat patvirtintas PCT patentas.

Disertacijos struktūra

Šią disertaciją sudaro skyriai:

1 skyrius – literatūros apžvalga. Literatūros apžvalgoje aprašoma žaizdų gydymo problemos, gijimo fiziologija. Apžvelgiama sidabro naudojimo istorija, veikimo mechanizmai, DTAD:Ag dangų gamyba bei apdirbimas. Trumpai apžvelgiami rinkoje esantys gydomieji pleistrai, taip pat vaistinės formos bei tvarsčiai su sidabru.

2 skyrius – medžiagos ir metodai. Skyriuje aprašomi naudoti reagentai bei trumpai pristatomi naudoti tyrimų metodai bei įranga.

3 skyrius – rezultatai ir jų analizė. Skyriuje aprašoma dangų ant nailono audinio analizės, mikrobiologiniai eksperimentai, sidabro jonų difuzijos ypatybės ir eksperimentų su gyvūnais tyrimų rezultatai ir rezultatų analizė.

4 skyrius – išvados. Pristatomos darbo išvados.

Disertacijos apimtis – 132 puslapiai, 26 paveikslėliai ir 6 lentelės, 8 priedai. Disertacijos pabaigoje pateiktas literatūros sąrašas, kurį sudaro 256 šaltiniai.

Autoriaus indėlis

Disertacijoje pateikiami rezultatai buvo pasiekti atliekant eksperimentus Kauno technologijos universitete (KTU) bei Lietuvos sveikatos mokslų universitete (LSMU). Autorius pasiūlė idėją sukurti išorinio poveikio vaistinę formą su sidabru, sukūrė pleistro struktūrą ir pagamino pleistrų prototipus. Dauguma eksperimentų ir tyrimų buvo suplanuota ir atlikta disertacijos autoriaus, įskaitant mikrobiologijos bei bandymus su gyvūnais. Vitoldas Kopustinskas ir dr. Andrius Vasiliauskas užgarino DTAD:Ag dangas ant nailono audinio pagrindų, SEM mikroskopija ir EDS dangų sudėties analizę atliko prof. Tomas Tamulevičius, Irina Abelit atliko AAS spektroskopiją.

Tyrimams atlikti buvo naudojamasi bendru KTU ir LSMU projektu NANOBIOSENSOR, autorius dirbo jaunesniuoju mokslo darbuotoju ir su LSMU mokslininkų komanda atliko mikrobiologijos eksperimentus.

Antras bendras LSMU ir KTU projektas NANOSMARTPLASTER buvo skirtas sukurti disertacijoje aprašomą vaistinę formą, autorius buvo projekto iniciatorius, atliko eksperimentus, susijusius su pleistro prototipo ruošimu, kartu su LSMU mokslininkais atliko mikrobiologinius tyrimus bei bandymus su laboratoriniais gyvūnais. Rezultatų domenų analizė buvo atlikta konsultuojantis su prof. Sigitu Tamulevičiumi, prof. Tomu Tamulevičiumi ir doc. Modestu Ružausku.

LITERATŪROS APŽVALGA

Žaizdų gijimas yra sudėtingas biologinis procesas, kurį kontroliuoja organizme vykstančios sudėtingos biocheminės reakcijos ir fiziologiniai procesai, kurie taip pat kontroliuoja pažeistų audinių hemostazę, t. y. kraujagyslių spindžio susiaurėjimą pažeistoje vietoje ir užkimšimą fibrino siūlais [42, 46, 49]. Sužeidimai dažniausiai nėra sterilūs ir į žaizdą patekusios bakterijos sukelia uždegimą [34, 35] – organizmo imuninės sistemos atsaką į svetimkūnius [36, 49]. Po uždegimo stadijos organizmo audiniai ir kraujagyslės atsistato, atauga, maturacijos stadijos metu pradeda formuotis randinis audinys, t. y. baigiasi audinių gijimas [33, 41].

Žaizdos, užkrėstos meticilinui atspariu stafilokoku, gali tapti lėtinėmis, neišgydomomis ar mirtinomis [60–62], o stipraus poveikio antimikrobinė medžiaga, kaip sidabras ir jo junginiai, galėtų būti pritaikyti gydymui dėl savo mažo toksiškumo ir didelio efektyvumo [91, 102, 106].

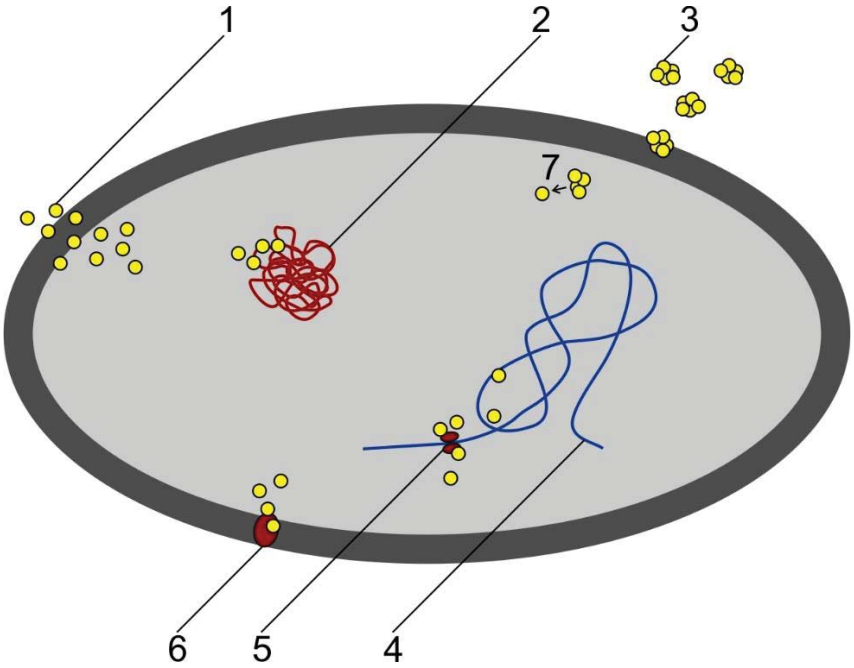

1 pav. Sidabro nanodalelių ir sidabro jonų antimikrobinio poveikio mechanizmai [10]: sidabro jonai (1) prasiskverbia per bakterijos ląstelės sienelę arba pereina per membranos kanalus (6) ir prisijungia prie DNR (2) molekulės, sutrikdo ribosomų galimybę (5) nukopijuoti informacinę ribosominę RNR (4) ir sutrikdo baltymų sintezės procesą. Sidabro nanodalelės (3) gali padaryti mechaninę žalą ląstelės membranai pereidamos kiaurai, taip pat gali išskirti sidabro jonus viduje ląstelės (7)

Taip pat sidabras labai tinkamas gydant sunkias infekcijas dėl savo plataus veikimo modelio (1 pav.). Bakterijos netampa atsparios sidabrui, todėl sidabras gali būti naudojamas gaminant pleistrus [85, 87, 98] ir kituose preparatuose bei gydant įvairias infekcijas [31, 85, 90].

Kita vertus, sidabras (jo nanodalelės ir jonai) turi būti įdėtas į kietą paviršių ar skystą terpę, kad būtų išvengta toksiško sidabro poveikio dėl per didelio suvartoto kiekio. Vienas daug žadančių metodų yra deimanto tipo anglies dangų gamyba įterpiant sidabro nanodaleles, kurios efektyviai gali išskirti sidabro jonus į drėgną terpę ir palaikyti stiprų antimikrobinį poveikį [29–32].

Sidabro nanodalelių toksiškumas priklauso nuo dalelių dydžio: pavojingiausios yra mažesnės nei 10 nm dalelės [104]. Nanodalelių nepageidaujamas poveikis gali būti ženkliai sumažinamas patalpinant jas DTAD matricoje, kurioje gali būti įvairaus dydžio dalelės dangų gamybos metu naudojant nesubalansuotą magnetroną ir radijo dažnio ėsdinimą deguonies plazma dangoms apdirbti [150–153]. Rinkoje egzistuota įvairūs gaminiai su sidabru: kremai, geliai, pleistrai su sidabro tinkleliu. Šiame darbe aprašomas sukurtas originalios konstrukcijos pleistro prototipas panaudojant DTAD:Ag, užgarintas ant nailono audinio su 3D silikono korio tipo tinkleliu, kuris užpildytas želatinos ir agaro mišiniu – tarnaujantis kaip sidabro jonų kaupimo sluoksnis, bei buvo ištirtos pleistro sidabro jonų difuzijos, antimikrobinės ir gydomosios savybės.

MEDŽIAGOS, EKSPERIMENTINĖ ĮRANGA IR TYRIMŲ METODIKA

Eksperimentuose naudotos medžiagos

Buvo naudotas benzilpenicilinas (Benzylpenicillinum natricum, 1000000 tarptautinių vienetų (T. V.) stikliniame buteliuke, Penicillin G. Sandoz). Nailono audinys (atlasinio pynimo, audinio ataudų tankis 100 cm^{-1}) ir silicio plokštelė buvo naudoti kaip padėklai magnetroninio dulkinimo procesuose bei kaip padėklai bakterijoms SEM mikroskopijai atlikti. Miuler Hinton agaras (Thermo Scientific, Leicestershire, UK) buvo naudojamas kaip mitybinė terpė bakterijoms, kuris buvo supilamas ir atvėsinamas į 94 mm Petri lėkšteles.

Argono dujos 99,999 %, C_2H_2 dujos 99,999 %, bei deguonies 99,9 % švarumo dujos buvo naudojamos magnetroninio dulkinimo ir ėsdinimo plazma procesuose. Pleistro gamybai buvo panaudota: celiuliozės skaidulos (vidutinės, C6288 Sigma, Sigma Aldrich, St. Louis, MO, USA), želatina (53028 FLUKA, Sigma Aldrich) ir agaras (A1296 SIGMA, Sigma Aldrich), medicininės paskirties silikono guma „A-103“ (www.factor2.com), pintas valas „BERKLEY MICRO ICE 0,006 mm“ ir dezinfekcijai 96 % spiritas (AB „Stumbras“). Eksperimentams su bakterijomis *in vitro* buvo naudotos standartizuotos sidabro nanodalelės (10 nm), 0,02 mg/ml vandeniniame buferyje (Sigma Aldrich).

Bandinių gamyba, apdorojimas ir analizė

Eksperimentuose buvo naudotas nuolatinės srovės nesubalansuotas magnetronas. Plonasluoksnių dangų gamybos metu buvo naudojamas sidabro taikinys ir acetilelo dujos. Keičiant magnetrono parametrus (elektros įtampą ir galią)

bei reguliuojant dujų srautą į magnetrono kamerą buvo pagamintos plonasluoksnės dangos (100 nm) ant nailono audinio su skirtingomis sidabro koncentracijomis. Iš viso buvo pagamintos trys bandinių grupės, kuriuose sidabro koncentracijos (at %) buvo: 1) 0,46 %; 2) 3,12 %; 3) 5,31 %.

Pagamintų dangų paviršius buvo apdorojamas deguonies plazma. Procesas leidžia padidinti dangų paviršiaus šiurkštumą bei pakeisti cheminę dangų sudėtį [35]. Šiame darbe naudojant „Plasma-600-T“ (JSC Kvartz) prietaisą buvo atliktas sausasis dangų paviršiaus ėsdinimas. Bandinių grupės buvo patalpintos į įrenginio kamerą ir ėsdintos radijo dažnio (13,56 MHz) deguonies plazma (99,9 % švarumo), slėgis kameroje buvo – 133 Pa, galia – 0,3 W/cm², ėsdinimo laikas buvo nuo 5 iki 30 sekundžių.

Bandinių analizė buvo atlikta naudojant skenuojantį elektroninį mikroskopą (SEM) su elektroninės dispersijos spektroskopu (EDS) „FEI Quanta 200 FEG“, pagamintą „Bruker Quantax“. EDS matavimai buvo atlikti naudojant 5 keV greitinančią įtampą. Nanodalelių dydžių ir pasiskirstymo analizė iš SEM nuotraukų buvo atlikta naudojant kompiuterinę programą „Image J (NIH)“ ir MATLAB (MathWorks).

Sidabro jonų koncentracijos matavimai naudojant AAS

Sidabro jonų difuzijai (kai bandiniai buvo laikomi mėgintuvėliuose su vandeniu) iš dangų paviršiaus (6 cm^2) į išgrynintą vandenį (1 ml) ištirti buvo naudojama atominės absorbcijos spektroskopija (AAS). Tyrimo metu sidabro jonų koncentracija buvo matuojama („A Perkin Elmer Model 403“) spektrometru. Bandinių grupės buvo laikomos distiliuotame vandenyje nuo 20 min. iki 48 val. Po to vanduo buvo filtruojamas ir atliekami matavimai.

Mikrobiologiniai metodai

Mikrobiologiniuose eksperimentuose buvo naudojama referentinė *S. aureus* padermė (ATCC25923) bei bakterijų padermės, išskirtos iš patologinės medžiagos: LTSa603, LTSaDA01, LTSaM01, ir meticilinui atspari *S. aureus* padermė (LTSa635).

Paruoštų bandinių antimikrobinio efektyvumo nustatymui buvo naudojamas diskų difuzijos testas: ant paruošto agaro Petri lėkštelėje buvo sėjamos *S. aureus* bakterijos naudojant tamponėlį ant sustingusio agaro, po to buvo dedamas DTAD:Ag mėginys, kuris buvo sudrėkinamas prieš uždedant ant agaro paviršiaus. Petri lėkštelės buvo laikomos 16–20 val. termostate 35 ºC temperatūroje. Antimikrobiniam poveikiui įvertinti buvo liniuote matuojamos skaidrios zonos aplink bandinį, eksperimentai buvo atlikti 4 kartus mėnesio eigoje.

Serijinių praskiedimų metodas buvo naudojamas nustatant antimikrobinių medžiagų poveikį *in vitro* (mėgintuvėlyje), naudojant šį metodą buvo nustatyta, koks skaičius kolonijas formuojančių vienetų (KFV) buvo sunaikintas. Metodo esmė: iš pirmo mėgintuvėlio (10 ml), kuriame yra bakterijų koncentratas, paimama (1 ml) dalis tirpalo ir perkeliama į fiziologiniu ar distiliuotu vandeniu (9 ml) užpildytą mėgintuvėlį, taip pirminis tirpalas praskiedžiamas 10 kartų (10^1). Jei paimamas 1 ml jau praskiesto tirpalo iš antrojo mėgintuvėlio ir perkeliama į trečią mėgintuvėlį su

fiziologiniu ar distiliuotu vandeniu, tirpalas mėgintuvėlyje tampa praskiestas šimtą kartų (10^2), procesas gali būti tęsiamas, kol randama (KFV) ant agaro paviršiaus po „išsėjimo ant lėkštelės“ metodo.

Metodas naudojamas siekiant sužinoti tikslų gyvų bakterijų skaičių suspensijoje (1 ml). Atliekant eksperimentus 0,1 ml bakterijų suspensijos iš praskiesto tirpalo buvo užlašintas ant agaro paviršiaus, suspensija paskleista po visa agaro paviršių naudojant sulenktą kilpelę. Po procedūros lėkštelės buvo patalpintos į termostatą ir KFV skaičiavimas buvo atliekamas 16–20 val.

Eksperimentai su laboratoriniais gyvūnais

Bandymai su gyvūnais buvo atlikti gavus leidimą iš Valstybinės maisto ir veterinarijos tarnybos. Eksperimentams buvo naudojamos jūros kiaulytės, kurios buvo laikomos narvelyje po dvi, su specialia slėptuve, automatine girdykla, ir gyvūnai buvo šeriami specializuotu sausu pašaru.

Eksperimentų metu buvo nuskustas kailis nugaros srityje, atliktas negilus pjūvis skalpeliu ir užklijuotas bandomasis pleistras. Papildomai buvo naudojama speciali liemenė, kuri neleido gyvūnams nusikrapštyti priklijuoto pleistro. Gijimas buvo vertinamas kas 24 valandas, eksperimentai trukdavo iki 4 dienų.

REZULTATAI IR EKSPERIMENTŲ DUOMENŲ APTARIMAS

DTD:Ag dangų gamyba ant nailono audinio padėklų ir jų cheminė sudėtis

Trys bandinių grupės (BG) su DLC:Ag dangomis ant nailono audinio, su sidabro 1) 0,46 at. %, 2) 3,12 at. %, 3) 5,31 at. % koncentracijomis buvo pagamintos naudojant nuolatinės srovės nesubalansuotą magnetroninį dulkinimą.

1 lentelė. Magnetroninio dulkinimo proceso nustatymai

Mėginio Nr.	Dulkinimo trukmė (s)	Ar dujų srautas (sccm)	C2H2 dujų srautas (sccm)	Magnetrono įtampa (V)	Magnetrono srovė (A)
1	520	70	21,1	553–625	0,07–0,12
2	235	70	21,1	568–741	0,07–0,22
3	200	80	7,8	625–656	0,10–0,11

Magnetroninio dulkinimo nustatymai (1 lentelė) atliko svarbų vaidmenį plonasluoksnių dangų formavimo procesuose ir buvo nustatyta, kad DTAD:Ag savybės gali būti valdomos keičiant acetileno, argono dujų srautų santykius bei kontroliuojant magnetroninio dulkinimo laiką [195].

Pirmoji mėginių grupė buvo paruošta pagal nustatymus: dulkinimo trukmė buvo 520 s ir argono dujų srautas – 70 sccm, acetileno dujų – 21,1 sccm. Antroji mėginių grupė buvo pagaminta taikant tuos pačius dujų srautų parametrus, bet buvo sutrumpintas magnetroninio dulkinimo laikas nuo 520 s iki 235 s bei padidina magnetrono įtampa ir srovė (1 lentelė).

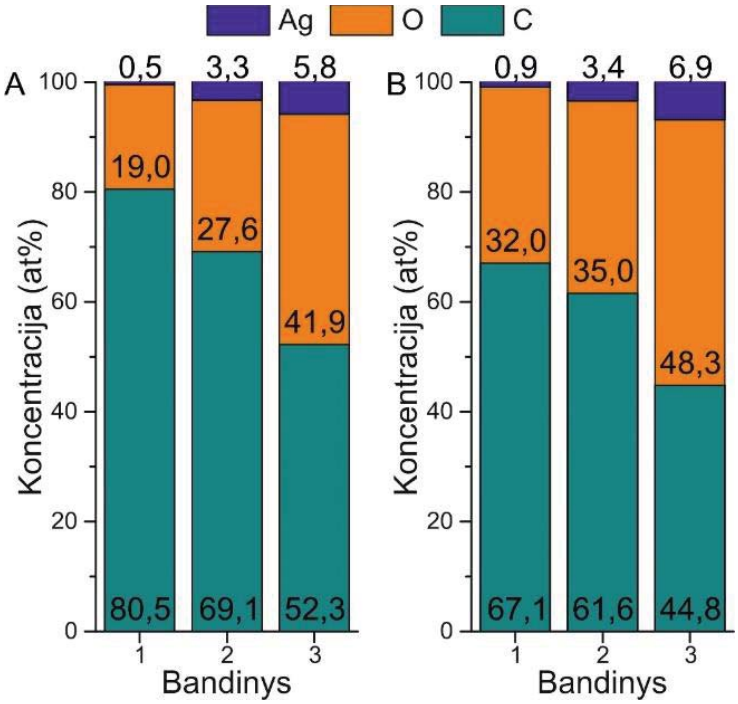

2 pav. Bandinių su DTAD:Ag cheminė sudėtis: plonasluoksnių dangų cheminių elementų pasiskirstymas ant silicio plokštelės po 5 s (A) ėsdinimo ir po 20 s ėsdinimo deguonies plazma (B)

Buvo pastebėta, kad didesni magnetrono srovės ir įtampos parametrai bei mažesni dujų srautai ir trumpesnis dulkinimo greitis turėjo įtakos didesniam sidabro nusėdimo kiekiui dangose [96, 196, 197], kaip buvo pastebėta gaminant trečią bandinių grupę.

Atlikus deguonies plazma ėsdintų dangų EDS matavimus, buvo nustatyta, kad visose trijose mėginių grupėse (žr. 2 pav.) po 5 ir 20 sekundžių ėsdinimo anglies koncentracija dangose sumažėjo ir atitinkamai padidėjo sidabro koncentracija.

Sidabro nanodalelių dydžių pasiskirstymas DTAD:Ag dangų matricoje

Buvo nustatyta, kad mėginiuose vidutinis nanodalelių dydis 23 nm, jos buvo tolygiai paskirsčiusios ant DLC:Ag paviršiaus, o sidabro nanodalelių dydis buvo nuo 3 iki 63 nm (3 pav.). Bandinių grupėse su maža sidabro koncentracija dominavo mažų matmenų sidabro nanodalelės, bandinių grupėje su didesnėmis sidabro koncentracijomis vyravo didesnio skersmens nanodalelės.

Pirmoje bandinių grupėje po ėsdinimo deguonies plazma 20 s dalelių vidutinis dydis buvo 16,1 nm (± 5,8 nm), antrojoje bandinių grupėje – 23,7 nm (± 9,6 nm), trečioje – sidabro nanodalelių dydis buvo 28,8 nm (± 12,6 nm). Atlikus duomenų analizę buvo pastebėta, kad bandiniuose su mažiausia sidabro koncentracija vyravo

mažiausios nanodalelės (9–12 nm ir 6–9 nm), o su didžiausia sidabro koncentracija vyravo didesnio diametro nanodalelės (27–30 nm).

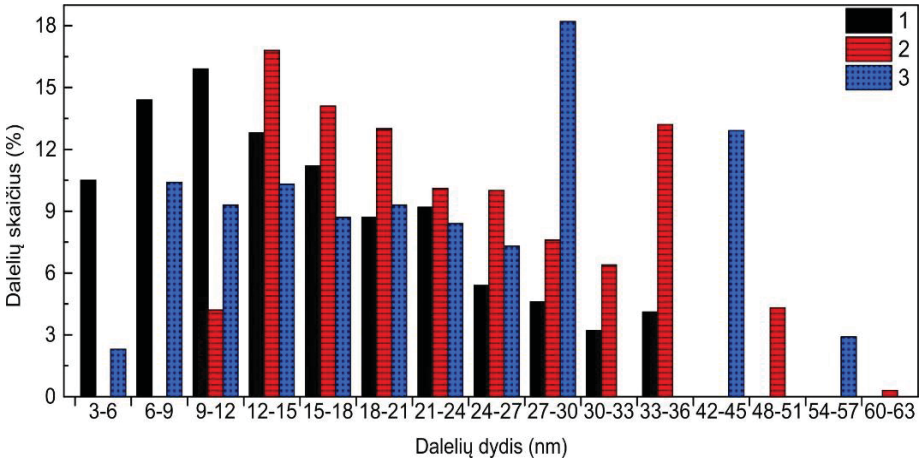

3 pav. Sidabro nanodalelių dydžių pasiskirstymas: diagramoje pateikiama bandinių grupės (1–3) dalelių dydžių pasiskirstymas nuo 3 iki 63 nm DTAD matricoje

Sidabro jonų difuzija

Sidabro jonų difuzijos greičiui įvertinti buvo atlikti testai naudojant 20 s deguonies plazma ėsdintas bandinių grupes, kurios buvo sukarpytos į 6 cm^2 gabaliukus. Mėginiai distiliuotame vandenyje buvo laikomi nuo 20 iki 1440 min. Atlikus atominės absorbcijos spektroskopiją buvo išmatuotas sidabro jonų difuzijos greitis ir jonų koncentracija (ppm) iš 6 cm^2 bandinio ploto į 1 ml išgryninto vandens skirtingais laiko intervalais (žr. 4 pav.).

Nustatyta, kad po 20 min pirmosios bandinių grupės, sidabro jonų difuzija buvo labai lėta, po 60 min. sidabro jonų koncentracija buvo mažesnė nei 0,1 ppm, po 24 val. tik 0,5 ppm. Antra bandinių grupė turėjo geriausias difuzijos savybes – po 60 min. sidabro jonų koncentracija pasiekė 1 ppm, po 24 val. atitinkamai – 4 ppm.

Trečiosios mėginių grupės sidabro jonų difuzija buvo lėtesnė nei antrosios bandinių grupės, po 1 valandos buvo 0,8 ppm, o po 24 valandų išsiskyrusių iš dangos sidabro jonų koncentracija vandenyje buvo 3,5 ppm.

Atlikus visų rezultatų analizę nustatyta, kad nanodalelių dydis atliko esminį vaidmenį vertinant sidabro jonų difuzijos efektyvumą. Žinoma, kad nanodalelės turi didelį paviršiaus plotą [96, 223], todėl ženkliai padidėjo sidabro jonų difuzijos greitis priklausomai nuo vyraujančių nanodalelių dydžio bandiniuose.

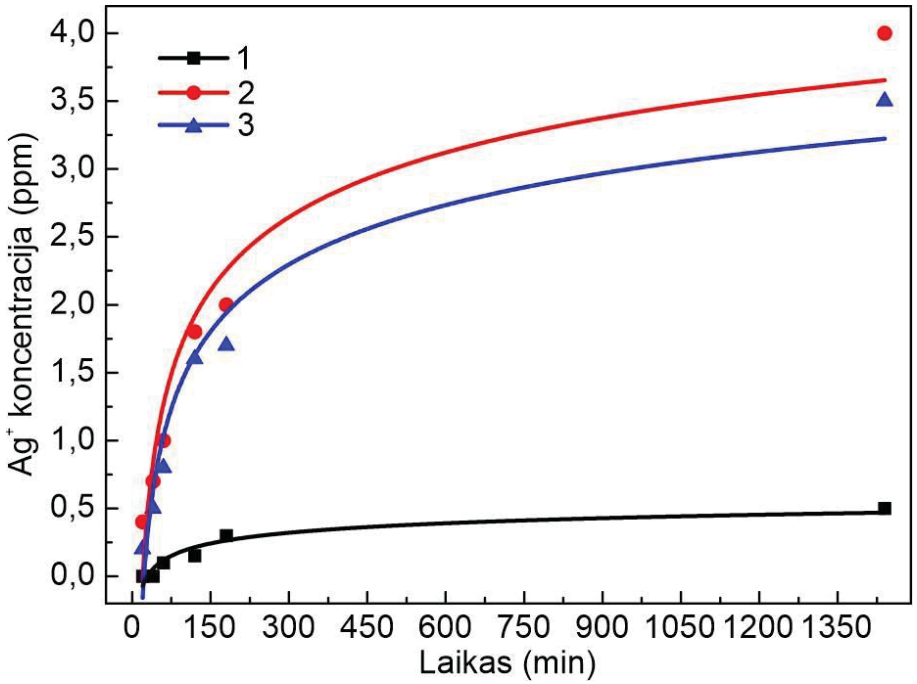

4 pav. Bandinių grupių su DTAD:Ag dangomis sidabro jonų difuzijos greitis ir susidariusi sidabro jonų koncentracija vandenyje po atitinkamų laiko intervalų: bandinių grupės 1 – 0,9 at. %; 2 – 3,4 at. %; 3 – 6,9 at. % sidabro koncentracija, paviršiaus ploto santykis su vandens tūriu buvo 6 cm^2 – 1 ml, mirkymo vandenyje laikas – nuo 20 min. iki 1440 min

Pleistro prototipo pagaminimas

Antrasis tvarsčio prototipas (žr. 5 pav.) buvo pagamintas atlikus mikrobiologinių ir bandymų su gyvūnais (pirmo pleistro prototipo) duomenų analizes.

Prototipui taip pat buvo panaudota antros bandinių grupės (3,4 at. % Ag) nailono audinio gabaliukai, kurie buvo ėsdinti 20 sekundžių deguonies plazma. Bandiniai buvo dezinfekuoti naudojant UV lempą 4 valandas. Siekiant išvengti papildomo užteršimo, mėginiai buvo laikomi plastikinėse Petri lėkštelėse. Po dezinfekcijos, paruošti 20x40 mm skersmens nailono bandiniai buvo padengti plonu celiuliozės pluošto sluoksniu, sumaišyti su želatina ir valcuoti naudojant 50 mm skersmens nerūdijančio plieno volelį, naudojant 5 kg / cm^2 slėgį. Užnešto 0,01–0,02 mm celiuliozės sluoksnio paskirtis buvo sulaikyti bet kokias daleles bei nešvarumus, kurie galėtų patekti nuo nailono audinio į žaizdą.

Sidabro jonų kaupimo sluoksnis (SJKS) buvo patobulintas naudojant 3D tinklelio struktūrą (korio tipo), pagamintą iš silikono, vienos akutės dydis 2 mm x 2 mm, pertvarų storis buvo 0,3 mm, o viso tinklelio storis – 2 mm Sidabro jonų kaupimo sluoksnis (tinklelio akučių užpildas) buvo paruoštas naudojant želatinos ir agaro (90 % / 10 % santykis) suspensiją (40–45 °C), kuri buvo supilta į Petri

lėkštelę. Lėkštelėje ant dugno buvo padėtas silikoninis tinklelis, ir želatinos-agaro mišinys buvo pilamas iki 2 mm, kad pilnai apsemtų tinklelį ir neliktų neužpildytų geliu akučių. Sukietėjus želatinos ir agaro geliui, visas sidabro jonų kaupimo sluoksnis buvo užklijuotas ant nailono audinio su celiuliozės sluoksniu naudojant šiltą (38–40 °C) želatinos-agaro gelį, galiausiai pleistras buvo surinktas (susiūtas naudojant 0,006 mm sterilų pintą valą) ant lipnios medicininės plėvelės su mikroskylutėmis.

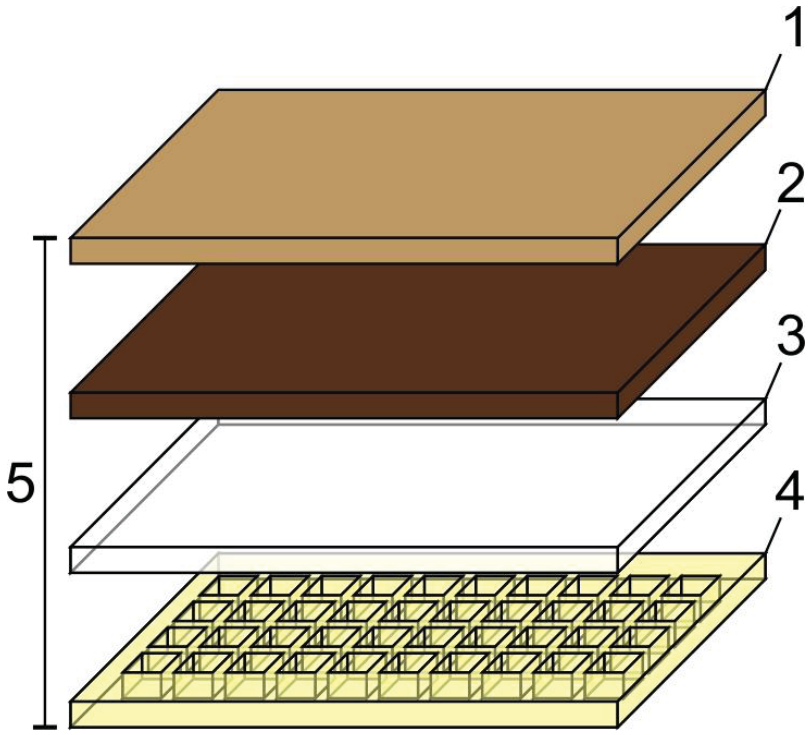

5 pav. Antrasis tvarsčio prototipas su sluoksniais (5): lipni medicininė plėvelė (1), DLC:Ag danga užgarintas nailono audinys (3,4 % Ag (at)) (2), celiuliozės sluoksnis (3), sidabro jonų kaupimo sluoksnis (4)

Sidabro jonų kaupimo sluoksnio antimikrobinis poveikis

Antros bandinių grupės (3,4 at. % Ag) ir tvarsčio prototipo mikrobiologinių eksperimentų tyrimai buvo atlikti naudojant labai patogeniškas *S. aureus* bakterijų padermes LTSa635 (MRSA), LTSaDA01, LTSaM01 ir LTSa603 (žr. 6 pav.).

Atlikus eksperimentų rezultatų (su bakterijų padermėmis LTSaDA01, LTSaM01 ir TSa603) analizę buvo pastebėta, kad po 20 min antra bandinių grupė su 3,4 at. % Ag sunaikino 10–15 % *S. aureus* bakterijų, tuo tarpu pagamintas pleistro prototipas sunaikino 63–65 % (žr. 5 pav.) bakterijų populiacijos.

Po 60 min. rezultatai su bakterijomis (LTSaDA01, LTSaM01, LTSa603): skaičius sumažėjo daugiau kaip 60 % naudojant antrą bandinių grupę, bet pleistro

prototipo antimikrobinis poveikis buvo stipresnis – po 60 min kolonijas formuojančių vienetų (KFV) skaičius sumažėjo apie 80 %. Atliktų tyrimų rezultatai rodo, kad pleistro prototipo didžiausias privalumas yra jo antimikrobinis veikimo greitis, nes po 120 min tiek pleistro prototipas, tiek antra bandinių grupė sunaikino daugiau kaip 90 % bakterijų populiacijos.

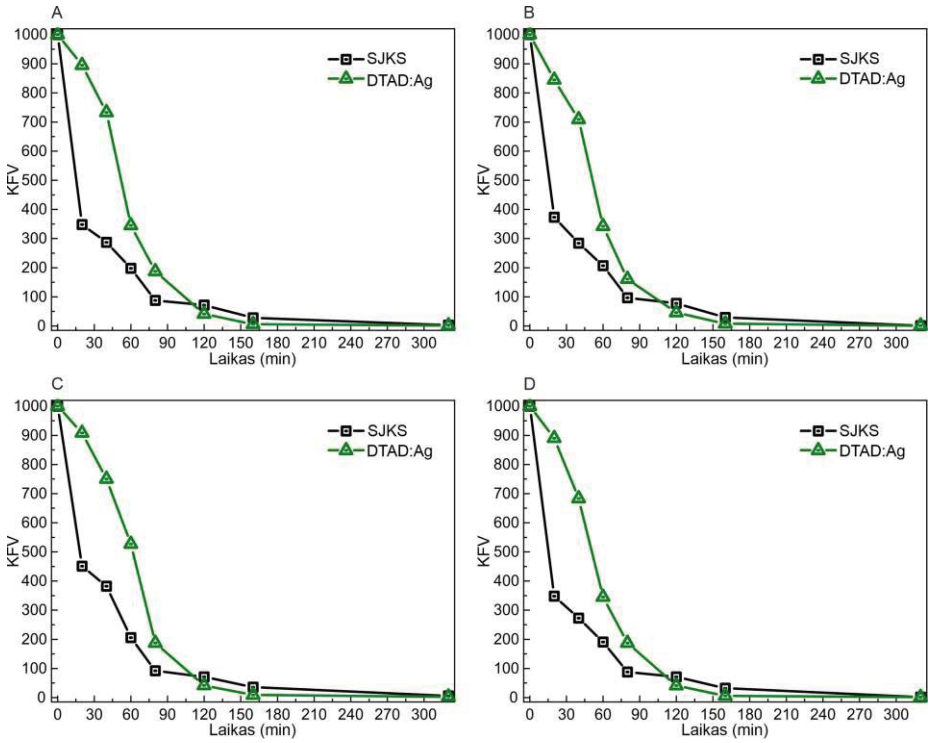

6 pav. Antimikrobiniai tyrimai su *S. aureus* bakterijų padermėmis: (A) LTSaDA01; (B) LTSaM01; (C) LTSa635 (MRSA) ir (D) LTSa603, bakterijų koncentracija – 1 Mf = $3x10^8$ CFV, suspensijos atskiedimas 10^{-5} ir DTAD:Ag – tvarsčio pagrindas, SJKS – pirmasis tvarsčio prototipas su sidabro jonų kaupimo sluoksniu

Remiantis tyrimų rezultatais buvo nustatyta, kad paruoštas tvarsčio prototipas su SJKS turėjo stipresnes ir greitesnes antimikrobines savybes lyginant BG (3,4 at. %). Nustatyta, kad sidabro nanodalelės vaidina svarbų vaidmenį sidabro jonų kaupimo sluoksniui, ir šis sluoksnis gali greitai ištirpinti ir atiduoti į aplinką visus sukauptus sidabro jonus. Tokia technologija gali būti taikoma tvarsčiams, kai antimikrobinis poveikis turi būti greitas siekiant išvengti infekcijos žaizdoje [59, 224].

Pleistro bandymai su laboratoriniais gyvūnais

Eksperimentų su laboratoriniais gyvūnais metu pleistro prototipas buvo panaudotas *S. aureus* bakterijomis užkrėstų ir neužkrėstų žaizdų gydymui. Atlikus

bandymus su neužkrėstomis žaizdomis buvo stebimas greitas žaizdos gijimas, jokių stiprių uždegimo požymių nebuvo pastebėta.

Žaizdų audiniai buvo šviesiai rausvos spalvos, žaizda traukėsi nuo įpjovų kraštų. Antrą dieną, dėl kapiliarų tinklo regeneracijos, žaizdos audiniai buvo tamsesnės rausvos spalvos, o žaizdos ilgis buvo mažesnis lyginant su pirmąja diena. Pleistras neprilipo prie žaizdos audinių ir buvo nuimamas nepažeidžiant gyjančių audinių.

Eksperimentai su MRSA užkrėstomis žaizdomis (7 pav.): po pirmosios gydymo dienos žaizdų audiniai buvo rausvos spalvos, o lyginant su kontroliniais bandymais, buvo matomas minimalūs patinimas ir paraudimas. Mikrobiologiniai tyrimai parodė, kad bakterijų skaičius sumažėjo iki 50 % po to, kai buvo pritaikytas tvarsčių prototipas, lyginant su kontroliniais bandymais. Po antrosios dienos bakterijų kolonijų skaičius sumažėjo nuo 91 iki 54, o gijimo procesas buvo įvertintas kaip geras. 3 dieną bakterijų nebuvo rasta žaizdų audiniuose ir žaizda susitraukė.

Sidabro jonų kaupimo sluoksnis gali sumažinti chemines reakcijas su sidabro nanodalelėmis ir palaikyti stiprų antimikrobinį aktyvumą [105, 169, 245] žaizdos paviršiuje. Lėtas sidabro jonų išsiskyrimas sumažina galimą toksiškumą bei dangos su sidabro nanodalelėmis gali būti veiksmingos ilgesnį laiką [92, 105, 240].

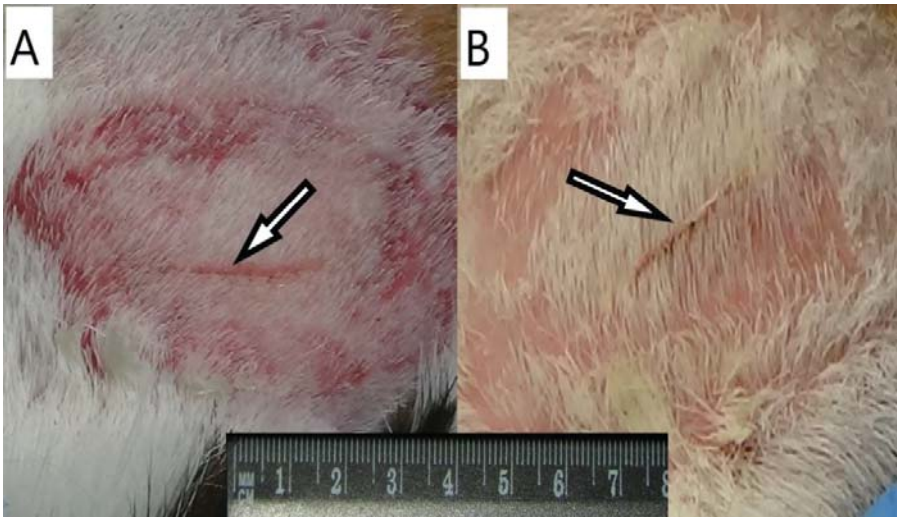

7 pav. MRSA užkrėstos žaizdos gydymas su pleistro prototipu: A – po dviejų dienų, B – po keturių dienų gydymo

IŠVADOS

1. Pagamintos trys bandinių grupės su DTAD:Ag danga naudojant nuolatinės srovės nesubalansuotą magnetroną buvo apdirbtos ėsdinimu deguonies plazma (0,3 W/cm^2), 20 sekundžių; pirmoje bandinių grupėje sidabro koncentracija padidėjo nuo 0,46 iki 0,93, antroje – nuo 3,1 iki 3,4 ir trečioje nuo 5,3 iki 6,9 at %. Sidabro nanodalelių dydis priklausė nuo sidabro koncentracijos dangoje, sidabro nanodalelių dydis buvo nuo 3 iki 63 nm, vidutinis dalelių dydis pirmoje bandinių grupėje buvo 16,1, antroje – 23,7 ir trečioje – 28,8 nm.
2. Atlikus eksperimentus buvo pastebėta, kad deguonies plazma 20–25 sekundes ėsdinti bandiniai turėjo stipriausias antimikrobines savybes prieš visas *S. aureus* padermes lyginant su plazma neėsdintomis dangomis.
3. Buvo nustatyta, kad mažesnė nei 1 ppm sidabro jonų koncentracija turėjo antimikrobines savybes prieš *S. aureus* bakteriją (0,5 Mf), bet stipriausios antimikrobinės savybės pasireiškė esant 4 ppm sidabro jonų koncentracijai bakterijų suspensijoje. Antra bandinių grupė (3,4 at. % Ag) turėjo geriausias antimikrobines savybes prieš visas *S. aureus* bakterijų padermes ant agaro paviršiaus bei bandymuose *in vitro* sunaikino 83 % bakterijų per 120 min.
4. Atlikus SEM bandinių analizę buvo nustatyta, kad sidabro nanodalelės ir sidabro jonai sukelia bakterijų ląstelių sienelių pažeidimus. Po gautų duomenų analizės buvo nustatyta, kad sidabro nanodalelės turėjo stipresnį antimikrobinį efektą (sunaikino 80 % bakterijų) nei tos pačios koncentracijos sidabro jonai (sunaikino 76 % bakterijų).
5. Buvo sėkmingai sukurtas pleistro prototipas panaudojant DTAD:Ag su 3,4 at. % Ag ant nailono audinio su celiuliozės membrana ir sidabro jonų kaupimo sluoksniu. Remiantis mikrobiologinių tyrimų rezultatais buvo nustatyta, kad tokia tvarsčio konstrukcija buvo iki 50 % efektyvesnė po 20 min ir pagrindinis pranašumas buvo antimikrobinis veikimo greitis per pirmąsias 60 min lyginant su DTAD:Ag bandiniais. Neprilipimo prie audinių savybės buvo patvirtintos po eksperimentų su laboratoriniais gyvūnais.
6. Remiantis eksperimentų su laboratoriniais gyvūnais duomenimis, buvo patvirtinta, kad pleistro prototipas pagreitino užkrėstų žaizdų gijimą 40 % bei 100 % sunaikino bakterijas žaizdoje trečiąją gydymo dieną. Pleistras sumažino randus, nesukėlė jokių alerginių reakcijų bei liekamųjų reiškinių ant odos, be to, laboratorinių gyvūnų gaišimo atvejų per visą bandymų laikotarpį nebuvo.

ABSTRACT

Diamond like carbon (DLC) coatings were applied for preparation of external use pharmaceuticals (bandages) for efficient treatment of the microorganisms polluted wounds. During the microbiology experiments it was determined that silver dopped DLC coatings are suitable for antimicrobial properties containing bandage preparation and it could be applied on infected wounds for efficient healing.

The DLC coatings containing various concentrations of silver were deposited using unbalanced DC magnetron with pure silver target in acetylene atmosphere and changing power, voltage and gas flow speed into chamber, the coatings thickness and structure were controlled. Diamond like carbon coatings (100 nm thickness) on silicon wafer, textile was investigated by energy dispersive X-ray spectroscopy (EDS), scanning electron microscopy, and for silver ion diffusion from DLC:Ag coatings to water - atomic absorption spectroscopy. To improve coatings, the radio frequency (13.56 MHz) oxygen plasma etching was performed. Improvements strongly increased the silver ion release rate and the antimicrobial properties. After atomic absorbtion measurements, it was confirmed the Ag ion migration, from coatings to the purified water, was up to 4 ppm. For antimicrobial properties, the standard microbiology methods - disk diffusion method, spread-plate technique, serial dilution methods were applied. According to the tests results, the unetched DLC:Ag coatings had the weak antimicrobial properties comparing with the same coatings, which were improved by etching of radio frequency oxygen plasma.

After atomic absorption and microbiology experiments the group of samples containing 3.41 at. % of silver sputtered on nylon fabric fabric was applied for preparation of bandage prototype. The gelatin/agar water rich media was selected for the silver ion accumulation inside the bandage prototype, which increased the silver ion release rate and antimicrobial efficiency up to 50 %. The proposed bandage prototype was tested using laboratory animals. Small infected wounds were treated applying the bandage prototype on skin surface and healing process was monitored. It was obtained that after 72 h. the bacteria in wound's bed were killed and healing process was up to 40 % faster comparing with ordinary cotton bandage respectively. It was confirmed the silver ions and nanoparticles damaged the bacteria cells walls and killed them as antibiotic benzylpenicillin. SEM data analysis showed the bacteria cell wall changes after silver ions application *in-vitro*, which correlated with applied benzylpenicillin concentrations during the tests.

5. REFERENCES

[1] MELSNER, J. J., I. BERDICEVSKY and M. ZILBERMAN. In vitro microbial inhibition and cellular response to novel biodegradable composite wound dressings with controlled release of antibiotics. *Acta Biomaterialia*. 7, (2011), 325–336. doi.org/10.1016/j.actbio.2010.07.013.

[2] KNETSCH, M. L. W. and L. H. KOOLE. New Strategies in the Development of Antimicrobial Coatings: The Example of Increasing Usage of Silver and Silver Nanoparticles. *Polymers* 2011, 3, 340-366. doi:10.3390/polym3010340.

[3] FUKUDA, A., et al. The Role of Flies in the Maintenance of Antimicrobial Resistance in Farm Environments. *Microbial Drug Resistance*. doi.org/10.1089/mdr.2017.0371.

[4] TAN, S .Y. and Y. TATSUMURA. Alexander Fleming (1881–1955): Discoverer of penicillin. *Singapore Med J. (*2015) 56(7): 366-367 doi: 10.11622/smedj.2015105

[5] STROHSAHL, C. M., L. MILLER and T. D. KRAUSS. Detection of methicillin-resistant Staphylococcus aureus (MRSA) using the NanoLantern™ Biosensor. *Proc. of SPIE. Vol.* 7167 71670S-2. doi.org/10.1117/12.808872.

[6] GRAHAM, J. P., et al. Antibiotic resistant enterococci and staphylococci isolated from flies collected near confined poultry feeding operations. *Science of The Total Environment.* Vol., 407, (2009), 2701-2710. doi.org/10.1016/j.scitotenv.2008.11.056.

[7] CUI, D., et al. Use of and microbial resistance to antibiotics in China: a path to reducing antimicrobial resistance. *Journal of International Medical Research.* 2017, Vol. 45(6), 1768–1778. doi.org/10.1177/0300060516686230.

[8] ONWUGAMBA, F. C., et al. The role of 'filth flies' in the spread of antimicrobial resistance. *Travel Medicine and Infectious Disease*. Volume 22, 2018, pages 8-17.

[9] ZHANG, J., et al. Housefly (*Musca domestica*) and blow fly (*Protophormia terraenovae*) as vectors of bacteria carrying colistin resistance genes. Appl. Environ. Microbiol. 84:e01736-17. doi: 10.1128/AEM.01736-17.

[10] LEAPER, D. J. Silver dressings: their role in wound management. *Int. Wound. J.* 2006;3:282–294. doi.org/10.1111/j.1742-481X.2006.00265.x

[11] ONIK, G., et al. Physical medicine modalities most frequently applied in the lower limbs chronic wounds treatment in Poland. *Polish Annals of Medicine.* Vol. 24, (2017), 92-98. doi.org/10.1016/j.poamed.2016.09.001.

[12] MORTON, L. M. and T. J. PHILLIPS. Wound healing and treating wounds. *American Academy of Dermatology.* Volume 74, (2016), 589–605. doi.org/10.1016/j.jaad.2015.08.068.

[13] DACOSTA, R. S., et al. Point-of-Care Autofluorescence Imaging for Real-Time Sampling and Treatment Guidance of Bioburden in Chronic Wounds: First-in-Human. *PLoS ONE*. 10(3), 0116623. doi:10.1371/journal.pone.0116623.

[14] KOPPEN, C. J. And R. W. HARTMANN (2015) Advances in the treatment of chronic wounds: a patent review. *Expert Opinion on Therapeutic Patents.* 25, 8, 931-937. doi.org/10.1517/13543776.2015.1045879

[15] ZAKARIENĖ, G., et al.Diamond like carbon Ag nanocomposites as a control measure against Campylobacter jejuni and Listeria monocytogenes on food preparation surfaces. *Diamond & Related Materials.* 81, (2018), 118–126. doi.org/10.1016/j.diamond.2017.12.007.

[16] CHUDOBOVA, D., et al. Complexes of Silver(I) Ions and Silver Phosphate Nanoparticles with Hyaluronic Acid and/or Chitosan as Promising Antimicrobial Agents for Vascular Grafts. *Int. J. Mol. Sci.* 2013, 14, 13592-13614; doi:10.3390/ijms140713592.

[17] GUO, L., et al. Polymer/nanosilver composite coatings for antibacterial applications. *Colloids and Surfaces A: Physicochem. Eng. Aspects,* 439, (2013), 69– 83. doi.org/10.1016/j.colsurfa.2012.12.029.

[18] JAIN, J., et al. Silver Nanoparticles in Therapeutics: Development of an Antimicrobial Gel Formulation for Topical Use. *Molecular pharmaceutics* Vol. 6, No. 5, 1388–1401. doi: 10.1021/mp900056g.

[19] BERTHET, M., et al. Nanoparticle-Based Dressing: The Future of Wound Treatment? *Trends in Biotechnology,* 2017, Vol. 35, No. 8., 770-784. doi.org/10.1016/j.tibtech.2017.05.005.

[20] THET, N. T., et al. Prototype Development of the Intelligent Hydrogel Wound Dressing and Its Efficacy in the Detection of Model Pathogenic Wound Biofilms. *ACS Appl. Mater. Interfaces,* 2016, 8, 14909−14919. doi: 10.1021/acsami.5b07372.

[21] TRAN, P. L., et al. The ability of a colloidal silver gel wound dressing to kill bacteria *in vitro* and *in vivo*. *J Wound Care*. (2017), 1, 26, (sup4), S16-S24. doi:10.12968/jowc.2017.26.Sup4.S16

[22] MEHRABANI, M. G., et al. Preparation of biocompatible and biodegradable silk fibroin/chitin/silver nanoparticles 3D scaffolds as a bandage for antimicrobial wound dressing. *Int J Biol Macromol.* Vol. 114, (2018), 961-971. doi:10.1016/j.ijbiomac.2018.03.128.

[23] MORONES-RAMIREZ, J. R., et al. Silver enhances antibiotic activity against gram-negative bacteria. *Sci. Transl. Med., Vol. 5, Issue 190, pp. 190ra81, (2013).* doi: 10.1126/scitranslmed.3006276.

[24] OKTAR, F. N., et al. Molecular Mechanism and Targets of the Antimicrobial Activity of Metal Nanoparticles. *Current Topics in Medicinal Chemistry.* 2015, 15. 1583-1588.

[25] ANH, T. T. H., et al. Elastin-based silver-binding proteins with antibacterial capabilities. *Nanomedicine* (2013). 8(4), 567–575. https://doi.org/10.2217/nnm.13.47.

[26] PALADINI, F., et al. Surface chemical and biological characterization of flax fabrics modified with silver nanoparticles for biomedical applications, *Materials Science & Engineering C,* (2015). doi: 10.1016/j.msec.2015.03.035.

[27] GALDIERO, S., et al. Silver Nanoparticles as Potential Antiviral Agents. *Molecules,* 2011, 16, 8894-8918; doi:10.3390/molecules16108894.

[28] XU, J., Large-area uniform hydrogen-free diamond-like carbon films prepared by unbalanced magnetron sputtering for infrared anti-reflection coatings. *Diamond & related materials* 17, (2008). 194–198. doi.org/10.1016/j.diamond.2007.12.010.

[29] BATORY, D., et al. Silver implanted diamond-like carbon coatings. *Vacuum. Vol.* 110, (2014). 78 - 86. doi.org/10.1016/j.vacuum.2014.09.001.

[30] REISFELD, R., T. SARAIDAROV and V. LEVCHENKO. Formation and structural characterization of silver nanoparticles in ormosil sol–gel films. *Optica Applicata,* Vol. XXXVIII, No. 1, 2008.

[31] DEEPACHITRA, R., et al. Nanoparticles embedded biomaterials in wound treatment. *Journal of Chemical and Pharmaceutical Sciences*. Volume 8, Issue 2, April-June 2015. ISSN: 0974-2115.

[32] POWERS, J. G., et al. Wound healing and treating wounds Chronic wound care and management. *Journal of the American Academy of Dermatology.* Volume 74, Issue 4, April 2016, Pages 607-625. doi: 10.1016/j.jaad.2015.08.070.

[33] ERICKSON, J. R. and K. ECHEVERRI. Learning from regeneration research organisms: The circuitous road to scar free wound healing. *Developmental Biology.*

433, (2018), 144–154. doi.org/10.1016/j.ydbio.2017.09.025. doi.org/10.1016/j.ydbio.2017.09.025.

[34] WU, S., et al. Plasma-Modified Biomaterials for Self-Antimicrobial Applications. *ACS Appl. Mater. Interfaces* 2011, 3, 2851–2860. doi: 10.1021/am20039.

[35] SATO, K., Y. UMESONO and M. MOCHII. A transgenic reporter under control of an es1 promoter/enhancer marks wound epidermis and apical epithelial cap during tail regeneration in Xenopus laevis tadpole. *Developmental Biology* 433 (2018) 404–415. doi.org/10.1016/j.ydbio.2017.08.012

[36] SULAEVA, I., et al. Bacterial cellulose as a material for wound treatment: Properties and modifications. A review. *Biotechnology Advances.* 33, (2015), 1547–1571. doi: 10.1016/j.biotechadv.2015.07.009.

[37] DAVIDSON, J. M. Animal models for wound repair. *Arch Dermatol Res.* (1998), 290, (Suppl. 1): S1. doi.org/10.1007/PL00007448.

[38] CATANZANO, O., et al. Ultrasmall silver nanoparticles loaded in alginate–hyaluronic acid hybrid hydrogels for treating infected wounds. *International journal of polymeric materials and polymeric biomaterials*. Vol., 66, (2017), 12, 626–634. doi.org/10.1080/00914037.2016.1252358.

[39] CATANZANO, O., et al. Ultrasmall silver nanoparticles loaded in alginate hyaluronic acid hybrid hydrogels for treating infected wounds. *International journal of polymeric materials and polymeric biomaterials.* 2017, Vol. 66, No. 12, 626–634. doi.org/10.1080/00914037.2016.1252358.

[40] BISHARA, S., et al. Effect of silver on burn wound infection control and healing: Review of the literature. *Burns,* 33, (2007) 139 – 148. doi.org/10.1016/j.burns.2006.06.010.

[41] Shuqiang, L., et. al. Antibacterial Hydrogels. Adv. Sci. 2018, 5, 1700527. DOI: 10.1002/advs.201700527.

[42] ZAHEDIA, P., et al. A review on wound dressings with an emphasis on electrospun nanofibrous polymeric bandages. *Polym. Adv. Technol.* 2010, 21 77–95. doi.org/10.1002/pat.1625.

[43] PATIL, K. R. and C. R. PATIL. Anti-inflammatory activity of bartogenic acid containing fraction of fruits of Barringtonia racemosa Roxb. in acute and chronic animal models of inflammation. *Journal of Traditional and Complementary Medicine,* 7, (2017), 86 - 93. doi.org/10.1016/j.jtcme.2016.02.001.

[44] ABBOUD, E. C., et al. Do silver-based wound dressings reduce pain? A prospective study and review of the literature. *Burns.* Vol 40, (2014), S40 – S47. doi.org/10.1016/j.burns.2014.09.012.

[45] FLORIAN, P., et al. Antibacterial properties of silver containing diamond like carbon coatings produced by ion induced polymer densification. *Surface & Coatings Technology* 205 (2011). 4850–4854. doi.org/10.1016/j.surfcoat.2011.04.078.

[46] HEYDARNEJAD, M. S., et al. Sliver nanoparticles accelerate skin wound healing in mice (Mus musculus) through suppression of innate immune system. *Nanomed. J., Vol.* 1, *No.* 2, *Winter* 2014. doi: 10.7508/NMJ.2014.02.003.

[47] BACHLER, G., N. GOETZ and K. HUNGERBÜHLER. A physiologically based pharmacokinetic model for ionic silver and silver nanoparticles. *International Journal of Nanomedicine.* 2013:8 3365–3382. doi: 10.2147/IJN.S46624.

[48] BAGHDADIA, M. B. and S. TAJBAKHSHA. Regulation and phylogeny of skeletal muscle regeneration. *Developmental Biology,* 433, (2018), 200–209. doi.org/10.1016/j.ydbio.2017.07.026.

[49] MEI, L., et al. Nanofibers for improving the wound repair process: the combination of a grafted chitosan and an antioxidant agent. *Polym. Chem.,* 2017, 8,1664.

[50] TANDARA, A. A. and T. A. MUSTOE. Oxygen in Wound Healing—More than a Nutrient. *World J. Surg.* 28, 294–300, 2004.

[51] NARAYAN R. J., et al. Antimicrobial properties of diamond-like carbon-silver-platinum nanocomposite thin films. *Journal of Materials Engineering and Performance* volume 14, pages 435–440(2005) doi: https://doi.org/10.1361/105994905X56197.

[52] BELKAID, Y. and J. A. SEGRE. Dialogue between skin microbiota and immunity. *Science*. 2014, 346, (6212), 954-959. doi: 10.1126/science.1260144.

[53] ANSELME, K., et al. The interaction of cells and bacteria with surfaces structured at the nanometre scale. *Acta Biomater*. 2010, 6(10), 3824-46. doi: 10.1016/j.actbio.2010.04.001.

[54] WOODHAMS, D. C., et al. Managing Amphibian Disease with Skin Microbiota. *Trends in Microbiology*. Vol. 24, (2016), 161-164. doi.org/10.1016/j.tim.2015.12.010.

[55] SMEDEN, J. and J. A. BOUWSTRA. Stratum corneum lipids: their role for the skin barrier function in healthy subjects and atopic dermatitis patients. *Curr. Probl. Dermatol.* 49, 8–26 (2016). doi: 10.1159/000441540.

[56] WONG, S. L., et al. Diabetes primes neutrophils to undergo NETosis, which impairs wound healing. *Nature Medicine.* Volume 21, pages 815–819 (2015).

[57] ELAMENYA, L. K., et al. Antimicrobial Susceptibility of Bacteria that cause Wound Sepsis in the Paediatric Surgical Patients at Kenyatta National Hospital. *Afr. J. Pharmacol. Ther.* 2015, 4(1), 21-27.

[58] NANDA, A., and M. SARAVANAN. Biosynthesis of silver nanoparticles from staphylococcus aureus and its antimicrobial activity against MRSA and MRSE. *Nanomed. Nanotechnol. Biol. Med.* 2009, 5, 452–456. doi.org/10.1016/j.nano.2009.01.012.

[59] GE, L., et al. Nanosilver particles in medical applications: Synthesis, performance, and toxicity. *Int. J. Nanomed.* 2014, 9, 2399–2407. doi: 10.2147/IJN.S55015.

[60] BENNETT, M., Design, Fabrication, and Characterization of Electroceutical Bandages for Treatment of Chronically Infected Wounds. https://etd.ohiolink.edu/pg_10?0::NO:10:P10_ACCESSION_NUM:osu1462837586. Viewed - 2018.12.21

[61] MUSTOE, T. Understanding chronic wounds: a unifying hypothesis on their pathogenesis and implications for therapy. *The American Journal of Surgery.* 187, (2004), 65S–70S.

[62] KUO, D., et al. Novel Quorum-Quenching Agents Promote Methicillin-Resistant *Staphylococcus aureus* (MRSA) Wound Healing and Sensitize MRSA to β-Lactam Antibiotics. *Antimicrob Agents Chemother.* 59, 1512–1518. doi: 10.1128/AAC.04767-14.

[63] YEO, E.D., et al. Degree of the hazards of silver-containing dressings on MRSA-infected wounds in Sprague-Dawley and streptozotocin-induced diabetic rats. *Wounds: a Compendium of Clinical Research and Practice*. 2015, 27(4), 95-102.

[64] BARILLO, D. J., and D. E. MARX. Silver in medicine: A brief history BC 335 to present. *Burns.* Vol 40, (2014), S3 – S8. doi.org/10.1016/j.burns.2014.09.009.

[65] DUCHEYNE, P., Kevin HEALY, Dietmar W. HUTMACHER, David W. GRAINGER, C. James KIRKPATRICK. *Comprehensive Biomaterials II***.** P – 80. 2nd edition. eBook ISBN: 9780081006924.

[66] ALBRIGHT, C., F. R. NACHUM and M. D. LECHTMAN. Electrolytic silver ion generator for water sterilization in Apollo spacecraft water systems. *Apollo applications program.* NASA Contract. Rep. 1967; Report Number: NASA CR-

65738. Wieved (05 - 2018)
[67] CONRAND, A. H., et al. Ag+ alters cell growth, neurite extension, cardiomyocyte beating, and fertilized egg constriction. *A Viat. Space EnViron. Med.* 1999, 70, 1096–1105.
[68] MELAIYE, A. and W. J. YOUNGS. Silver and its application as an antimicrobial agent. Expert Opin. *Ther. Pat.* 2005, 15, 125–130. doi.org/10.1517/13543776.15.2.125.
[69] TRAVAN, A., et al. Non-cytotoxic silver nanoparticle-polysaccharide nanocomposites with antimicrobial activity.*Biomacromolecules 10 (2009) 1429.* doi: 10.1021/bm900039x.
[70] STOJKOVSKA, J., et al. Controlled production of alginate nanocomposites with incorporated silver nanoparticles aimed for biomedical applications *J. Serb. Chem. Soc.* 77 (12) 1709–1722 (2012) JSCS–4383. doi: 10.2298/JSC121108148S.
[71] MORRISON, M. L., et al. Electrochemical and antimicrobial properties of diamondlike carbon-metal composite films. *Diamond & Related Materials.* 15, (2006), 138 – 146. doi.org/10.1016/j.diamond.2005.08.031.
[72] QUELEMES, P. V., et al. Development and Antibacterial Activity of Cashew Gum-Based Silver Nanoparticles. *Int. J. Mol. Sci.* 2013, 14, 4969-4981; doi:10.3390/ijms14034969
[73] CAMPOS, V., et al. Simple and rapid method for silver nanoparticles incorporation in polymethyl methacrylate (PMMA) substrates. *Superficies y Vacío.* 30(4), 51-55, December 2017. ISSN: 1665-3521.
[74] GORUP, L.F., et al. (2017) Nanostructured Functional Materials: Silver Nanoparticles in Polymer for the Generation of Antimicrobial Characteristics. *Recent Advances in Complex Functional Materials.* pp 271-292. doi.org/10.1007/978-3-319-53898-3_11.
[75] GREEN, J.B.D., et al. A review of immobilized antimicrobial agents and methods for testing. *Biointerphases* 2011. 6. MR13–MR28.
[76] OSINSKA-JAROSZUK, M., et al. Vascular prostheses with covalently bound gentamicin and amikacin reveal superior antibacterial properties than silver-impregnated ones—An *in vitro* study. *Eur. J. Vasc. Endovasc. Surg.* 2009, 38, 697–706. doi:10.1016/j.ejvs.2009.09.003.
[77] BARILLO, D. J., et al. A literature review of the military uses of silver-nylon dressings with emphasis on wartime operations. *Burns.* Vol 40, (2014), S24 – S29. doi.org/10.1016/j.burns.2014.09.017.
[78] MOONEY, E. K., C. Lippitt and J. Friedman. Safety and efficacy report: silver dressings. *Plast Reconstr Surg.* 2006; 117(2), p 666-669. doi: 10.1097/01.prs.0000200786.14017.3a.
[79] PAUL, R. Diamond-Like-Carbon Coatings for Advanced Biomedical Applications. *Glob J Nanomed* 2(5): GJO.MS.ID.555598 (2017).
[66] TANGA, C., et al. Silver nanoparticles-loaded activated carbon fibers using chitosan as binding agent: Preparation, mechanism, and their antibacterial activity. *Applied Surface Science,* 394, (2017), 457–465. doi.org/10.1016/j.apsusc.2016.10.095.
[81] CHOI, H. W., et al. Characteristic of silver doped DLC films on surface properties and protein adsorption. *Diamond & Related Materials* 17, (2008). 252–257. doi.org/10.1016/j.diamond.2007.12.034.
[82] GURUNATHAN, S., et al. Green synthesis of silver nanoparticles using *Ganoderma neo-japonicum* Imazeki: a potential cytotoxic agent against breast cancer cells. *International Journal of Nanomedicine,* 2013:8 4399–4413. doi: 10.2147/IJN.S51881.

[83] LANSDOWN, A. B., B. SAMPSON and A. ROWE. Sequential change in trace metal, metallothionein and calmodulin concentrations in healing skin wounds. *Journal of Anatomy,* 195(3), 375-386.

[84] HAIDER, A., and I. K. KANG. Preparation of Silver Nanoparticles and Their Industrial and Biomedical Applications: A Comprehensive Review. *Advances in Materials Science and Engineering.* Volume 2015, Article ID 165257, 16 pages. doi.org/10.1155/2015/165257.

[85] BOONKAEW, B., et al. Antimicrobial efficacy of a novel silver hydrogel dressing compared to two common silver burn wound dressings: Acticoat™ and PolyMem Silver®. *Burns,* Vol. 40, 2014, 89-96. doi.org/10.1016/j.burns.2013.05.011.

[86] CATANZANO, O., et al. Alginate–hyaluronan composite hydrogels accelerate wound healing process. *Carbohydrate Polymers*. Vol. 131, (2015), 407-414. doi.org/10.1016/j.carbpol.2015.05.081.

[87] PARK, M., et al. Effect of discarded keratin-based biocomposite hydrogels on the wound healing process *in vivo*. *Materials Science and Engineering: C*, Vol. 55, (2015), 88-94. doi.org/10.1016/j.msec.2015.03.033.

[88] MONTASER, A.S., et al. Preparation and characterization of alginate silver nicotinamide nanocomposites for treating diabetic wounds. *International Journal of Biological Macromolecules.* 92, (2016), 739–747. doi.org/10.1016/j.ijbiomac.2016.07.050.

[89] DUMANTEPE, M., et al. Efficacy of intralesional recombinant human epidermal growth factor in chronic diabetic foot ulcers. *Growth Factors*. 33:2, 128-132. doi.org/10.3109/08977194.2015.1031898.

[90] ABDELGAWAD, A. M., S. M. HUDSON and O. J. ROJAS. Antimicrobial wound dressing nanofiber mats from multicomponent (chitosan/silver-NPs/polyvinyl alcohol) systems. *Carbohydrate Polymers.* 100, (2014), 166-178. doi.org/10.1016/j.carbpol.2012.12.043.

[91] BIAO, L., et al. Synthesis and characterization of proanthocyanidins-functionalized Ag nanoparticles. *Colloids and Surfaces B: Biointerfaces,* 169, (2018), 438–443. doi.org/10.1016/j.colsurfb.2018.05.050.

[92] ABALKHIL, T. A., et al. Bactericidal activity of biosynthesized silver nanoparticles against human pathogenic bacteria. *Biotechnology & biotechnological equipment,* 2017 vol. 31, no. 2, 411–417. doi.org/10.1080/13102818.2016.1267594.

[93] LOPEZ-CARBALLO, G., et al. Silver Ions Release from Antibacterial Chitosan Films Containing in Situ Generated Silver Nanoparticles. *J. Agric. Food Chem.* 2013, 61, 260−267. doi**:** 10.1021/jf304006y.

[94] DUNN, K., and V. EDWARDS-JONES. The role of ActicoatTM with nanocrystalline silver in the management of burns. *Burns,* 30 Suppl. 1 (2004), S1 - S9. doi.org/10.1016/S0305-4179(04)90000-9.

[95] WANG, X., et al. Adsorption of bovine serum albumin on silver surfaces enhances the release of silver at pH neutral conditions. *Phys. Chem. Chem. Phys.,* 2015, 17, 18524—18534. doi: 10.1039/C5CP02306H.

[96] CLOUTIER, M., et al. On the long term antibacterial features of silver-doped DLC coatings deposited via a hybrid plasma process. *Biointerphases 9, 029013 (2014).* doi.org/10.1116/1.4871435.

[97] MARX, D. E. and D. J. BARILLO. Silver in medicine: The basic science. *Burns.* Vol. 40 (2014), S9 – S18.

[98] RUPARELIA, J. P., et al. Strain specificity in antimicrobial activity of silver and copper nanoparticles. *Acta Biomater.,* 2008, 4, 707–716. doi.org/10.1016/j.actbio.2007.11.006.

[99] BUI, V. K. H., et al. Chitosan Combined with ZnO, TiO2 and Ag Nanoparticles for AntimicrobialWound Healing Applications: A Mini Review of the Research Trends. *Polymers,* 2017, 9(1), 21. doi.org/10.3390/polym9010021

[100] BONDARENKO, O., et al. Bacterial plasma membrane is the main cellular target of silver nanoparticles in Escherichia coli and Pseudomonas aeruginosa. https://doi.org/10.1101/322727.

[101] PAL, S., Y. K. Tak and J. M. Song. Does the antibacterial activity of silver nanoparticles depend on the shape of the nanoparticle? A study of the Gramnegative bacterium *Escherichia coli*. *appl environ microbiol.,* 73:17, 12–20., 2007. doi: 10.1128/AEM.02218-06.

[102] RIEGER, K.A., et al. Antimicrobial Activity of Silver Ions Released from Zeolites Immobilized on Cellulose Nanofiber Mats. *Appl. Mater. Interfaces* 2016, 8, 3032−3040. doi: 10.1021/acsami.5b10130

[103] GRAVANTE, G., et al. Nanocrystalline silver: a systematic review of randomized trials conducted on burned patients and an evidence-based assessment of potential advantages over older silver formulations. *Ann Plast Surg*. 2009; 63(2), 201–205. doi: 10.1097/SAP.0b013e3181893825.

[104] CATANZANO, O., et al. Ultrasmall silver nanoparticles loaded in alginate–hyaluronic acid hybrid hydrogels for treating infected wounds. *International Journal of Polymeric Materials and Polymeric Biomaterials*, 66:12, 626-634, (2017). doi.org/10.1080/00914037.2016.1252358

[105] YALCINKAYA, E.E., et al. Cellulose nanocrystals as templates for cetyltrimethylammoniumbromide mediated synthesis of Ag nanoparticles and their novel usein PLA films. *Carbohydrate Polymers,* 157, (2017), 1557–1567. doi.org/10.1016/j.carbpol.2016.11.038.

[106] PERCIVAL, S.L., P.G. BOWLER and D. RUSSELL. Bacterial resistance to silver in wound care. *Journal of Hospital Infection* (2005), 60, 1–7. doi.org/10.1016/j.jhin.2004.11.014.

[107] KIM, M. H., et al. Thermal fabrication and characterization of Ag nanoparticle-activated carbon composites for functional wound-dressing additives. *Journal of Alloys and Compounds*, 735, (2018), 2670 - 2674. doi.org/10.1016/j.jallcom.2017.11.347.

[108] VOLOVA, T. G., et al. Antibacterial properties of films of cellulose composites with silver nanoparticles and antibiotics. *Polymer Testing., 65, (2018), 54–68.* doi.org/10.1016/j.polymertesting.2017.10.023.

[109] MARCIANO, F.R., et al. Wettability and antibacterial activity of modified diamond-like carbon films. *Applied Surface Science,* 255 (2009) 8377–8382. doi.org/10.1016/j.apsusc.2009.05.091.

[110] JANKAUSKAITĖ, V., et al. Bactericidal effect of graphene oxide/Cu/Ag nanoderivatives against Escherichia coli, Pseudomonas aeruginosa, Klebsiella pneumoniae, Staphylococcus aureus and Methicillin-resistant Staphylococcus aureus. *International Journal of Pharmaceutics,* 511, (2016), 90-97. doi.org/10.1016/j.ijpharm.2016.06.121.

[111] KASITHEVAR, M., et al. Antibacterial efficacy of silver nanoparticles against multi-drug resistant clinical isolates from post-surgical wound infections. *Microbial Pathogenesis,* 107 (2017), 327-334. doi.org/10.1016/j.micpath.2017.04.013.

[112] LI, X.Z., H. NIKAIDO and S.E. WILLIAMS. Silver-resistant mutants of Escherichia coli display active efflux of Ag+ and are deficient in porins. *J Bacteriol.* 1997, 179, 6127–32. doi: 10.1128/jb.179.19.6127-6132.1997.

[113] SILVER, S., L.T. PHUNG and G. J. SILVER. *Ind. microbiol. biotechnol.* (2006), 33: 627. doi.org/10.1007/s10295-006-0139-7.
[114] SILVER, S. Bacterial silver resistance: molecular biology and uses and misuses of silver compounds. *FEMS Microbiology Reviews.* Vol. 27, (2003), 341–353. doi.org/10.1016/S0168-6445(03)00047-0.
[115] KAUR, P., and D.V. VADEHRA. Mechanism of resistance to silver ions in *Klebsiella* pneumoniae. *Antimicrob Agents Chemother.* 1986, 29(1), 165–167. doi: 10.1128/AAC.29.1.165.
[116] LOVE, C.A., et al. Diamond like carbon coatings for potential application in biological implants—a review. *Tribology International* 63(2013), 141–150. doi.org/10.1016/j.triboint.2012.09.006.
[117] STERLING, J. P. Silver-resistance, allergy, and blue skin: Truth or urban legend. *Burns.* Vol 40, (2014) S19 – S23. doi.org/10.1016/j.burns.2014.10.007.
[118] WADHERA, A., and M. Fung. Systemic argyria associated with ingestion of colloidal silver. *Dermatol Online J.* 2005;11(1):12.
[119] XU, F., et al. Silver nanoparticles (AgNPs) cause degeneration of cytoskeleton and disrupt synaptic machinery of cultured cortical neurons. *Molecular Brain* 2013, 6:29. doi.org/10.1186/1756-6606-6-29.
[120] PARHAM, S., et al. In Situ Synthesis of Silver Nanoparticles for Ag-NP/Cotton Nanocomposite and Its Bactericidal Effect. *J. Chin. Chem. Soc.* 2017, 64, 1286–1293. doi.org/10.1002/jccs.201700157.
[121] CHANAN-KHAN, A., et al. Complement activation following first exposure to pegylated liposomal doxorubicin (Doxil): possible role in hypersensitivity reactions. *Ann Oncol.,* 2003; 14: 1430–1437. doi.org/10.1093/annonc/mdg374.
[122] SZEBENI, J., et al. Animal models of complement-mediated hypersensitivity reactions to liposomes and other lipid-based nanoparticles. *J. Liposome Res*., 2007;17: 107–117. doi.org/10.1080/08982100701375118.
[123] LEGLER, A. V., et al. Synthesis and antimicrobial activity of silver complexes with arginine and glutamic acid. *Pharm Chem J.* 2001, 35, 501–503. doi.org/10.1023/A:1014098810078.
[124] POON, V. K. M. and A. BURD. In vitro cytotoxity of silver: implication for clinical wound care. *Burns* 30, (2004), 140–147. doi.org/10.1016/j.burns.2003.09.030.
[125] ALBERS, C. E., et al. In vitro cytotoxicity of silver nanoparticles on osteoblasts and osteoclasts at antibacterial concentrations. *Nanotoxicology,* 2011*; Early Online,* 1–7. doi: 10.3109/17435390.2011.626538.
[126] BERTUCCIO, A. J. and R. D. TILTON. Silver Sink Effect of Humic Acid on Bacterial Surface Colonization in the Presence of Silver Ions and Nanoparticles. *Environ. Sci. Technol.* 51, 3, 1754-1763. doi: 10.1021/acs.est.6b04957.
[127] JAMUNA-THEVI, K., et al. Quantification of silver ion release, in vitro cytotoxicity and antibacterial properties of nanostuctured Ag doped TiO2 coatings on stainless steel deposited by RF magnetron sputtering. *Vacuum,* 86, (2011), 235 - 241. doi.org/10.1016/j.vacuum.2011.06.011.
[128] KORANI, M., et al. Acute and subchronic dermal toxicity of nanosilver in guinea pig. *International Journal of Nanomedicine.* 2011:6, 855–862. doi: 10.2147/IJN.S17065.
[129] KAWATA, K., M. OSAWA and S. OKABE. In Vitro Toxicity of Silver Nanoparticles at Noncytotoxic Doses to HepG2 Human Hepatoma Cells. *Environ. Sci. Technol.* (2009), 43, (15), 6046–6051. DOI: 10.1021/es900754q
[130] AURORE, V., et al. Silver-nanoparticles increase bactericidal activity and radical oxygen responses against bacterial pathogens in human osteoclasts. *Nanomedicine:*

Nanotechnology, Biology, and Medicine., 14, (2018), 601–607. doi.org/10.1016/j.nano.2017.11.006.

[131] MEŠKINIS, Š., et al. Structure of the silver containing diamond like carbon films: Study by multiwavelength Raman spectroscopy and XRD. *Diamond & Related Materials,* 40, (2013). 32–37. doi.org/10.1016/j.diamond.2013.09.004.

[132] NARAYAN, R. J., et al. Antimicrobial Properties of Diamond-like Carbon-Silver-Platinum Nanocomposite Thin Films. *Journal of Materials Engineering and Performance. Volume* 14(4) *August* 2005—435. doi: 10.1361/105994905X56197.

[133] PRINCEN, E. P. H. (1994). Deposition of diamond-like carbon coatings by unbalanced magnetron sputtering. TU Eindhoven. Fac. Werktuigbouwkunde, Vakgroep WPA, rapporten. Eindhoven. Technische Universiteit Eindhoven. https://pure.tue.nl/ws/files/4346098/430776.pdf

[134] ZENG, Z., et al. Synthesis of quenchable amorphous diamond. NATURE COMMUNICATIONS | 8: 322, (2017). https://www.nature.com/articles/s41467-017-00395-w.

[135] LINA, I.N., Y. H. CHENB and H. F. CHENG. Modification of emission properties of diamond films due to surface treatment process. *Diamond and Related Materials,* 9, (2000), 1574-1581. doi.org/10.1016/S0925-9635(00)00312-5.

[136] CALDERON, S., et al. Ag+ release inhibition from ZrCN–Ag coatings by surface agglomeration mechanism: structural characterization. J. Phys. D: Appl. Phys. 46 (2013) 325303. doi.org/10.1088/0022-3727/46/32/325303.

[137] NAKATANI, T., et al. Controlled Zeta Potential Using Plasma Processing and Evaluation of Cytocompatibility. *J. Photopolym. Sci. Technol.* Vol. 22, No. 4, 2009. doi.org/10.2494/photopolymer.22.455.

[138] KELLY, P. J. and R. D. ARNELL. Magnetron sputtering: a review of recent developments and applications. *Vacuum* 56 (2000) 159 - 172. doi.org/10.1016/S0042-207X(99)00189-X.

[139] KLINGENBERG, M., et al. Practical applications of ion beam and plasma processing for improving corrosion and wear protection. *Surface and Coatings Technology.* Vol. 158 –159, (2002), 164–169. doi.org/10.1016/S0257-8972(02)00194-9.

[140] CORTESE, B., et al. Superhydrophobic fabrics for oil–water separation through a diamond like carbon (DLC) coating. *J. Mater. Chem. A.* 2014, 2,6781.

[141] CASCHERA, D., et al. Flame retardant properties of plasma pre-treated/diamondlike carbon (DLC) coated cotton fabrics. *Cellulose.* (2015), 22:2797–2809. doi.org/10.1007/s10570-015-0661-8.

[142] ARNELL, R. D. and P. J. Kelly. Recent advances in magnetron sputtering. *Surface and Coatings Technology*. 112, (1999), 170–176. doi.org/10.1016/S0257-8972(98)00749-X.

[143] HAN. J. G. Magnetron sputtering technology. Available in PDF at: www.ispcconference.org/ispcdocs/ispc18/ispc18/content/slide00822.pdf.

[144] YAO, W., et al. A dynamic and thermodynamic model of diamond film Growth. *Diamond and Related Materials.* 9 _2000. 1664 - 1667. doi.org/10.1016/S0925-9635(00)00329-0.

[145] NARAYAN, R. J. Nanostructured diamondlike carbon thin films for medical applications. *Materials Science and Engineering C.* 25 (2005). 405 – 416. doi.org/10.1016/j.msec.2005.01.026.

[146] ARONSSON, B. O., J. LAUSMA and B. KASEMO. Glow discharge plasma treatment for surface cleaning and modification of metallic biomaterials. *Journal of*

Biomedical Materials Research. Vol. 35, 49–73 (1997). doi.org/10.1002/(SICI)1097-4636(199704)35:1<49::AID-JBM6>3.0.CO;2-M.

[147] HAKOVIRTA, M., X. M. HE and M. NASTASI. Optical properties of fluorinated diamond-like carbon films produced by pulsed glow discharge plasma immersion ion processing. *Journal of applied physics.* 88, 1456, (2000). https://doi.org/10.1063/1.373838.

[148] WUA, Y., et al. Preparation and properties of Ag/DLC nanocomposite films fabricated by unbalanced magnetron sputtering. *Applied Surface Science* 284, (2013). 165– 170. doi.org/10.1016/j.apsusc.2013.07.074.

[149] W. D. High-rate reactive DC magnetron sputtering of oxide and nitride superlattice coatings. *Vacuum*. Vol. 51, Issue 4 (1998), 641-646. doi.org/10.1016/S0042-207X(98)00265-6.

[150] VIRGANAVIČIUS, D., et al. Patterning of diamond like carbon films for sensor applications usingsilicon containing thermoplastic resist (SiPol) as a hard mask. *Applied Surface Science* 385 (2016) 145–152. doi.org/10.1016/j.apsusc.2016.05.100.

[151] YUNATA, E. E., and T. Aizawa. Micro-texturing into DLC/diamond coated molds and dies via high density oxygen plasma etching. *Manufacturing Rev.* 2015, 2, 13. doi.org/10.1051/mfreview/2015015.

[152] MASSI, M., et al. Plasma etching of DLC films for microfluidic channels. *Microelectronics Journal*. 34, (2003), 635–638. doi.org/10.1016/S0026-2692(03)00077-6.

[153] MANIMUNDA, P., et al. Shear-Induced Structural Changes and Origin of Ultralow Friction of Hydrogenated Diamond-like Carbon (DLC) in Dry Environment. *ACS Appl. Mater. Interfaces.* 2017, 9, 16704−16714. doi: 10.1021/acsami.7b03360.

[154] MEŠKINIS, Š., et al. Annealing Effects on Structure and Optical Properties of Diamond-Like Carbon Films Containing Silver. *Nanoscale Research Letters* (2016). 11:146. doi 10.1186/s11671-016-1362-4. doi.org/10.1186/s11671-016-1362-4.

[155] MASOUD, N., K. MARTUS and K. BECKER. Vacuum ultraviolet emissions from a cylindrical dielectric barrier discharge in neon and neon–hydrogen mixtures. *International Journal of Mass Spectrometry,* 233, (2004), 395–403. doi.org/10.1016/j.ijms.2004.02.007.

[156] DIFFEY, B. L. Sources and measurement of ultraviolet radiation. *Methods,* 28, (2002). 4–13. doi.org/10.1016/S1046-2023(02)00204-9.

[157] BINTSIS, T. Existing and potential applications of ultraviolet light in the food industry – a critical review. *J Sci Food Agric.* 80, 637-645, (2000). doi.org/10.1002/(SICI)1097-0010(20000501)80:6<637::AID-JSFA603>3.0.CO;2-1.

[158] XIONG, B., et al. Preventing UV induced cell damage by scavenging reactive oxygen species with enzyme-mimic Au–Pt nanocomposites. *Talanta.* Vol. 120, (2014), 262-267. doi.org/10.1016/j.talanta.2013.12.020.

[159] WÄLDCHEN, S., et al. Light-induced cell damage in live-cell super-resolution microscopy. *Nature, Scientific Reports.* Vol. 5, Article number: 15348 (2015). doi: 10.1038/srep15348.

[160] SÁNCHEZ, A. P., et al. Protective effects of citrus and rosemary extracts on UV-induced damage in skin cell model and human volunteers. *Journal of Photochemistry and Photobiology B: Biology.* 136, (2014), 12-18. doi.org/10.1016/j.jphotobiol.2014.04.007.

[161] RAVANAT, J. L. T. DOUKI and J. CADET. Direct and indirect effects of UV radiation on DNA and its components. *J Photochem Photobiol B.* 63, (2001), 88-102.

[162] ZIMMER, J. L., and R. M. SLAWSON. Potential Repair of *Escherichia coli* DNA following Exposure to UV Radiation from Both Medium- and Low-Pressure UV

Sources Used in Drinking Water Treatment. *Appl Environ Microbiol.* 2002 Jul; 68(7): 3293–3299. doi: 10.1128/AEM.68.7.3293-3299.2002.

[163] GRIFFINI, G., et al. Multifunctional Luminescent Down-Shifting Fluoropolymer Coatings: A Straightforward Strategy to Improve the UV-Light Harvesting Ability and Long-Term Outdoor Stability of Organic Dye-Sensitized Solar Cells. *Adv. Energy Mater.* 2015, 5, 1401312. doi.org/10.1002/aenm.201401312.

[164] GUTAROWSKA, B., et al. Historical textiles – a review of microbial deterioration analysis and disinfection methods. *Textile Research Journal.* Vol. 87, 2388-2406. doi.org/10.1177/0040517516669076.

[165] RAMAN, N. et al. Smart Textiles Coated with Eco-Friendly UV-Blocking Nanoparticles Derived from Natural Resources. *ACS Omega.* 2018, 3 (7), 7454-7465. doi: 10.1021/acsomega.8b00822.

[166] ROBERTSON, S. N., et al. Investigation of the antimicrobial properties of modified multilayer diamond-like carbon coatings on 316 stainless steel. *Surface and Coatings Technology.* Vol 314, (2017), 72-78. doi.org/10.1016/j.surfcoat.2016.11.035.

[167] AL-JUMAILI, A., et al. Review on the Antimicrobial Properties of Carbon Nanostructures. *Materials.* 10(9), (2017), 1066. doi:10.3390/ma10091066.

[168] ZHOU, H., et al. Investigation into the antibacterial property of carbon films. *Diamond & Related Materials*. 17, (2008), 1416–1419. doi.org/10.1016/j.diamond.2008.01.047

[169] GAO, S., et al. Novel conjugated Ag@PNIPAM nanocomposites for an effective antibacterial wound dressing. *RSC Adv.* 2015. 5. 25870. doi: 10.1039/c5ra01199j.

[170] BOCIAGA, D., et al. Silver-doped nanocomposite carbon coatings (Ag-DLC) for biomedical applications – Physiochemical and biological evaluation. *Applied Surface Science* 355, (2015), 388–397. doi.org/10.1016/j.apsusc.2015.07.117.

[171] HARRASSER, N., et al. Antibacterial efficacy of ultrahigh molecular weight polyethylene with silver containing diamond-like surface layers. *AMB Expr.* (2015), 5:64. doi.org/10.1186/s13568-015-0148-x.

[172] CAZALINI, E. M., et al. Antimicrobial and anti-biofilm properties of polypropylene meshes coated with metal-containing DLC thin films. *J Mater Sci: Mater Med.* (2017) 28:97. doi.org/10.1007/s10856-017-5910-y.

[173] MATUSCHEK, E., D. F. J. BROWN and G. KAHLMETER. Development of the EUCAST disk diffusion antimicrobial susceptibility testing method and its implementation in routine microbiology laboratories. *Clin Microbiol Infect* 2014; 20: O255–O266. doi.org/10.1111/1469-0691.12373.

[174] HODILLE, B. M., et al. Disk diffusion testing for detection of methicillin-resistant staphylococci: does moxalactam improve upon cefoxitin? *J Clin Microbiol* 54:2905–2909. doi: 10.1128/JCM.01195-16.

[175] WOLFENSBERGER, A., et al. Change of Antibiotic Susceptibility Testing Guidelines from CLSI to EUCAST: Influence on Cumulative Hospital Antibiograms. *PLoS ONE*. 8(11): e79130. https://doi.org/10.1371/journal.pone. 0079130

[176] Clinical and Laboratory Standards Institute (CLSI). Performance Standards for Antimicrobial Susceptibility Testing. 26th ed. CLSI supplement M100S (ISBN 1-56238-923-8 [Print]; ISBN 1-56238-924-6 [Electronic]). Clinical and Laboratory Standards Institute, 950 West Valley Road, Suite 2500, Wayne, Pennsylvania 19087 USA, 2016.

[177] KLANČNIK, A., et al. Evaluation of diffusion and dilution methods to determine the antibacterial activity of plant extracts. *Journal of Microbiological Methods.*81, Issue 2, May 2010, Pages 121-126. https://doi.org/10.1016/j.mimet.2010.02.004

[178] HARTMAN, D. Perfecting Your Spread Plate Technique. *J Microbiol Biol Educ*. 2011; 12(2): 204–205. doi: 10.1128/jmbe.v12i2.324
[179] CORMIER, J. and J. JANES. A double layer plaque assay using spread plate technique for enumeration of bacteriophage MS2. *Journal of Virological Methods*. Volume 196, February 2014, Pages 86-92. https://doi.org/10.1016/j.jviromet.2013.10.034.
[180] BIOSAN densitometer. [Wiewed at Web page 2018-04] https://www.biosan.lv/en/products/katalog/densitometers/den-1
[181] https://microbeonline.com/preparation-mcfarland-turbidity-standards/ wieved 2018-04-20
[182] McFARLAND STANDARD. Wiewed 2018-04. Available in PDF at: http://www.dalynn.com/dyn/ck_assets/files/tech/TM53.pdf
[183] ZAPATA, A. and S. RAMIREZ-ARCOS. A Comparative Study of McFarland Turbidity Standards and the Densimat Photometer to Determine Bacterial Cell Density. *Curr Microbiol*. 2015, 70: 907. https://doi.org/10.1007/s00284-015-0801-2
[184] HOPWOOD, D. Fixatives and fixation: a review. *The Histochemical Journal*.1969, Volume 1, 323–360. doi.org/10.1007/BF01003278.
[185] KNIGGENDORF, A. K., et al. Effects of ethanol, formaldehyde, and gentle heat fixation in confocal resonance Raman microscopy of purple nonsulfur bacteria. *Microscopy research technique.*Vol.74, 2011**,** 177-183. doi.org/10.1002/jemt.20889.
[186] DANILATOS, G. D. and R. Postle. The environmental scanning electron microscope and its applications. *Scanning Electron Microscopy.* (1982),1-16.
[187] MONTEIRO, J. M., et al. Cell shape dynamics during the staphylococcal cell cycle. *Nature communications.* 6:8055, (2015). doi: 10.1038/ncomms9055.
[188] ZAJMI, A., et al. Ultrastructural Study on the Antibacterial Activity of Artonin E versus Streptomycin against *Staphylococcus aureus* Strains. *PLoS ONE.* 10(6), e0128157, (2015). doi.org/10.1371/journal.pone.0128157
[189] REIMER, Ludwig. Scanning Electron Microscopy: Physics of Image Formation and Microanalysis. Springer, Nov 11, 2013. Pages 1-2, 12. eBook ISBN 978-3-540-38967-5
[190] EGERTON, R. F. Physical Principles of Electron Microscopy. *Physical Principles of Electron Microscopy.*121-147. doi: 10.1021/es104205a.ISBN 978-3-319-39877-8
[191] Image J, the software working guide. [Wiewed at Web page 2018-06] https://imagej.net/User_Guide/Working_with_ImageJ
[192] PICCOLO, B. and R. T. O'CONNOR. Atomic absorption spectroscopy. *JAOCS.* Vol., 45, 11, (1968), 789-792. doi.org/10.1007/BF02631956.
[193] WALSH, A., et al. Atomic absorption and atomic fluorescence methods of analysis: their merits and limitations. *Phil. Trans. Roy. Soc. London*. A305, 485-498, (1982). doi.org/10.1098/rsta.1982.0046
[194] HASWELL, S. J. 1991. Atomic Absorption Spectrometry; Theory, Design and Applications. *Elsevier, Amsterdam*. Analytical Spectroscopy Library; v. 5; 1991; 549 p; Elsevier; Amsterdam (Netherlands); ISBN 0-444-88217-0
[195] TAMULEVIČIUS, S., et al. Piezoresistive properties of amorphous carbon based nanocomposite thin films deposited by plasma assisted methods. *Thin Solid Films.* 538, (2013), 78–84. doi.org/10.1016/j.tsf.2012.11.122.
[196] ZAPOROJTCHENKO, V. Residual stress in polytetrafluoroethylene-metal nanocomposite films prepared by magnetron sputtering. *Thin Solid Films. 518, (2010), 5944–5949.* doi.org/10.1016/j.tsf.2010.05.097.
[197] SAFI, I. Recent aspects concerning DC reactive magnetron sputtering of thin films: a review. *Surface and Coatings Technology.* 127 _2000. 203

219. doi.org/10.1016/S0257-8972(00)00566-1.
[198] YAREMCHUK, I., et al. Modeling of the plasmonic properties of DLC-Ag nanocomposite films. *Phys. Status Solid. A.,* 211, No. 2, 329–335 (2014). doi.org/10.1002/pssa.201330067.
[199] LIN, T., et al. High resolution transmission electron microscopy study of the initial growth of diamond on silicon. *Diamond and Related Materials.* 9, 2000. 1703 - 1707. doi.org/10.1016/S0925-9635(00)00303-4.
[200] JONES, B. J. and N. NELSON. Sticking non-stick: Surface and Structure control of Diamond-like Carbon in Plasma Enhanced Chemical Vapour Deposition. *Journal of Physics: Conference Series.* 768 (2016) 012011.
[201] KORNER, E., et al. Formation and distribution of silver nanoparticles in a functional plasma polymer matrix and related AgR release properties. *Plasma Process. Polym.* 2010, 7, 619–625. doi.org/10.1002/ppap.200900163.
[202] CHEKAN, N.M., et al. Biological activity of silver-doped DLC films. *Diamond & Related Materials* 18 (2009). 1006–1009. doi.org/10.1016/j.diamond.2009.02.024.
[203] TAMULEVIČIUS, T., et al. Refractive index sensor based on the diamond like carbon diffraction grating. *Thin Solid Films* 519 (2011) 4082–4086. doi.org/10.1016/j.tsf.2011.01.099.
[204] CASCHERA, D., et al. Ultra Hydrophobic/Superhydrophilic Modified Cotton Textiles through Functionalized Diamond-Like Carbon Coatings for Self-Cleaning Applications. *Langmuir.* 2013, 29, 2775−2783. doi: 10.1021/la305032k.
[205] TAMULEVIČIUS, T., et al. Structuring of DLC:Ag nanocomposite thin films employing plasma chemical etching and ion sputtering. *Nuclear Instruments and Methods in Physics Research B* 341 (2014) 1–6. doi.org/10.1016/j.nimb.2013.09.052.
[206] N. Kitahara a,∗, T. Sato a, H. Isogawa b, Y. Ohgoe a, S. Masuko b, F. Shizuku b, K.K. Hirakuri a. Antibacterial property of DLC film coated on textile material. Diamond & Related Materials 19 (2010) 690–694
[207] GORZELANNY, C., et al. Silver nanoparticle-enriched diamond-like carbon implant modification as a mammalian cell compatible surface with antimicrobial properties. *Nature, Scientific Reports.* 6:22849. doi: 10.1038/srep22849.
[208] WANG, Y, M. et al. Recent studies on diamond surfaces. *Diamond and Related Materials.* 9 2000. 1582 1590. doi.org/10.1016/S0925-9635(00)00292-2.
[209] KUTSAY, O., et al. Surface properties of amorphous carbon films. *Diamond & Related Materials* 17, (2008). 1689–1691. doi.org/10.1016/j.diamond.2008.02.020.
[210] FURNO, F., et al. Silver nanoparticles and polymeric medical devices: a new approach to prevention of infection. *Journal of Antimicrobial Chemotherapy. (*2004) 54, 1019–1024. https://doi.org/10.1093/jac/dkh478.
[211] IVANOVA, A.A., et al. Hybrid biocomposite with a tunable antibacterial activity andbioactivity based on RF magnetron sputter deposited coating andsilver nanoparticles. *Applied Surface Science,* 329, (2015), 212–218. doi.org/10.1016/j.apsusc.2014.12.153.
[212] RINALDI, S., L. Tarpani, and L. Latterini. "UV Treatment of the Stabilizing Shell for Improving the Photostability of Silver Nanoparticles," *Journal of Nanomaterials*. 2016, Article ID 7510563, 7 pages, 2016. https://doi.org/10.1155/2016/7510563.
[213] BOIS, L., et al. Chemical growth and photochromism of silver nanoparticles into a mesoporous titania template. *Langmuir* 26, (2010), 1199–1206. doi: 10.1021/la902339j.
[214] ZAPOROJTCHENKO, A. V., et al. Tuning of the ion release properties of silver nanoparticles buried under a hydrophobic polymer barrier. *J. Nanopart. Res.* (2012).,

14:928.
[215] WANG, B., et al. In situ construction of Ag NPs in bio-inspired multilayer films for long-term bactericidal and biofilm inhibition properties. *Polymer Testing.,* 62, (2017), 162-170. doi.org/10.1016/j.polymertesting.2017.06.023.
[216] RAI, M., A. YADAV and A. GADE. Silver nanoparticles as a new generation of antimicrobials. *Biotechnology Advances,* 27, (2009), 76–83. doi.org/10.1016/j.biotechadv.2008.09.002.
[217] PAZOS, E., et al. Nucleation and Growth of Ordered Arrays of Silver Nanoparticles on Peptide Nanofibers: Hybrid Nanostructures with Antimicrobial Properties. *J. Am. Chem. Soc.* 2016, 138, 5507−5510. doi: 10.1021/jacs.6b01570.
[218] REED, R. B., et al. Potential Environmental Impacts and Antimicrobial Efficacy of Silverand Nanosilver-Containing Textiles. *Environ. Sci. Technol.* 2016, 50, 4018−4026. doi: 10.1021/acs.est.5b06043.
[219] ERTEM, E., et al. Core−Shell silver nanoparticles in endodontic disinfection solutions enable long-term antimicrobial effect on oral biofilms. *ACS Appl. Mater. Interfaces* 2017, 9, 34762−34772. doi: 10.1021/acsami.7b13929.
[220] LIU, H. L., et al. Antibacterial properties of silver nanoparticles in three different sizes and their nanocomposites with a new waterborne polyurethane. *Int. J. Nanomed*. 2010, 5, 1017–1028. doi: 10.2147/IJN.S14572.
[221] MEI, L., et al. Silver Nanocluster-Embedded Zein Films as Antimicrobial Coating Materials for Food Packaging. *ACS Appl. Mater. Interfaces* 2017, 9, 35297−35304. doi: 10.1021/acsami.7b08152.
[222] GIESSEN, T. W. and A. P. SILVER. Converting a Natural Protein Compartment into a Nanofactory for the Size-Constrained Synthesis of Antimicrobial Silver Nanoparticles. *Environ. Sci. Technol.* 2011, 45 (10), pp 4422–4428. doi: 10.1021/acssynbio.6b00117.
[223] ZHANG, W., et al. Modeling the Primary Size Effects of Citrate-Coated Silver Nanoparticles on Their Ion Release Kinetics. *Environ. Sci. Technol*. 2011, 45(10), pp 4422–4428. doi: 10.1021/es104205a.
[224] BACHLER, G., N. GOETZ and K. HUNGERBÜHLER. A physiologically based pharmacokinetic model for ionic silver and silver nanoparticles. *International Journal of Nanomedicine.* 2013:8 3365–3382. doi: 10.2147/IJN.S46624.
[225] KRUKA, T., et al. Nanostructured multilayer polyelectrolyte films with silver nanoparticles as antibacterial coatings. *Colloids and Surfaces B: Biointerfaces*. 137, (2016), 158–166. doi.org/10.1016/j.colsurfb.2015.06.016.
[226] NATEGHI, M. R., and H. HAJIMIRZABABA. Effect of silver nanoparticles morphologies on antimicrobial properties of cotton fabrics. *The Journal of The Textile Institute*. 105, 806-813. doi.org/10.1080/00405000.2013.855377.
[227] SONG, Y., et al. Silver-Incorporated mussel-inspired polydopamine coatings on mesoporous silica as an efficient nanocatalyst and antimicrobial agent. *ACS Appl. Mater. Interfaces.* 2018, 10, 1792−1801. doi: 10.1021/acsami.7b18136.
[228] BORRELLI, N. F., et al. Physics and Chemistry of Antimicrobial Behavior of Ion-Exchanged Silver in Glass. *ACS Appl. Mater. Interfaces* 2015, 7, 2195−2201. doi: 10.1021/am508159z.
[229] TAHERI, S., et al. Substrate independent silver nanoparticle based antibacterial coatings. *Biomaterials,* 35, (2014), 4601 - 4609. doi.org/10.1016/j.biomaterials.2014.02.033
[230] PETKOVA, P., et al. Sonochemical coating of texiles with hybrids ZnO/chitosan antimicrobial nanoparticles. *ACS Appl. Mater. Interfaces,* 2014, *6, 1164–1172.* doi: 10.1021/am404852d.

[231] HERMANS, M. H. Silver-containing dressings and the need for evidence. *AJN*. 2006, 106 (12), 60–68.
[232] SHEN, W., et al. The bactericidal mechanism of action against Staphylococcus aureus for AgO nanoparticles. *Materials Science and Engineering C.,* 75 (2017) 610–619. doi.org/10.1016/j.msec.2017.02.080.
[233] STROMINGER, J. L., et al. Composition of the cell wall of Staphylococcus aureus: its relation to the mechanism of action of penicillin. *The Journal of biological chemistry* 234, (1959), 3263-8.
[234] YOURASSOWSKY, E., et al. Paradoxicalaction of penicillin G on Staphylococcus aureus: a time study of the effect ofa zonal antibiotic concentration gradient on bacterial growth. *Antimicrobialagents and chemotherapy*. 8, (1975), 262–265. doi: 10.1128/AAC.8.3.262.
[235] BLUMBERG, P. M., and J. L. STROMINGER. Interaction of penicillin with the bacterial cell: penicillin-binding proteins and penicillin-sensitive enzymes. *Bacteriological Reviews*. 38, (1974), 291–335.
[236] TIPPER, D. J., and J. L. STROMINGER. Mechanism of action of penicillins: a proposal basedon their structural similarity to acyl-d-alanyl-d-alanine. *Proceedings of the National Academy of Sciences.* 54, (1965), 1133–1141. doi.org/10.1073/pnas.54.4.1133.
[237] GUNTUPALLI, R., et al. Detection and identification of methicillin resistant and sensitive strains of *Staphylococcus aureus* using tandem measurements. *Journal of Microbiological Methods.* 90, (2012), 182–191. doi.org/10.1016/j.mimet.2012.05.003.
[238] LORAN, S., A. YELON and E. SACHER. Short communication: Unexpected findings on the physicochemical characterization of the silver nanoparticle surface. *Applied Surface Science*, 428, (2018), 1079–1081. doi.org/10.1016/j.apsusc.2017.09.251.
[239] VIMALA, K., et al. Fabrication of Curcumin Encapsulated Chitosan-PVA Silver Nanocomposite Films for Improved Antimicrobial Activity. *Journal of Biomaterials and Nanobiotechnology*, 2011, 2, 55-64. doi.org/10.1016/j.aca.2016.02.025.
[240] AHMAD, M.B., et al. Synthesis of Silver Nanoparticles in Chitosan, Gelatin and Chitosan/Gelatin Bionanocomposites by a Chemical Reducing Agent and Their Characterization. *Molecules* 2011, 16, 7237-7248. doi:10.3390/molecules16097237
[241] AHMADI, F., et al. Effect of Silver Nanoparticles on Common Bacteria in Hospital Surfaces. *Jundishapur J Mirobiol.* 2013; 6(3): 209-14. doi: 10.5812/jjm.4585.
[242] ROE, D., et al. Antimicrobial surface functionalization of plastic catheters by silver nanoparticles. *J Antimicrob Chemother*. 2008;61(4):869-876. doi.org/10.1093/jac/dkn034.
[243] ROLLIN, G., et al. Intracellular Survival of *Staphylococcus aureus* in Endothelial Cells: A Matter of Growth or Persistence. *Front Microbiol.* 2017; 8: 1354. doi.org/10.3389/fmicb.2017.01354.
[244] WRIGHT, B. I., K. LAM and A. G. BURET. Early healing events in a porcine model of contaminated wounds: Effect of nanosilver in MMP's cell apoptosis and healing. *J Dermatol.* 1991; 124: 519–526. doi.org/10.1046/j.1524-475X.2002.10308.x.
[245] RICHARDS, H. L., et al. Metal Nanoparticle Modified Polysulfone Membranes for Use in Wastewater Treatment: A Critical Review. *Journal of Surface Engineered Materials and Advanced Technology,* Vol.2 No.3A, July 27, 2012. doi.org/10.4236/jsemat.2012.223029.
[246] DORSETT-MARTIN, W. A. Rat models of skin wound healing: A review. *Wound*

rep. reg. 2004; 12:591–599. doi.org/10.1111/j.1067-1927.2004.12601.x.
[247] PANNERSELVAM, B., et al. An in vitro study on the burn wound healing activity of cotton fabrics incorporated with phytosynthesized silver nanoparticles in maleWistar albino rats. *European Journal of Pharmaceutical Sciences,* 100, (2017), 187–196. doi.org/10.1016/j.ejps.2017.01.015.
[248] JOHNSON, K., et al. Systemic cell cycle activation is induced following complex tissue injury in axolotl. *Developmental Biology.* 433, (2018), 461–472. doi.org/10.1016/j.ydbio.2017.07.010.
[249] INNES, M. E., et al. The use of silver coated dressings on donor site wounds: a prospective, controlled matched pair study. *Burns* 27 (2001) 621–627. doi.org/10.1016/S0305-4179(01)00015-8.
[250] THOMSON C.H. Biofilms: do they affect wound healing?. *Int Wound J.* 2011, 8, 63–67. doi: 10.1111/j.1742-481X.2010.00749.x.
[251] RIGO, C., et al. Active Silver Nanoparticles for Wound Healing. *Int. J. Mol. Sci.* 2013, *14*, 4817-4840; doi:10.3390/ijms14034817.
[252] BIDGOLI, S. A., et at. Toxicity Assessment of Nanosilver Wound Dressing in Wistar Rat. *Acta Medica Iranica.* Vol. 51, No. 4 (2013).
[253] LAZIĆ, V., et al. A study of the antibacterial activity and stability of dyed cotton fabrics modified with different forms of silver. *J. Serb. Chem. Soc.* 77, (2), (2012), 225–234. doi: 10.2298/JSC110505167L.
[254] DARGAVILLE, T. R., et al. Sensors and Imaging for Wound Healing: A Review. *Biosensors and Bioelectronics,* 41, pp. 30-42. doi.org/10.1016/j.bios.2012.09.029.
[255] NIAKAN, S., et al. Comparison of the Antibacterial Effects of Nanosilver With 18 Antibiotics on Multidrug Resistance Clinical Isolates of *Acinetobacter baumannii*. *Jundishapur Journal of Microbiology.* 2013 ; 6(5): 1-5. ISSN 2008-4161.
[256] LIN, Y., et al. Functional nanonetwork-structured polymers and carbons with silver nanoparticle yolks for antibacterial application. *Chem. Commun.,* 2017, 53, 9777.

Curriculum Vitae

Name / surname: Tadas Juknius
Nationality: Lithuanian
Date of birth: May 15, 1987

Adress: Kaunas, Tvirtovės al. 83-18.
Lithuania
email tadasjuknius@inbox.lt
tel. +370 696 83 975

Work experience:

- Since Apr 2021 director, project manager of UAB CIVECOSAS.
- Since Mar 2020 director and project manager of UAB Romecic.
- Since Jan 2019 work with new innovations (personal projects)
- Sept 2018 to Dec 2018 innovator (in a feasibility study)
- Nov 2017 to Jun 2018 Project expert (mentor of young entrepreneurs)
- Nov 2017 to Dec 2018 Project supervisor
- Jun 2017 to Nov 2017 Deputy Project Manager
- May 2016 to Jun 2017 director of startup *UAB IKN*
- Apr 2015 to Dec 2015 work at NANOSMARTPLASTER project as a junior researcher representing Kaunas University of Technology
- Dec 2013 to Feb 2015 work at BIOCARDIOSTIM project as a specialist representing Kaunas University of Technology
- Nov 2013 to Jan 2015 work at PARMO project as a specialist representing Kaunas University of Technology.

Work in non-profit organizations:

- Dec 01, 2010 to Nov 08, 2011 President of a newly established Veterinary Academy students' association at Lithuanian University of Health Sciences.
- Nov 08, 2011 Veterinary Academy students' association member of the council. Member of the University Senate.
- Secretary of project Planning and Management of Student Career
- Since May 06, 2011 Study quality assessment expert at Centre for Quality Assessment in Higher Education.
- Dec 04, 2008 Vice-president; from Jan 06, 2010 to Dec 01, 2010 President of Student Representations at Veterinary Academy. Member of Veterinary academy senate. Member of the Faculty Council, the National Union of Student Representations of Lithuania.

Education:

- Veterinarian (scientific degree: master). Graduation date: Feb 27, 2013 graduation from Lithuanian Health Sciences University Veterinary Academy.

6. APPROBATION OF THE RESEARCH RESULTS

The dissertation results have been published in 3 scientific articles in scientific journals with the citation index of *Web of Science* (*Clarivate Analytics*). A PCT patent has been issued for the developed bandage structure.

The scientific results have been presented at 8 international conferences and one national conference, specifically, one oral presentation and 8 poster session presentations have been delivered. The author has personally presented the research results in all the conferences.

Two patents have been obtained: one national and one WIPO (PCT).

List of publications related to the dissertation

1. Juknius, Tadas; Tamulevičius, Tomas; Gražulevičiūtė, Ieva; Klimienė, Irena; Matusevičius, Algimantas Petras; Tamulevičius, Sigitas. *In-situ* measurements of bacteria resistance to antimicrobial agents employing leaky mode sub-wavelength diffraction grating // Sensors and Actuators B 204 (2014) 799–806. http://dx.doi.org/10.1016/j.snb.2014.08.049. ISSN 0925-4005. [Science Citation Index [IF (E): 4.097 (2014)]
2. Juknius, Tadas; Ružauskas, Modestas; Tamulevičius, Tomas; Šiugždinienė, Rita; Juknienė, Indrė; Vasiliauskas, Andrius; Jurkevičiūtė, Aušrinė; and Tamulevičius, Sigitas. Antimicrobial Properties of Diamond-Like Carbon/Silver Nanocomposite Thin Films Deposited on Textiles: Towards Smart Bandages // Materials 2016, 9, 371; doi: 10.3390/ma9050371. ISSN 1996-1944. [Science Citation Index [IF (E): 2.467 (2017)]
3. Juknius, Tadas; Juknienė, Indrė; Tamulevičius, Tomas; Ružauskas, Modestas; Pamparienė, Ina; Oberauskas, Vaidas; Jurkevičiūtė, Aušrinė; Vasiliauskas, Andrius; and Tamulevičius, Sigitas. Preclinical Study of a Multi-Layered Antimicrobial Patch Based on Thin Nanocomposite Amorphous Diamond Like Carbon Films with Embedded Silver Nanoparticles. Materials 2020, 13, 3180; doi: 10.3390/ma13143180. ISSN 1996-1944. [Science Citation Index IF (E): 3.057 (2019)]

Patents

1. KAUNAS UNIVERSITY OF TECHNOLOGY (LT). Sensible plaster, Inventors: Tadas JUKNIUS. LT patent No. LT 6502. The State Patent Bureau of the Republic of Lithuania.
2. KAUNAS UNIVERSITY OF TECHNOLOGY (LT). The WIPO (PCT) patent Smart Patch. Inventors: Tadas JUKNIUS. Number: WO2018002817A1.

List of conferences related to the dissertation

1. Juknius, Tadas; Tamulevičius, Tomas; Gražulevičiūtė, Ieva; Virganavičius, Dainius; Klimienė, Irena; Matusevičius, Algimantas Petras; Tamulevičius, Sigitas. The response of a pure bacterial culture to the effect of antimicrobial agents employing a leaky mode diffraction grating waveguide sensor // 56th scientific conference for young students of physics and natural sciences. 2013, March 20-23 Vilnius, Lithuania. p. 171. Poster session P3-10.
2. Juknius, Tadas; Tamulevičius, Tomas; Gražulevičiūtė, Ieva; Klimienė, Irena; Matusevičius, Algimantas Petras; Tamulevičius, Sigitas. In-Situ measurements of bacteria resistance to antimicrobial agents employing refractometric method based on sub-wavelength diffraction grating // Advanced materials and technologies 2013: book of abstracts p. 43. Advanced materials and technologies 2013 August 27-31, Palanga, Lithuania.
3. Juknius, Tadas; Tamulevičius, Tomas; Gražulevičiūtė, Ieva; Klimienė, Irena; Matusevičius, Algimantas Petras; Tamulevičius, Sigitas. Investigation of *S. aureus* response to benzylpenicillin in real time employing refractive index sensor based on a sub-wavelength diffraction grating // XII Conference on optical chemical sensors and biosensors. 2014 April 13-16, Athens, Greese. p. 50, Poster session OS-18.
4. Juknius, Tadas; Tamulevičius, Tomas; Klimienė, Irena; Matusevičius, Algimantas Petras; Tamulevičius, Sigitas. Silver and diamond like carbon nanocomposite coatings for medical applications. // Nanotechnology: research and development: conference book. Lithuanian Academy of Sciences, Vilnius, Lithuania 2014 May 15-16 p. 75. Poster session P2-3.
5. Juknius, Tadas; Tamulevičius, Tomas; Tamuliavičienė, Asta; Klimienė, Irena; Matusevičius, Algimantas Petras; Meškinis, Šarūnas; Tamulevičius, Sigitas. Antibacterial properties of silver containing amorphous diamond like carbon films // E-MRS Spring Meeting 2014, May 26 to 30, Lille, France. Strasbourg: European Materials Research Society G.PI. 20.
6. Juknius, Tadas; Tamulevičius, Tomas; Klimienė, Irena; Matusevičius, Algimantas Petras; Meškinis, Šarūnas; Tamulevičius, Sigitas. // 9th International conference on surfaces, coatings and nanostructured materials. 2014 September 8-11, Dublin, Ireland. Abstract code: NANO-247.
7. Juknius, Tadas; Ružauskas, Modestas; Tamulevičius, Tomas; Tamulevičius, Sigitas. Silver nanoparticle's based plaster for efficient healing of infected wounds // 7th international conference on nanotechnologies and advanced materials. EuroNanoForum 2015 June 10-12. Riga, Latvia.
8. Juknius, Tadas; Ružauskas, Modestas; Tamulevičius, Tomas; Tamulevičius, Sigitas. Smart nanoplaster – a new way of wound treatment in daily life // Advanced materials and technologies 2015: book of abstracts P-46. Advanced materials and technologies 2015 August 27-31, Palanga, Lithuania.
9. Juknius, Tadas; Ružauskas, Modestas; Tamulevičius, Tomas; Jurkevičiūtė, Aušrinė; Tamulevičius, Sigitas. Smart bandage – one medical device that can control healing process // Life Sciences Baltics. 2016 September 14-15. Vilnius, Lithuania. Oral presentation on September 14.

Acknowledgements

I would like to express my appreciation to my scientific advisor prof. Sigitas Tamulevičius for the opportunity to implement my scientific ideas and create an innovative prototype. His valuable advice and immeasurable wisdom supported my work and creation process during all of my study years.

I am thankful to prof. Tomas Tamulevičius for advice and friendly scientific support and assistance in measurements.

My sincere thanks go to all collegues from the Institute of Materials Sciences for their stimulating discussions and support in overcoming numerous obstacles.

I am also grateful for the institute scientists, dr. Igoris Prosyčevas and Irina Abelit who helped me to perform atomic absorbtion spectroscopy measurements, to dr. Andrius Vasiliauskas, Vitoldas Kopustinskas and dr. Šarūnas Meškinis for assistance in the deposition of DLC coatings.

I want to say a big ‘thank you’ for scientists Assoc. Prof. Modestas Ružauskas, dr. Irena Klimienė, dr. Vaidas Oberauskas who shared experience and gave me valuable advice for microbiology and animal testing experiments from Lithuanian University of Health Sciences.

My deep gratitude goes to my family and my wife Indrė for their support and understanding.

Annex 1. Chemical composition (at.%) of prepared samples (Table 2)

	Chemical elements		
GoS 1		C	Ag
		99.46	0.47
		99.62	0.44
		99.54	0.46
	Average	**99.54**	**0.46**
	STDEV	0.08	0.015
GoS 2		96.81	3.15
		96.86	3.24
		96.98	2.98
	Average	**96.88**	**3.12**
	STDEV	0,09	0,13
GoS 3		94.56	5.14
		94.48	5.38
		95.02	5.42
	Average	**94.69**	**5.31**
	STDEV	0.3	0.15

Annex 2. Chemical composition (at. %) changes of prepared samples after RF plasma etching (Fig. 9)

		Chemical element		
		C	**Ag**	**O**
GoS 1	5 SEC	80.1	0.48	18.05
		79.3	0.52	21.1
		82.2	0.49	18.02
	Average	**80.5**	**0.5**	**19**
	STDEV	1.497776	0.020817	1.769642
	20 SEC	66.3	0.85	30.89
		67.2	1.02	31.98
		67.9	0.9	33.19
	Average	**67.1**	**0.9**	**32**
	STDEV	0.802081	0.087369	1.150522
		C	Ag	O
GoS 2	5 SEC	69.05	3.39	27.19
		70.01	3.05	26.89
		68.25	3.48	28.67
	Average	**69.1**	**3.3**	**27.6**
	STDEV	0.881211	0.226789	0.95296
	20 SEC	62.4	3.55	36.09
		60.59	3.29	35.96
		61.82	3.39	33.18
	Average	**61.6**	**3.4**	**35**
	STDEV	0.924247	0.131149	1.643847
		C	Ag	O
GoS 3	5 SEC	52.25	5.91	41.01
		53.39	6.05	42.02
		51.29	5.48	42.7
	Average	**52.3**	**5.8**	**41.9**
	STDEV	1.051285	0.297041	0.850353
	20 SEC	45.48	6.75	47.73
		44.89	7.24	49.17
		43.97	6.72	48.01
	Average	**44.8**	**6.9**	**48.3**
	STDEV	0.760986	0.291947	0.763501

Annex 3. Supplementary table and fit parameters of time versus Ag+ concentration (ppm) (Fig. 14)

GoS No	time min	Ag+ conc (ppm)
1	20	0.0
	40	0.0
	60	0.1
	120	0.15
	180	0.3
	1440	0.5
2	20	0.4
	40	0.7
	60	1.0
	120	1.8
	180	2.0
	1440	4.0
3	20	0.2
	40	0.5
	60	0.8
	120	1.6
	180	1.7
	1440	3.5

Equation $y = a\ln(-b\ln x)$ in Origin software – (Bradley) was used to approximate the experimental curve, and a high correlation coefficient $R^2 = 0.96$ was obtained for the constants a = 4.36 and b = - 0.32.

No.	*a*	*a* Standart Error	*b*	*b* Standart Error	Reduced Chi-Sqr	Adj. R-Square
1	4.15243	0.50241	-0.33147	0.01948	0.11831	0.93085
2	3.81252	0.42306	-0.32022	0.01627	0.08389	0.94132
3	0.60898	0.08924	-0.29694	0.01744	0.00373	0.90113

Annex 4. Experiment data of disk diffusion method (Fig. 16)

GoS No	Bacteria code (A-D) and clear zone on agar around sample				Etching time
	(A) LTSaDA01	B) LTSaM01	(C) LTSa635	(D) LTSa603	
1	**0** (0; 0; 0.5; 0)	**0** (0; 0.5; 0; 0)	**0** (0; 0; 0; 0)	**0** (0; 0; 0; 0.5)	5 s.
	0.5 (0.5; 0.5; 0.5; 0.5)	**0.5** (0.5; 0.5; 0.5; 0.5)	**0.5** (0.5; 0.5; 0.5; 0.5)	**0.5** (0.5; 0.5; 0.5; 0,5)	15 s.
	1.5 (1; 1.5; 1.5; 1.5)	**1.5** (1.5; 1.5; 1.5; 1.5)	**1** (0.5; 1; 1; 1)	**0.5** (0.5; 0.5; 0.5; 1)	20 s.
	1.5 (1.5; 1.5; 1.5; 1.5)	**1.5** (1.5; 1.5; 1.5; 1)	**1.5** (1.5; 1.5; 1; 1.5)	**1** (1; 1; 1; 1.5)	25 s.
	1 (1.5; 1; 1; 1)	**1** (1; 1; 1; 1)	**0,5** (1; 0.5; 0.5; 0.5)	**0.5** (0.5; 0.5; 0.5; 0.5)	30 s.
2	**0.5** (1; 0.5; 0.5; 0.5)	**0.5** (0.5; 1; 0.5 0.5)	**0.5** (0.5; 1; 0,5 0,5)	**0.5** (1; 0.5; 0.5; 0.5)	5 s.
	1.5 (1.5; 1.5; 1.5; 1)	**1.5** (1.5 1.5; 1.5; 1.5)	**1.5** (1; 1.5; 1.5; 1.5)	**1** (0.5; 1; 1; 1)	15 s.
	2.5 (2.5; 2.5; 2.5; 2)	**2.5** (2.5; 2.5; 2.5; 2.5)	**2.5** (2; 2.5; 2.5; 2.5)	**2** (2; 1.5; 2; 2)	20 s.
	2.5 (2.5; 2.5; 2.5; 2.5)	**2.5** (2.5; 2.5; 2; 2.5)	**2.5** (2.5; 2.5; 2.5; 2)	**2** (2; 2; 2; 1.5)	25 s.
	1 (1; 0.5; 1; 1)	**1.5** (1.5; 1.5; 1; 1.5)	**1** (1; 1; 1; 0.5)	**1** (1.5; 1; 1; 1)	30 s.
3	**1** (0.5; 1; 1; 1)	**0.5** (1; 0.5; 0.5; 0.5)	**1** (0.5; 1; 1.5; 1)	**1** (1; 0.5; 0.5; 1.5)	5 s.
	1.5 (1; 1.5; 2; 1.5)	**1.5** (1.5; 1.5; 1.5; 1.5)	**1.5** (1.5; 1.5; 1.5; 1)	**1** (1; 1.5; 1; 1)	15 s.
	2 (2.5; 2.5; 2.5; 2.5)	**2.5** (2.5; 2.5; 2.5; 2.5)	**2.5** (2.5; 2.5; 2.5; 2)	**2** (1.5; 2; 2; 2)	20 s.
	2 (2; 1.5; 2; 2)	**2.5** (2.5; 2.5; 2; 2.5)	**2.5** (2.5; 2; 2.5; 2.5)	**2** (1.5; 2; 2; 2)	25 s.
	1.5 (1.5; 1.5; 2; 1.5)	**1.5** (1.5; 1.5; 1.5; 1)	**2** (2.5; 2; 2; 2)	**1.5** (1.5; 2; 1.5; 1.5)	30 s.

The experiment value averages are in **bold**, the values of the individual tests are given in brackets**.** DLC:Ag coated nylon fabric groups of samples were RF oxygen plasma etched for 5-15-20-25-30 s.

Annex 5. Correlation of silver ion concentration and bacteria colony forming units (cfu (0.5 mf)) reduction in-time scale (Fig. 17 and Fig. 22)

Concentration ppm	Time, min.	CFU %	Live bacteria count^{x}
1	20	87.3	435
	40	75.5	379
	60	69.7	354
	120	62.9	322
	180	56.6	302
	340	54.4	294
3	20	83.5	416
	40	67.7	340
	60	59.5	302
	120	46.5	238
	180	39.5	211
	340	32.2	174
4	20	77.3	385
	40	60.6	304
	60	48	244
	120	35.9	184
	180	26.6	142
	340	20.7	112
Bandage SIAL antimicrobial effect	20	29.3	146
	40	19.5	98
	60	11.4	58
	120	7.4	38
	180	4.1	22
	340	0.4	2
CONTROL	20	100	498
	40	100	502
	60	100	508
	120	100	512
	180	100	534
	340	100	540

Experiment values are given in averages, the control value is 0.

Equation $y=y_0+A\cdot\exp(R_0\cdot x)$ in the Origin software – (Levenberg Marquardt) was used to approximate the experimental curves in Fig. 17 and Fig. 22.

Annex 6. Antibacterial tests result with *S. aureus* bacteria strains (Fig. 23)

Bacteria (A) LTSADA01; (B) LTSAM01; (C) LTSA635 (MRSA) AND (D) LTSA603, concentration: 1 mf = $3x10^8$ CFU, dilution 10^{-5} , SIAL – silver ion accumulation layer, experiment values are given in averages.

Bacteria (**LTSaDA01**) tests with bandage SIAL

	Time (min)/CFU							
t/min	**Kontrol**	**20**	**40**	**60**	**80**	**120**	**160**	**320**
test 1	1000<	324	282	188	86	67	32	6
test 2	1000<	376	288	208	90	78	30	0
test 3	1000<	344	290	198	88	70	23	2
Average	1000<	348	287	198	88	72	28	3

Bacteria (**LTSaM01**) tests without bandage SIAL

	Time (min)/CFU							
t/min	**Kontrol**	**20**	**40**	**60**	**80**	**120**	**160**	**320**
test 1	1000<	858	724	368	184	41	5	0
test 2	1000<	890	730	320	192	38	9	3
test 3	1000<	936	744	346	186	45	3	2
Average	1000<	895	733	345	187	41	6	2

Bacteria (**LTSaM01**) tests with bandage SIAL

	Time (min)/CFU							
t/min	**Kontrol**	**20**	**40**	**60**	**80**	**120**	**160**	**320**
test 1	1000<	364	272	198	96	76	30	0
test 2	1000<	386	282	218	102	82	36	4
test 3	1000<	368	298	204	92	72	22	0
Average	1000<	373	284	207	97	78	29	1

Bacteria (**LTSaM01**) tests without bandage SIAL

	Time (min)/CFU							
t/min	**Kontrol**	**20**	**40**	**60**	**80**	**120**	**160**	**320**
test 1	1000<	798	724	342	164	44	6	0
test 2	1000<	848	690	320	152	48	10	0
test 3	1000<	890	714	364	166	45	8	2
Average	1000<	845	709	342	161	46	8	1

Bacteria (**LTSa635**) tests with bandage SIAL

	Time (min)/CFU							
t/min	**Kontrol**	**20**	**40**	**60**	**80**	**120**	**160**	**320**
test 1	1000<	426	386	197	98	62	30	6
test 2	1000<	472	368	202	90	78	36	4
test 3	1000<	454	392	218	88	73	43	8
Average	1000<	451	382	206	92	71	36	6

Bacteria (**LTSa635**) tests without bandage SIAL

	Time (min)/CFU							
t/min	**Kontrol**	**20**	**40**	**60**	**80**	**120**	**160**	**320**
test 1	1000<	878	754	518	184	48	8	3
test 2	1000<	930	770	520	182	39	12	4
test 3	1000<	916	725	543	196	40	6	2
Average	1000<	908	750	527	187	42	9	3

Bacteria (**LTSa603**) tests with bandage SIAL

	Time (min)/CFU							
t/min	**Kontrol**	**20**	**40**	**60**	**80**	**120**	**160**	**320**
test 1	1000<	347	273	180	88	63	33	4
test 2	1000<	356	282	194	93	77	34	0
test 3	1000<	340	265	198	84	72	28	2
Average	1000<	348	273	191	88	71	32	2

Bacteria (**LTSa603**) tests without bandage SIAL

	Time (min)/CFU							
t/min	**Kontrol**	**20**	**40**	**60**	**80**	**120**	**160**	**320**
test 1	1000<	873	684	368	184	41	5	2
test 2	1000<	895	690	320	192	38	9	1
test 3	1000<	902	674	346	186	45	3	2
Average	1000<	890	683	345	187	41	6	2

Annex 7. Permission for experiments with laboratory animals

dr. M. Ružauko žiniai

2015 GAUTA 06 01 VMVT-78 Nr.

VALSTYBINĖ MAISTO IR VETERINARIJOS TARNYBA

LSMU Veterinarijos akademijos kanclerė Henrikas Žilinskas

LEIDIMAS ATLIKTI BANDYMO SU GYVŪNAIS PROCEDŪRŲ PROJEKTĄ

2015-05-27 Nr. G2-30
Vilnius

Vadovaujantis Lietuvos Respublikos gyvūnų gerovės ir apsaugos įstatymo 16 straipsnio 4 dalimi, Mokslo ir mokymo tikslais naudojamų gyvūnų laikymo, priežiūros ir naudojimo reikalavimais, patvirtintais Valstybinės maisto ir veterinarijos tarnybos direktoriaus 2012 m. spalio 31 d. įsakymu Nr. B1-866 „Dėl Mokslo ir mokymo tikslais naudojamų gyvūnų laikymo, priežiūros ir naudojimo reikalavimų patvirtinimo", Europos konvencija dėl eksperimentiniais ir kitais mokslo tikslais naudojamų stuburinių gyvūnų apsaugos (OL *2004 m. specialusis leidimas*, 15 skyrius, 4 tomas, p. 325) ir remiantis Lietuvos bandomųjų gyvūnų naudojimo etikos komisijos prie Valstybinės maisto ir veterinarijos tarnybos 2015-05-22 išvada Nr. 11 „Dėl leidimo atlikti bandymus su gyvūnais", l e i d ž i a m a

Lietuvos sveikatos mokslų universiteto Veterinarijos akademijai,
(ūkio subjekto (-ų), kuriame (-uose) ketinama atlikti bandymo su gyvūnais procedūrų projektą)

Tilžės g. 18, LT-47181 Kaunas, 302536989,
(adresai (-ai), kodai (-ai) Juridinių asmenų registre)

atlikti bandymo su gyvūnais procedūrų projektą

„Išmanaus antibakterinio pleistro kūrimas panaudojant sidabro nanostruktūras ir biopolimerus (NANOSMARTPLASTER)",
(bandymo su gyvūnais procedūrų projekto pavadinimas, vadovas, naudojami gyvūnai)

vadovas Modestas Ružauskas, naudojant 15 triušių ir 15 jūrų kiaulyčių,

Lietuvos sveikatos mokslų universiteto Veterinarijos akademijoje, Tilžės g. 18, LT-47181 Kaunas.
(bandymų su gyvūnais procedūrų projektą atliekančio vieto pavadinimas, adresas)

Leidimas atlikti bandymo su gyvūnais procedūrų projektą galioja iki 2015 m. gruodžio 31 d.

Direktoriaus pavaduotojas, pavaduojantis direktorių — Ž. Stanevičius — Zenonas Stanevičius

Annex 8. Laboratory animals experiment data (Table 6)

The changes of wound healing parameters

	Wound length			**Capillary net formation**			**Swelling**		
Day (1-3)	**1**	**2**	**3**	**1**	**2**	**3**	**1**	**2**	**3**
Patch 0	33	31	30	n	p	p	p	p	p
	32	31	28	n	p	p	p	p	p
	32	30	29	n	p/n	p	p	p	p
	34	33	30	n	p	p	p	p	p
	29	28	25	n	p	p	p	p	p
	30	29	27	n	p	p	p	p	p
	29	28	27	n	p	p	p	p	p
	28	27	25	n	p	p	p	p	p
AVERAGE	**30.875**	**29.625**	**27.625**	**n**	**p**	**p**	**p**	**p**	**p**
STDEV	2.167124	1.995531	1.995531						
Patch 1	31	29	25	n	p	n	p	n	n
	28	27	24	n	p	n	p	n	n/p
	29	28	26	n	p	n	p/n	n	n
	30	28	25	n	p	n	p	n	n
	32	29	26	n	p	n/p	p	n	n
	31	29	25	n	p	n	p	n	n
	30	28	26	n	p	n	p	n	n
	32	29	26	n/p	p	n	p	n	n
AVERAGE	**30.375**	**28.375**	**25.375**	**n**	**p**	**n**	**p**	**n**	**n**
STDEV	1.407886	0.744024	0.744024						
Patch 1A	28	26	24	p	p	n	p/n	n	n
	31	29	26	p	p	n	p	n	n
	29	27	23	p	p	n	p	n	n
	27	25	26	p/n	p	n	p	n	n
	29	27	26	p	p	n	p	n	n
	30	26	24	p	p	n	p	n	n
	28	26	24	p	p	n	p	n	n
	29	28	25	p	p	n	p	n	n
AVERAGE	**28.875**	**26.75**	**24.75**	**p**	**p**	**n**	**p**	**n**	**n**
STDEV	1.246423	1.28174	1.164965						
	30	28	27	p	p	n	n	n	n

Patch 2	33	31	30	p	p	n	n	n	n
	32	30	29	p	p	n	n	n	n
	33	31	29	p	p	n	n	n	n
	31	29	28	p	p	n	n	n	n
	34	32	30	p	p	n	n	n	n
	31	28	27	p	p	n	n	n	n
	32	29	28	p	p	n	n	n	n
AVERAGE	**32**	**29.75**	**28.5**	**p**	**p**	**n**	**n**	**n**	**n**
STDEV	1.309307	1.488048	1.195229						
Patch 3	26	23	18	p	p	n	n	n	n
	24	21	17	p	p	n	n	n	n
	25	22	18	p	p	n	n	n	n
	26	22	19	p	p	n	n	n	n
	26	23	19	p	p	n	n	n	n
	25	21	18	p	p	n	n	n	n
	26	22	18	p	p	n	n/p	n	n
	27	24	20	p	p	n	n	n	n
AVERAGE	**25.625**	**22.25**	**18.375**	**p**	**p**	**n**	**n**	**n**	**n**
STDEV	0.916125	1.035098	0.916125						

	Redness			**Scab formation**			**CFU number**		
Day (1-3)	**1**	**2**	**3**	**1**	**2**	**3**	**1**	**2**	**3**
Patch 0	p	p	p	p	p	p			
	p	p	p	p	p	p			
	p	p	p	p	p	p			
	p/n	p	p	p	p	p			
	p	p	p	p	p	p			
	p	p	p	p	p	p			
	p	p	p	p	p	p			
	p	p	p	p	p	p			
AVERAGE	**p**	**p**	**p**	**p**	**p**	**p**			
STDEV									
Patch 1	p	p	n	p	p	p	185	122	72
	p	p	n	p	p	p	179	134	84
	p	p	n	p	p	p	184	128	79
	p/n	p	n	p	p	p/n	188	129	82

	p	p	n	p	p	p	190	130	76
	p	p	n	p	p	p	181	118	65
	p	p	n	p	p	p	182	126	70
	p	p	n	p	p	p	186	134	78
AVERAGE	**p**	**p**	**n**	**p**	**p**	**p**	**184.375**	**127.625**	**75.75**
STDEV							3.662	5.553	6.386
Patch 1A	p	n	n	n	n	n	170	116	64
	p	n	n	n	n	n	170	108	69
	p/n	n	n	n	n	n	164	99	58
	p	n	n	n	n	n	168	95	51
	p	n	n	n	n/p	n	188	122	65
	p	n	n	n	n	n	183	112	67
	p	n	n	n	n	n	165	98	59
	p	n	n	n	n	n	171	101	76
AVERAGE	**p**	**n**	**n**	**n**	**n**	**n**	**172.375**	**106.375**	**63.625**
STDEV							8.568	9.664	7.633
Patch 2	n	n	n	n	n	n	92	59	0
	n	n	n	n	n	n	94	58	0
	n	n	n	n	n	n	91	64	0
	n	n	n	n	n	n	93	52	1
	n	n	n	n	n	n	88	56	0
	n	n	n	n	n	n	86	52	0
	n	n	n/p	n	n	n	89	41	0
	n	n	n	n	n	n	94	49	0
AVERAGE	**n**	**n**	**n**	**n**	**n**	**n**	**90.875**	**53.875**	**0.125**
STDEV							2.948	7.039	0.353
Patch 3	n	n	n	n	n	n			
	n	n	n	n	n	n			
	n	n	n	n	n	n			
	n	n	n	n	n	n			
	n	n	n	n	n/p	n			
	n	n	n	n	n	n			
	n/p	n	n	n	n	n			
	n	n	n	n	n	n			
AVERAGE	n	n	n	n	n	n			
STDEV									

p – positive, n – negative and p/n or n/p – hard to identify

UDK 539.216+615.463](043.3)
SL 344. 2021-12-06, 16,5 leidyb. apsk. l. Tiražas 14 egz. Užsakymas 288
Išleido Kauno technologijos universitetas, K. Donelaičio g. 73, 44249 Kaunas
Spausdino leidyklos „Technologija“ spaustuvė, Studentų g. 54, 51424 Kaunas